Ph. D. DISSERTATION

Metal Organic Frameworks Synthesis-Ultrasonic and Solvothermal Treatment with Organic/Inorganic Solvents Combinations

Jeju National University

Department of Nuclear and Energy Engineering

Farrukh Israr

December, 2015

Ph. D. DISSERTATION

	2015	Farrukh Israr	Metal Organic Frameworks synthesis-Ultrasonic and Solvothermal treatment with Organic/Inorganic Solvents Combinations

Metal Organic Frameworks Synthesis-Ultrasonic and Solvo-thermal Treatment with Organic/ Inorganic Solvents Combinations

Farrukh Israr

(Supervised by Professor Wongee Chun)

A thesis submitted in partial fulfillment of the requirement for the degree of Doctor of Nuclear & Energy Engineering.

December, 2015

This thesis has been examined and approved.

_____

Thesis Director, Wongee Chun, Prof. of Nuclear & Energy Engineering

Lee Heon-Ju_____

Choi Soo Seok_____

Kim Dong Kook_____

Park Choon Gun_____

(Name and Signature) Date: 2015.12

Department of Nuclear & Energy Engineering

GRADUATE SCHOOL

JEJU NATIONAL UNIVERSITY

To

My parents and family

Acknowledgements

In the name of Almighty Allah, the most merciful, the most beneficent. First, I would like to present my gratitude in front of Allah, Who gave me strength to accomplish this work.

I would like to thank my supervisor Prof. Wongee Chun for his trust, support, and supervision. The completion of this work would not be possible without his guidance and expertise. His thought-provoking seminars and discussions and a never-ending appetite for excellence I will admire and cherish forever. His encouragement and guidance during my high time and support and kindness during the down times have all been a source of motivation towards learning more and more. I am also thankful to my co-supervisor Associate Prof. Duk Kyung Kim as my mentor and Prof. Yoon Joon Lee for his useful lectures and discussions.

I want to thank my seniors and mentors including Dr. Joon Ho Hyun, Dr. Seung Jin Oh, Dr. Nauman Malik and Dr. Khalid Rehman. I had the company of wonderful friends in lab that helped and made research enjoyable including Yeong Min Kim, Moktar Hossain, Won Sik Kim, Ko Yoon Jung and Jung Haejun. The friends from university Dr. Muhammad Zubair, Junaid Ali, Shahid Aziz, Ghayas ud din Siddiqui, Dr. Murtaza Mehdi, Memoon Sajid, Dr. Anil Kumar, Safdar Ali, Rashid Ahmad, Sohail Khan, Kamran Ali, Wasim Abbas, Gul Hassan Orakzai, Zubair Amjad, Afaq Ahmed, Dr. Thiyagarajan, Dr. Sarwan, and Dr. Jamil Choudhry made my stay in Jeju easy. I would like to mention my friend Dr. Sebastian who guided me in various technical aspects during my research. Finally, I want to thank my good friends Dr. Zahid Manzoor and Shawkat Ali with whom I spent my most of time during my stay in Jeju.

The support from family was the fuel for the whole journey and I want to thank my parents, my wife, young Murtaza and my younger sister for their love and support. Love you all.

Contents

List of Figures

List of Tables

ABSTRACT

Metal organic frameworks (MOF) are a class of materials which are formed by a combination of metal with organic linkers. The properties of organic ligands such as bond angles, length, bulkiness and chirality plays an important part in determination of resultant framework. The metal ions can also adopt various geometries and affect the structure of MOFs. These solids have stable and ordered structures with high surface areas. Metal organic frameworks (MOFs) have different names such as porous coordination networks (PCNs) or porous coordination polymers (PCPs), yet all of these refer to same kind of materials. These materials have attracted a huge attention over the last three decades because of their applications in gas storage, gas separation, catalysis, luminescent and fluorescent materials, and drug storage and drug delivery.

By convention, metal organic frameworks have been synthesized by solvo thermal process which involves a reaction of organic ligands with metal salts at relatively low temperature (below 300°C). Additionally, other methodologies such as electrochemical, mechanochemical, microwave assisted heating and sonochemical routes have also been employed successfully with appreciable product yields.

Copper and Nickel based MOFs were synthesized from ultrasonic and solvo thermal techniques and their properties were investigated. Cu-BTC has been synthesized by ultrasonic treatment while using different combinations of organic and inorganic solvents. The solvent combination Dimethylformamide (DMF)/De-ionized water (H_2O) produced a MOF product of highest surface area (1434m^2/g) in one of these reactions. The product yield tend to vary with sonication time and applied power of sonication. Particle size and morphology vary with the type of solvent combination being employed.

The ultrasonic technique was also used to synthesize Ni-BTC by reacting Nickel metal precursor ($NiNO_3.6H_2O$) with benzenetricaroxylic acid at various probe temperatures and power levels. The probe temperatures and intermediate power level are the key operating principles for obtaining meaningful product yield. The Ni-BTC has also been synthesized by solvo thermal reactions. Seven different solvent combinations were used at identical operating conditions. The product yields were consistent but surface areas and other physico-chemical properties of MOFs tend to differ with each solvo thermal reaction mixture.

An intermediate/low temperature hydrothermal process approach was adopted for synthesis of Fe-BTC. This low temperature and short time reaction approach made the synthesis economically feasible and less time consuming compared to conventional processes. High temperature stability of synthesized MOF was investigated by comparing the XRD patterns of as prepared and heat treated samples of Fe-BTC.

Outline of Thesis

An outline of the different chapters of this thesis is as follow:

Chapter 1 introduces the metal organic frameworks (MOFs). The synthesis techniques of metal organic frameworks and their industrial applications in general.

Chapter 2 discusses the brief introduction of characterization techniques which have been used to examine the metal organic frameworks (MOFs).

Chapter 3 demonstrates the results of Cu-BTC synthesis through ultrasonic treatment. Different combinations of inorganic and organic solvent were used in these experiments and their outcomes were compared.

Chapter 4 shows the results of Ni-BTC synthesis through ultrasonic treatment. The effects of process parameters upon the properties of synthesized MOFs were recorded and presented.

Chapter 5 illustrates the solvothermal of Ni-BTC. Several organic and inorganic solvents were employed in synthesis processes. Each process showed characteristic yield and physical properties of synthesized MOF.

Chapter 6 demonstrates the hydrothermal synthesis of Fe-BTC at intermediate temperature and short reaction time.

Chapter 7 illustrates the hydrothermal synthesis of a Nickel based MOF in a cost effective and low energy consuming way.

Chapter 8 concludes this thesis by summarizing number of results from the present research work.

Chapter 9 is devoted to the acknowledgements related to the funding for this research work.

I. Introduction

1.1 Basic concept of Metal Organic Frameworks

The bridging of organic ligands with metal nodes forms extended metal-ligands networks which are called Metal organic frameworks (MOFs)[1,2]. MOFs have attracted a huge interest over the last three decades[3]. The MOFs have large surface areas and tunable pore sizes and structures. MOFs consist of metal atoms or metal clusters as nodes, which are linked through organic ligands. These metal–ligand network materials are synthesized from molecular building blocks (Fig. 1.1). The metal ions act nodes and are cations in MOF structure. In order to balance the charge anions are necessary. These anions come from negatively charged bridging ligands such as carboxylates (Fig. 1.2)

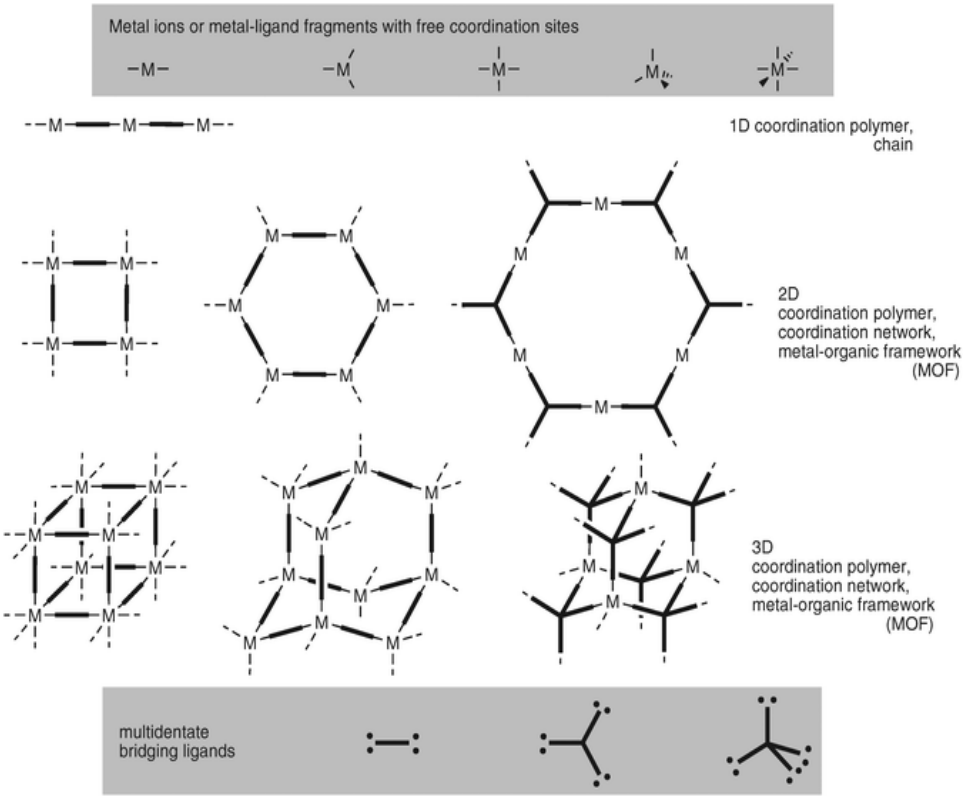

Fig. 1.1 Construction of MOFs from molecular building blocks. [4]

Benzene-multicarboxylate ligands, are frequent choices for metal–organic networks[1][5–11].Benzene-1, 4-dicarboxylate (Fig. 1.2)[12–14] can link with four metal ions[15–18] or it can form long bridges through benzene ring with variety of resulting structures [19,20]. Benzene-1, 3-dicarboxylate[21] is considered as good oxygen donor for building metal–organic networks. Benzene-1, 3, 5-tricarboxylic acid is a rigid, planar molecule and provides three anions as bridging ligands in the synthesis of multidimensional MOFs.

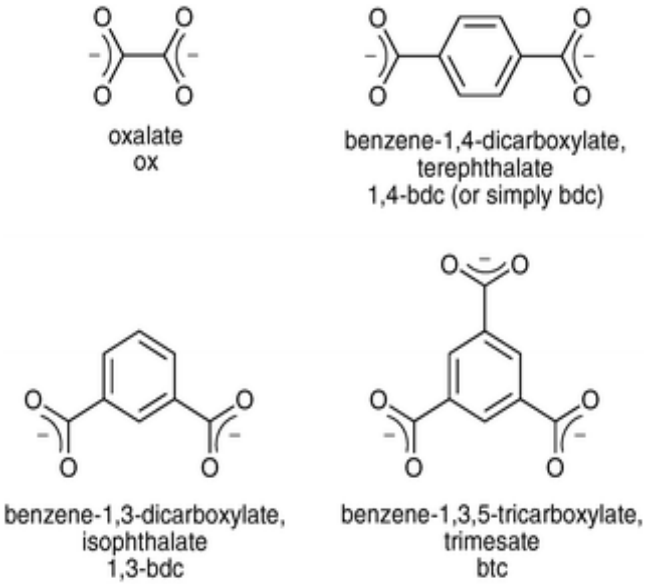

Fig. 1.2 Examples for anionic di- or tricarboxylate bridging ligands for MOFs.[22,23]

Then there are neutral bridging ligands (Fig. 1.3) as well where charge balance is achieved by anions from the original metal salt, for example, Cl^{-1}, NO_3^{-1}, SO_4^{-2}, and BF_4^{-1}. The compounds such as 4, 4-bipyridine, pyrazine, 1, 4-diaza-bicyclo octane, bis (pyridine-4-yl)-1, 2-ethene and 2, 4,6-tris(4-pyridyl)-1, 3, 5-triazine are few example of neutral organic linkers.

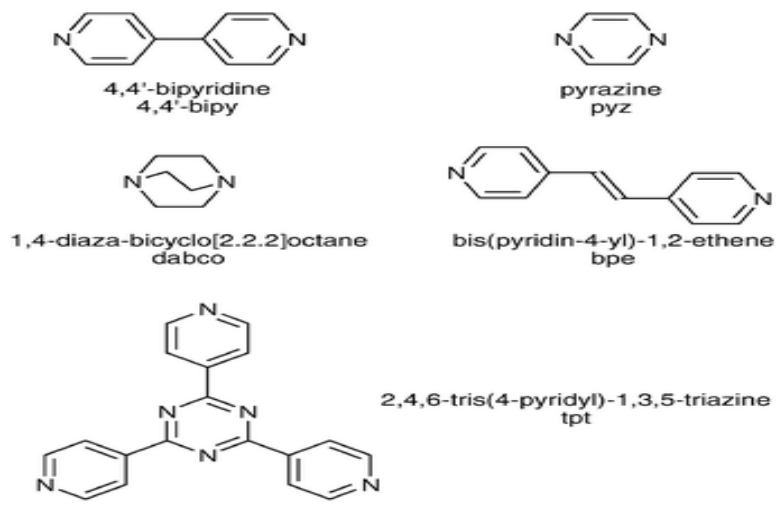

Fig. 1.3 Examples of neutral nitrogen-heterocyclic bridging ligands for MOFs[23–26]

1.2 Categories of MOFs based on linkers

There is a variety of linkers which can be employed for the construction of metal organic frameworks. These are discussed briefly here.

1.2.1 Carboxylate based MOFs

MOFs that make use of organic carboxylate ligands (RCO2 -) are known as carboxylate based MOFs. The Fig. 1.4 [27]shows an example of large pore size iron (III) carboxylic metal organic framework. The strength of these MOFs is moderate which allows the reversibility in the formation of framework and correction [28] in initial structural errors. The bonding mode in carboxylate MOFs is predictable which allows for structure prediction and derivatization [29,30]. Carboxylates can bind in a monodentate and bidentate fashions but most of the important carboxylate systems are found in a bidentate fashion [31,32]. The known metal-carboxylate clusters are termed as secondary building units (SBUs) [33]. With mixing of an SBU with a ligand

of a given geometry (linear, trigonal, etc.), a certain number of possible structures could be formed, which can lead to a greater degree of predetermined design. Furthermore, isoreticular MOF families [34,35] are obtained by altering the size of linker, while maintaining the geometry. The size, polarity and functionality of the pore is adjusted accordingly. The isoreticular carboxylate MOFs have large pore volumes and some have Brunauer-Emmett-Teller (BET) surface areas in excess of 7,000 m^2/g. These MOFs thus have been studied extensively for gas storage applications [36][37]. Transition metal-carboxylates have bond strengths on the order of 180 kJ/mol per M-O-C bond [35]

Carboxylate-based MOFs have remarkably high surface area and uniform pore size distribution. The drawback for carboxylate MOFs is their lack of stability in air and water [38,39] which poses a significant problem if they are to be used in industrial or commercial applications. Divalent metal carboxylates undergo hydrolysis quite easily and are soluble in acid solution. The MOFs based on pyrazolate ligands are much more robust.

1.2.2 Phosphonate based MOFs

The phosphonate based MOF structures are less common as compared to the carboxylate ones. This is because of certain factors;

1. The ease of making simple phosphonate structures in the form of dense layered materials.
2. Phosphonate phases are insoluble and precipitate in less a ordered way due to which growth of single crystal is difficult.
3. The phosphonate has complex coordination chemistry because of varying stages in deprotonation

Regardless of all these factors, it is interesting to use phosphonate ligands for preparing attractive compounds with different structures and properties. In general, mild synthetic conditions are required for organo phosphonic acids to form the metal phosphonates. The resulting structures of metal phosphonates are determined by many synthesis variables such as the phosphonate source, the metal source, the metal/P ratio, the solvent, the concentration, the pH, and the reaction temperature. Phosphonates form stronger bonds than carboxylates do with metal atoms. Monovalent metal phosphonates are highly soluble. The solubility decreases as the valence of metal increases. Divalent metal phosphonates has enough solubility such that their single crystals can be obtained. In case of trivalent and tetravalent metal phosphonates, these are difficult to crystalline because of their high insolubility. The trivalent and tetravalent metal phosphonates precipitate as poorly ordered layered materials.

The porous phosphonates are referred as unconventional MOFs, or UMOFs. UMOFs are poorly crystalline but show great thermal stability and are insoluble in highly acidic media. These materials are used ion exchange materials, proton conductors, catalysts, and sorbents. The well-known phosphonate framework structures are formed and reported with a variety of lanthanide elements, p-block elements and transition metals[40–46]. A microporous phosphonate $[Cu_3(H_3L)(OH)(H_2O)_3]\cdot H_2O\cdot MeOH$ (H_8L = 1,3,5,7-tetrakis(4-phosphonatophenyl)adamantine) [40] has been reported by Shimizu and co-workers. This structure has an interpenetrated diamondoid related topology with both the $[Cu_3(\mu\text{-}OH)]$ trimer unit and the phosphonate ligands acting as the tetrahedral nodes (Fig. 1.5). The other two similar kind of phosphonates are $[Al_2(O_3PC_4H_8PO_3)(H_2O)_2F_2]\cdot 2H_2O$ and $[Al_2(O_3PC_3H_6PO_3)(H_2O)_2F_2]\cdot H_2O$ with three-dimensional structures [47,48]

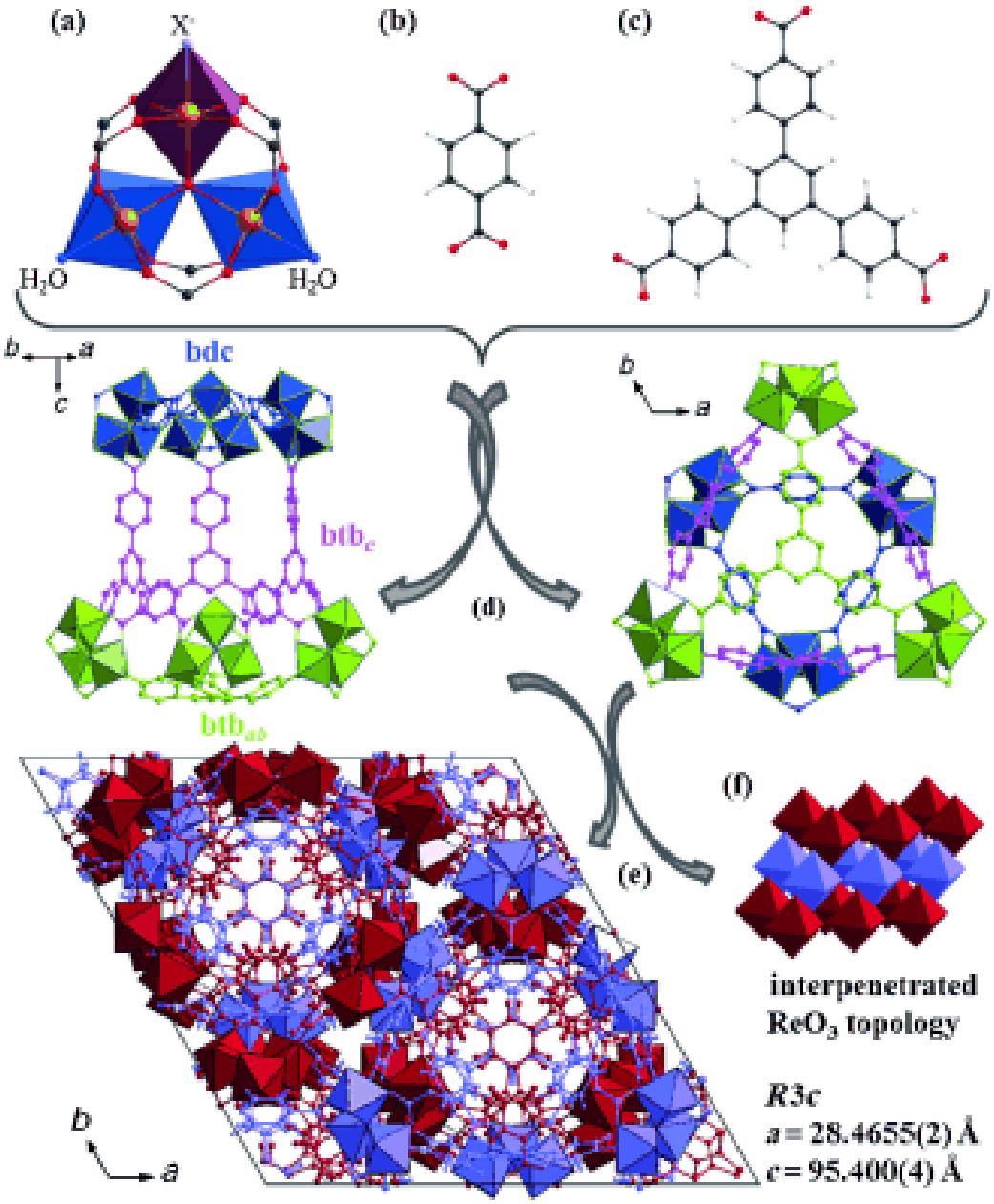

Fig. 1.4 a) Oxo-centered trimer of FeO_6 octahedra in MIL-142A (Fe atoms: orange, O atoms: red, water molecules: blue, counteranion: purple); b) terephthalate (bdc); c) 1,3,5-benzenetrisbenzoate (btb); d) views of the hybrid superoctahedra along the *b* (left) and *c* axis (right); e) view of the structure of MIL-142 along the *c* axis; f) schematic representation of the interpenetrated ReO_3 topology.

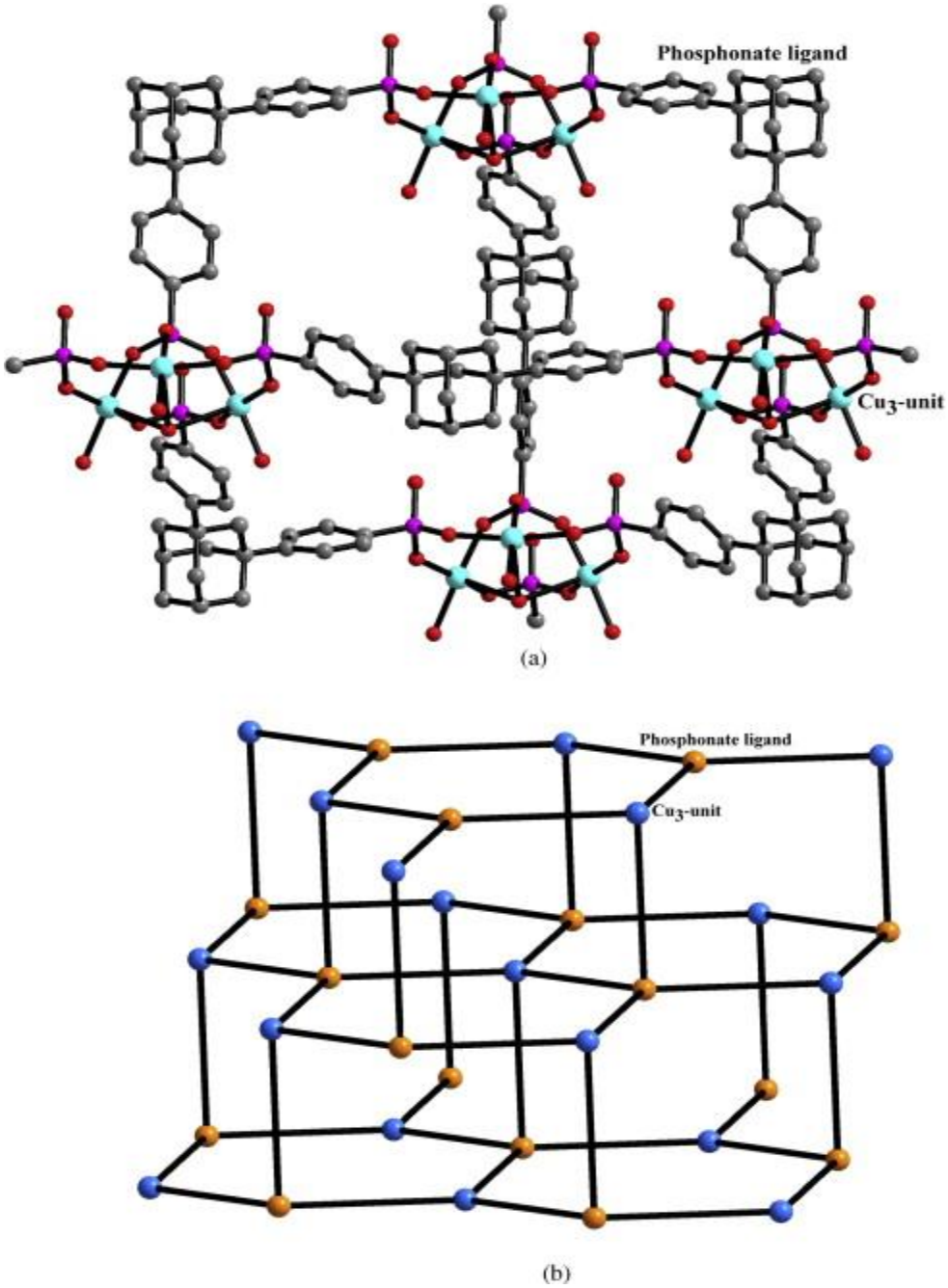

Fig. 1.5 (a) The connectivity between the [Cu_3(μ-OH)] trimer units and 1,3,5,7-tetrakis (4-phosphonatophenyl) adamantine in the MOF, [$Cu_3(H_3L)(OH)(H_2O)_3]\cdot H_2O\cdot$MeOH ($H_8L$ = 1,3,5,7-tetrakis(4-phosphonatophenyl)adamantane) (b) The connectivity between the [Cu_3(μ-OH)] trimer unit (light blue sphere) and 1,3,5,7-tetrakis (4-phosphonatophenyl)adamantane (orange sphere) forming the diamond structure.

1.2.3 Sulphonate based MOFs

With most of the sulphonate frameworks prepared so far has lower dimensionality [48]. There is not a lot much research has been done for investigation of sulphonated MOFs. The sulphonated MOFs are also difficult to synthesize because of lack of reactivity of the organo sulphonic acid. The sulphonate anions produce less coordinated products because of their low reactivity. The structures are not robust and do not have permanent porosity. The lower reactivity along with the tendency of ligand to appear in spherical geometry in sulphonates makes it difficult to predict the possible coordination bonding mode. The sulphonates structures of barium, copper and lanthanides have been reported been reported [49–55]. Among the sulphonates structures that have been synthesized, two dimensional layered structures of silver are considered the most important [56].

1.2.4 Zeolitic Imidazolate frameworks

The aluminosilicate zeolite are the most popular framework with which the current class of metal organic frameworks are associated. Earlier, the formation of aluminum phosphate structures during the 80s acted as a pioneer landmark such that virtually all the metals are now part of this family of frameworks structures. There is a continuous effort to develop newer metal organic frameworks that can resemble the topological features of the aluminosilicate zeolites. In such direction, structures based on 4-connected networks are important. In 4-connected imidazolate frameworks, divalent metal ions (Zn^{+2}, Co^{+2}) replace the Si and imidazolate (Im^{-}) substitute for O^{-2} of zeolite.

The imidazolate structures of Fe^{+2}, Co^{+2}, Cu^{+2} and Zn^{+2} are dense and have low symmetry. The synthesis of porous and symmetrical Zn-imidazolate structure was one of the earliest effort for the formation of open structure [57]. Zinc-imidazolates are analogous to zeolite such as sodalite (SOD), analcime (ANA), and rho (RHO) (Fig. 1.6). Yaghi and co-workers [58–61] have put good effort to emphasize many different imidazolate frameworks of diverse topologies.

Feng and co-workers synthesized zinc-imidazolate structures by using mixtures of imidazole and its derivatives along with solvent mixtures [62] and [63]. ZIF are very robust and the presence of reactive sites makes them interesting candidate for catalytic properties.

1.2.5 Porphyrin based MOFs

Porphyrins have important properties regarding their use in photochemistry, catalysis etc. it has rigid building unit which promotes various possibilities for functionalization. The porphyrins as building unit has resulted in interesting structures such as sheets, chains and molecular tapes [64]. The porphyrins can accommodate different metal ions at the center of rings, this ability of porphyrins based compounds is attractive for device purposes.

The porphyrins have good thermal and chemical stability under hydrothermal conditions. The meso-tetra (4-pyridyl) porphyrin and meso-tetra (4-carboxylphenyl) porphyrin ligands produce three dimensional structures in which porphyrin molecules are connected with individual metal centers in to extended structures. This way homometallic as well as heterometallic organic compounds can be formed [65,66] and [67]. The Fig. 1.7 shows an example of a porphyrin based compound where carboxylate group and bipyridine units are involved in formation of compound. The paddle wheel building units $Co_2(COO)_4$, cis-ZnDCPP, and 4,4′-bipyridine are connected to

produce two dimensional layers. Sapphyrins are other systems which have higher available electrons. Sapphyrins can extend this family of compounds further [68].

1.2.6 Carborane based MOFs

Carboranes based MOFs possess quite a bit rigidity, thermal and chemical stability. An example of carborane based MOF $[Zn_3(OH)(p\text{-}CDC)_{2.5}(DEF)_4]$ (p-CDC^{-2} = depronated form of 1, 12 - dihydroxy dicarbonyl - 1, 12 – dicarba – closo – dodecarborane; DEF = diethylformamide) [69,70] is shown in Fig. 1.8.

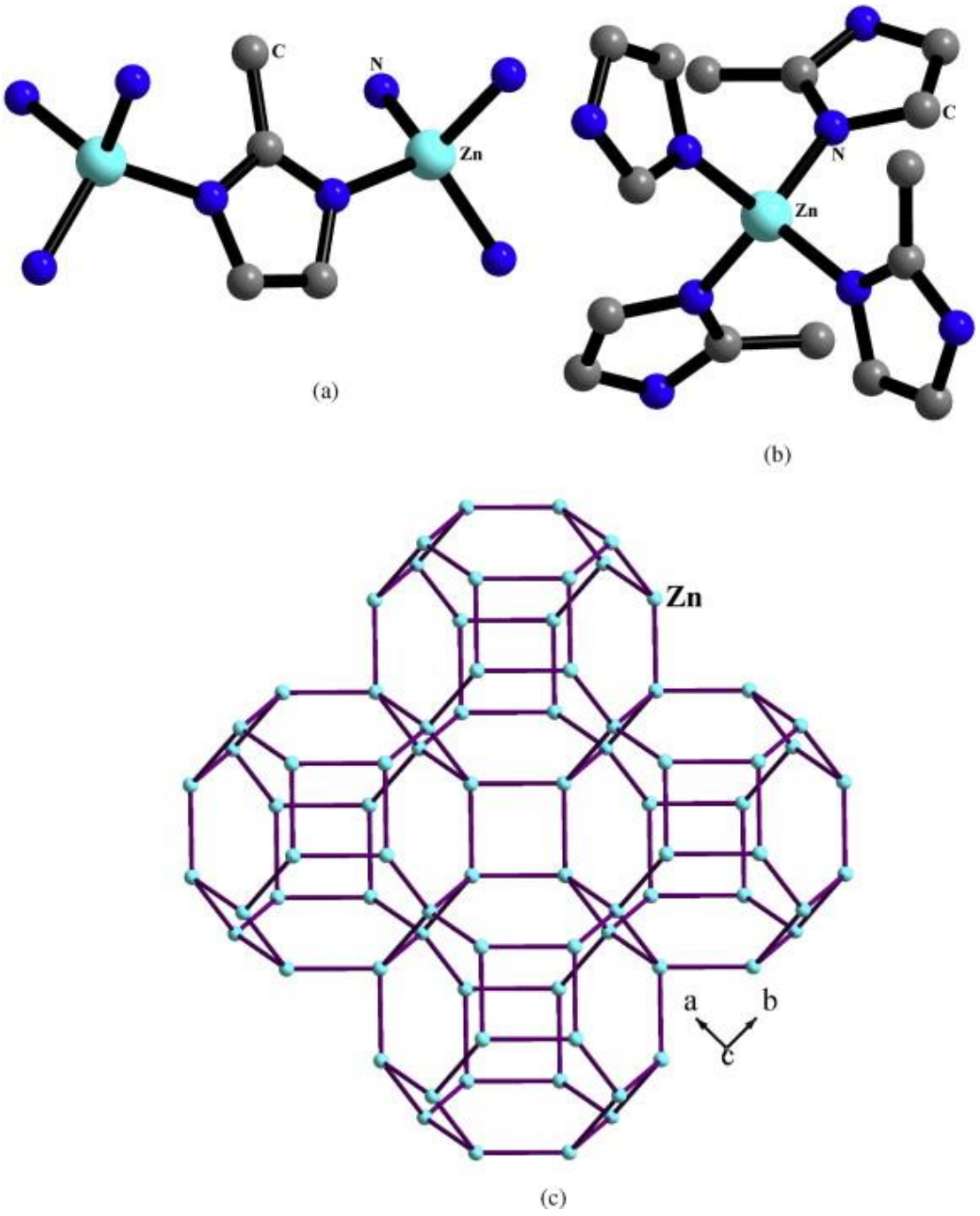

Fig. 1.6 (a) The connectivity between 2-methylimidazolate and Zn^{+2} ions in $[Zn(mim)_2]$ (mim = 2-methylimidazolate), (ZIF-8). (b) The connectivity of the Zn^{+2} ions. Four 2-methylimidazolate units connect with one Zn^{+2} ion. (c) The connectivity between Zn^{+2} ions through 2-methylimidazolate units forming the sodalite network.

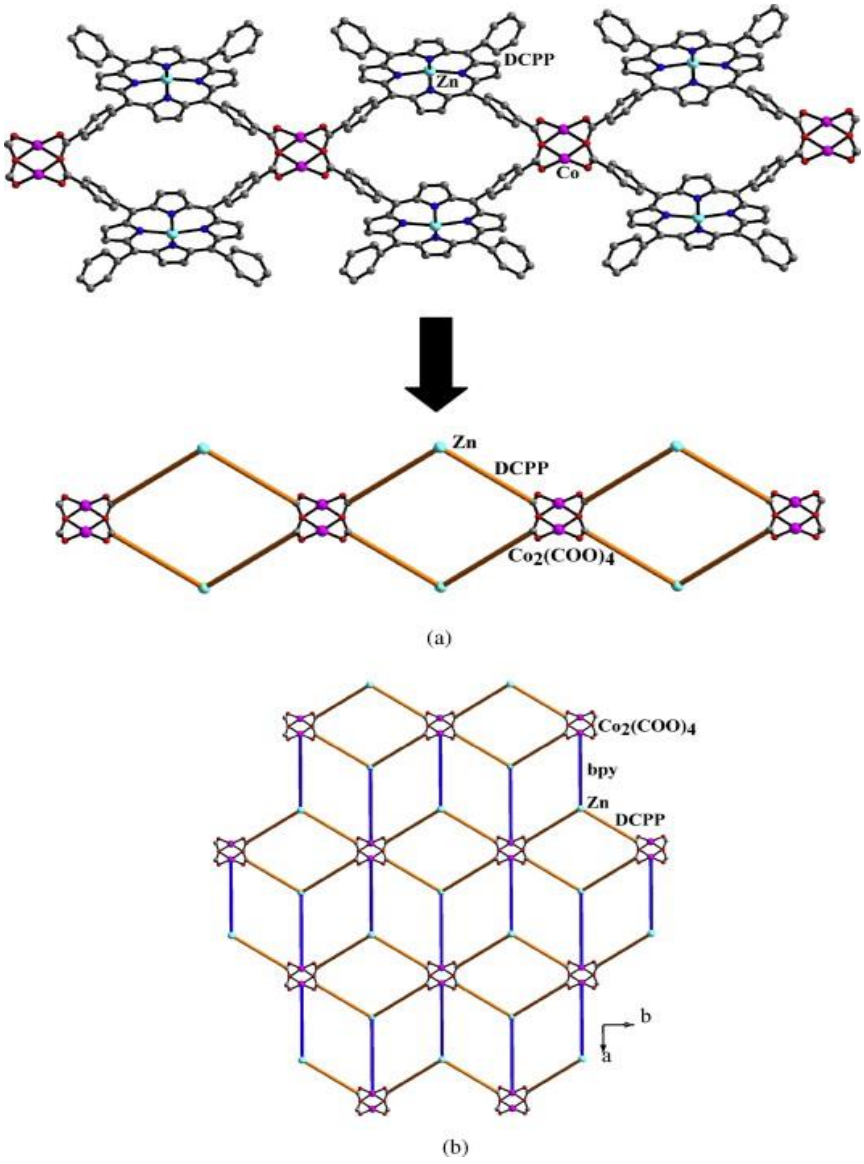

Fig. 1.7 (a) The connectivity between the cobalt paddle–wheel units and the cis-ZnDCPP forming one-dimensional motif in [Co(cis-ZnDCPP)(bpy)]·4DMF·H_2O (cis-ZnDCPP = zinc 5,10-di(4-carboxyphenyl)-15,20-diphenylporphyrin; bpy = 4,4′-bipyridine; DMF = dimethyl formamide). (b) The connectivity between the paddle–wheel building units, $Co_2(COO)_4$, cis-ZnDCPP, and the 4,4′-bipyridine forming the two-dimensional layers. The layers have close resemblance to the $CdCl_2$ layers.

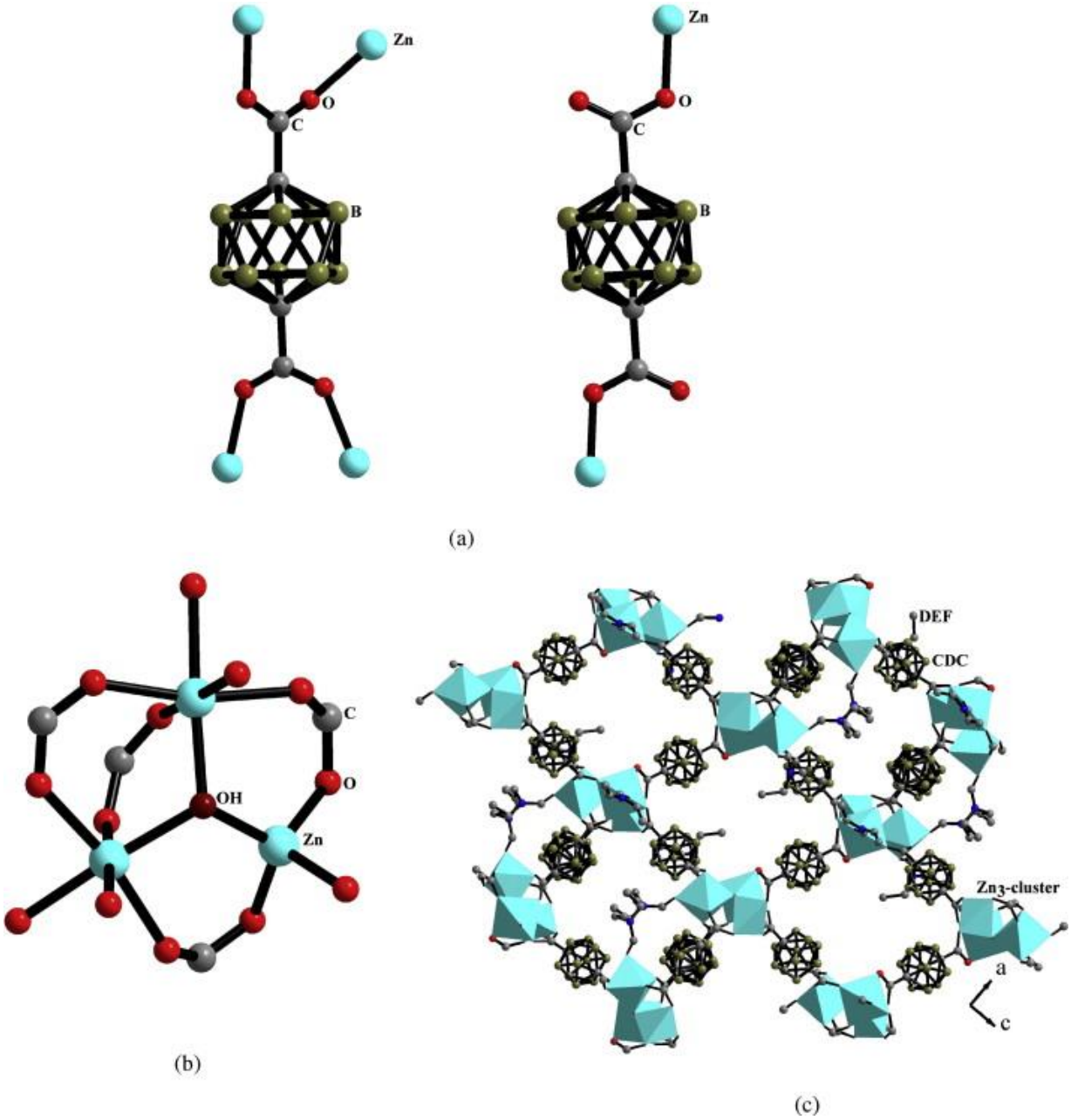

Fig. 1.8 (a) The connectivity of *p*-CDC^{2-} with the Zn^{+2} ions in $[Zn_3(OH)(p\text{-}CDC)_{2.5}(DEF)_4]$ (*p*-CDC^{2-} = deprotonated form of 1,12-dihydroxydicarbonyl-1,12-dicarba-closo-dodecaborane; DEF = diethylformamide) (b) Structure of Zn_3 cluster formed by the connectivity of μ_3-OH and Zn^{+2} ions. (c) The connectivity between the Zn_3 cluster and the *p*-CDC^{2-} units forming the three-dimensional structure.

1.3 Synthesis of MOFs

MOFs are synthesized by various approaches as shown in Fig. 1.9. In most synthesis methodologies, the reactions are liquid phase based where metal salts are mixed with organic linker in the presence of solvents. The selection of solvent is based upon factors such as reactivity, solubility, redox potential and stability constant. Solvent is also important in determining the thermodynamics and activation energy for reaction. The description of various MOFs synthesis approaches are given as:

1.3.1 The slow evaporation method

The slow evaporation method is a room temperature process in which low boiling solvents are evaporated. By evaporation of solvents the solution of starting materials is made concentrated. This method does not require any external energy source. This method is good for growing simple molecular or ionic crystals by tuning the rate of nucleation and crystal growth. For crystal growth, reactant concentration has to be adjusted such that the critical nucleation concentration is surpassed. This is done by change of temperature or by solvent evaporation. The solvent evaporation creates a concentration gradient which initiate the formation of MOF. Though sometimes it is preferred but real disadvantage of such process is that it requires more time compared with other well-known conventional methods. In cases when a mixture of solvents is involved, it can increase the solubility of the reagents and can make the process faster by quicker evaporation of low-boiling solvents [71–74].

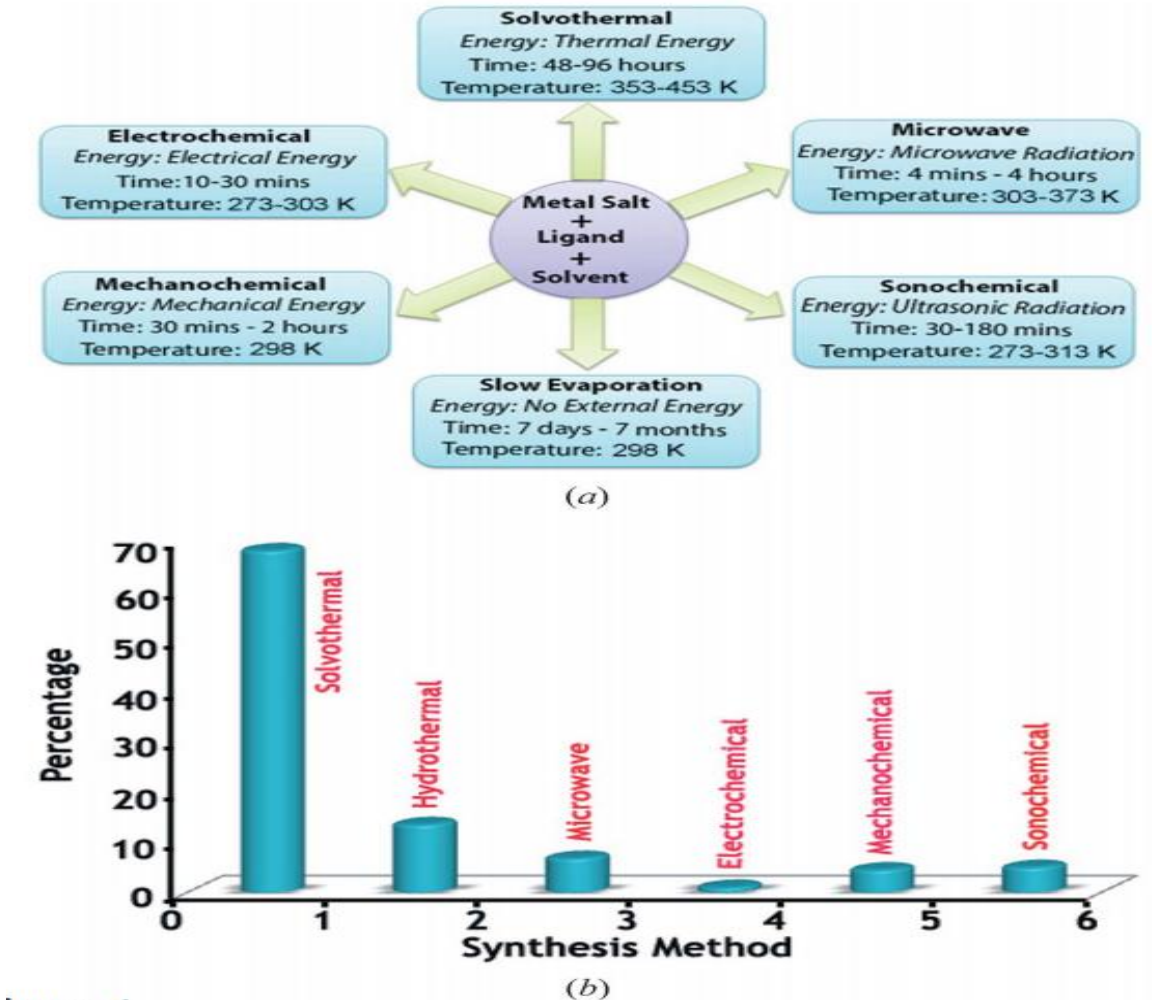

Fig. 1.9 (a) Synthesis conditions commonly used for MOF preparation;
(b) Indicative summary of the percentage of MOFs synthesized using the various preparation routes.

1.3.2 Solvothermal synthesis

Solvothermal reactions are operated under autogenous pressure above the boiling point of the solvent. The reaction is carried out in a closed vessel under autogenous pressure. The non-solvothermal processes take place below or at the boiling point at ambient pressure[75]. The most commonly used organic solvents are dimethyl formamide, diethyl formamide, acetonitrile, acetone, ethanol, methanol *etc*. In order to avoid problems of differing solubility

for the different starting materials, mixtures of solvents have also been used. The temperatures of solvothermal reactions vary with respect to the requirements of particular reaction. In general, MOFs synthesis takes place at temperatures ranging from room temperature to about 250°C. The heat energy can be provided through conventional electric heating such as oven via convection. For low temperature operations glass vial are used but for high temperature reactions, Teflon liners are employed [76]. The hydrothermal method has been used successfully for the synthesis of an enormous number of inorganic compounds and inorganic organic hybrid materials.

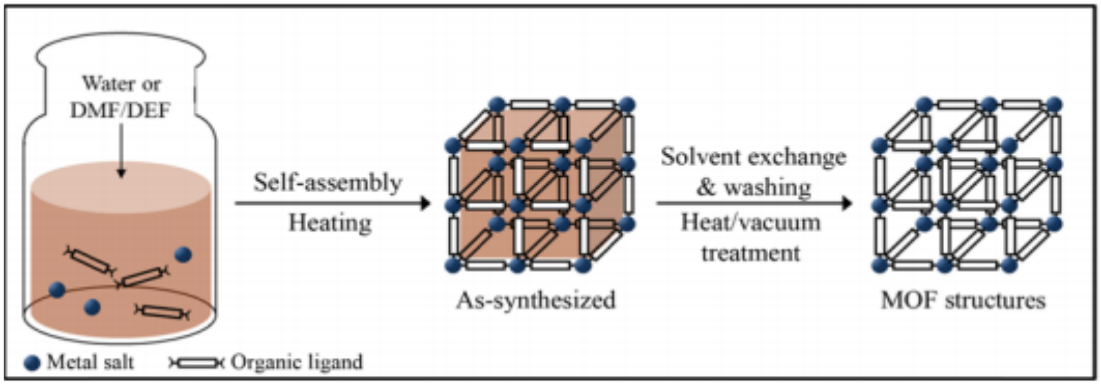

Fig. 1.10 Conventional solvothermal synthesis of MOF structures.

1.3.3 Microwave assisted synthesis

Microwave-assisted synthesis involves heating a solution with microwaves for a period of few minutes to an hour for producing nano sized crystals. In microwave assisted process the interaction of electromagnetic waves with mobile electric charges take place. In case of solids, an electrictical resistance with in the solid produce heating. In case of solution, polar molecules align and oscillate in the presence of electromagnetic field. Through the application of appropriate frequency, collisions between the molecules take place which lead to an increase in system

temperature. In this process, high heating rates and homogeneous heating of reactants system is achieved. Microwave ovens for materials synthesis has the provision for temperature and pressure monitoring and this way precise control of reaction conditions is possible. The main aims in microwave assisted process are:

1. The acceleration of crystallization.
2. Nano-scale product formation.
3. Improved product purity.
4. Selectively synthesizing polymorphs.

It is considered as a rapid method for synthesis of MOFs and has been used extensively to produce nano sized metal oxides[77]. The quality of the crystals obtained by microwave-assisted processes are generally the same as those produced by the regular solvothermal processes, but the synthesis is much quicker[78].

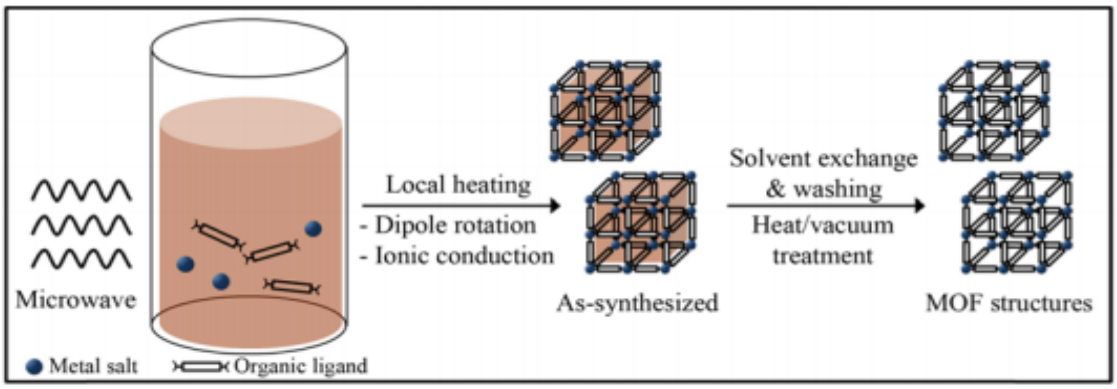

Fig. 1.11 Microwave-assisted solvothermal synthesis of MOF structures.

1.3.4 Electrochemical synthesis

The electrochemical synthesis of MOFs uses a conducting reaction medium which contains a conducting salt and dissolved linker molecules whereas metallic ions are supplied through anodic deposition. The electrochemical route is also possible to run a continuous process to obtain a higher solids content compared to normal batch reactions[79]. This process was initially reported in 2005 at BASF [80]. The purpose of its use was to exclude nitrates, perchlorates and chlorides during the synthesis which can cause problems for large scale production processes.

In this process metal ions are continuously introduced anodic dissolution in the reaction media. The reaction medium contains linker molecules and a conducting salt. Cathode metal deposition is protected by using protic solvent or compounds such as acrylonitrile, acrylic and maleic easter.

The pioneering work for the production of MOFs from electrochemical process was established from BASF [80]. Different combinations of anode materials (Zn, Cu, Mg, Co) and organic linkers [1,3,5-H_3BTC, 1,2,3-H_3BTC, H_2BDC and H_2BDC-OH] were used in the synthesis of MOFs. Electrochemical MOF synthesis has several advantages:

1. Faster synthesis at lower temperatures than conventional synthesis.
2. Recycling of solvent solution is trouble free because of absence of any kind of anions.

3. Virtual total utilization of the linker can be achieved.

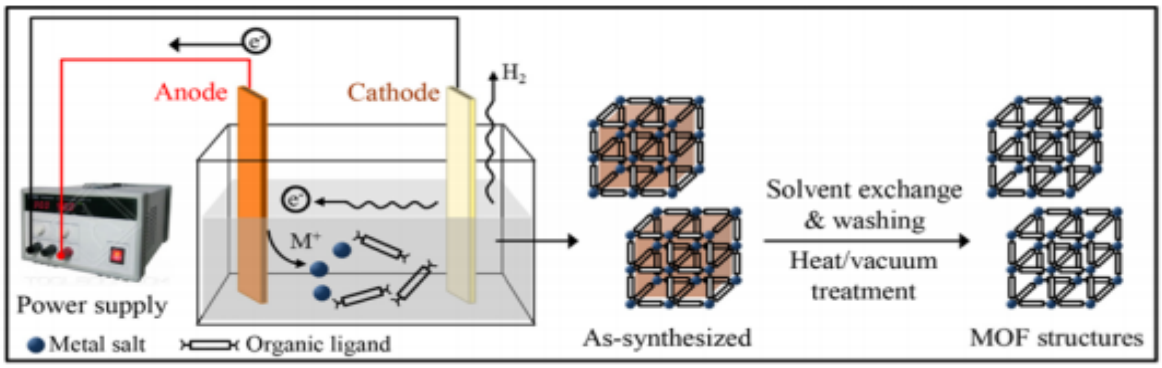

Fig. 1.12 Electrochemical synthesis of MOF structures

1.3.5 Mechanochemical synthesis

Mechanical force can induce different physical phenomena and chemical reactions. In mechanochemical synthesis, Mechanical breakage of intramolecular bonds initiate chemical transformation which results in formation of MOFs. Mechanochemical process has a history in synthetic chemistry[81]. It has been employed to perform pharmaceutically active cocrystals, organic synthesis, inorganic solid-state chemistry and polymers [82–84]. Mechanochemical reactions can occur at room temperature under solvent-free conditions, which is especially advantageous when organic solvents can be avoided[83]. In short reaction times of 10-60 minutes, Quantitative yields of small MOF particles can be obtained. In certain cases, metal oxides are preferred as a starting material, which results in water as the only side product[79]. The interesting advantages of using mechanochemical MOF synthesis are:

1. Reaction can be done at room temperature under solvent free conditions, especially when organic solvents can be avoided[83].
2. High yield is attainable within a short reaction time of 10-60 minutes.

3. Product particles are smaller in size.
4. For starting materials, metal salts can be replaced by metal oxides which reduces the production of unwanted by-products.

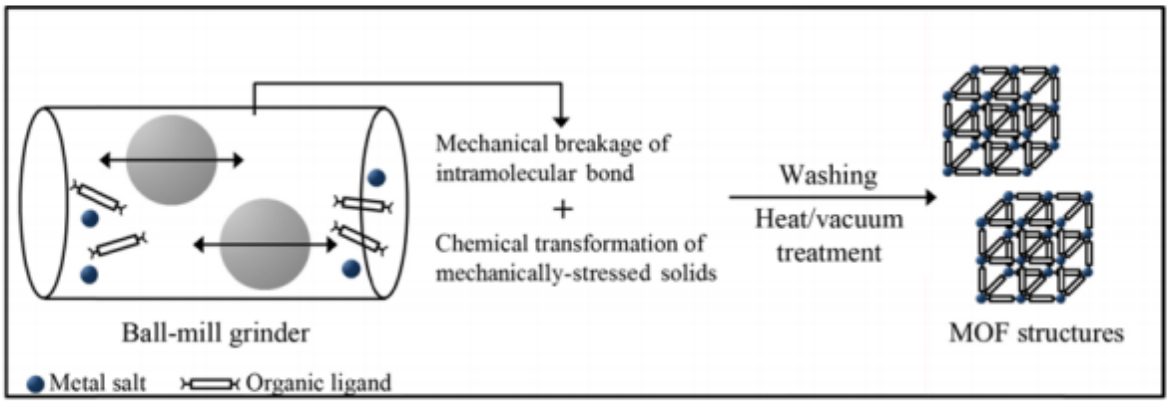

Fig. 1.13 Mechanochemical synthesis of MOFs

1.3.6 Sonochemical synthesis

In ultrasonic synthesis, high intensity ultrasonic radiations (20 kHz-10MHz) are applied through which molecules undergo chemical change. Ultrasound induces chemical or physical changes due to a cavitation process involving the formation, growth and instantaneous collapse of bubbles in a liquid, which creates local hot spots of a short lifetime with high temperature and pressure. The extreme conditions promote chemical reactions by immediate formation of crystallization nuclei. Due this rapid nucleation centers formation, crystallization time is considerably reduced as compared with conventional hydrothermal methods

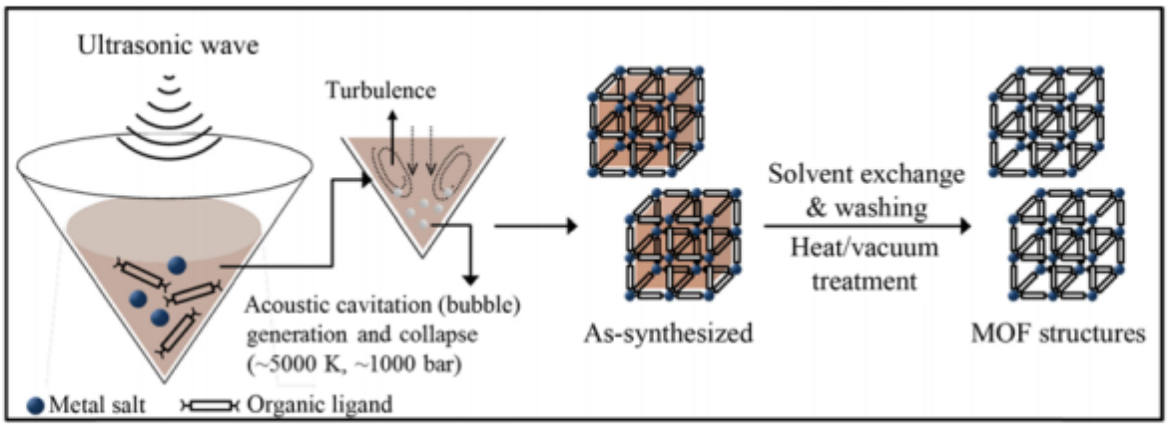

Fig. 1.14 Ultrasonic synthesis of MOFs

In general, the wavelength is much larger than the molecular dimensions. Therefore direct interaction of ultrasonic wave with molecules cannot create the chemical reaction. However when high energy ultrasound interacts with liquids, cyclic alternating areas of low pressures and high pressures are created within the liquid. Within the low pressure region, the pressure drops below the vapor pressure of reactant which produce small bubbles. These small bubbles then grow in size as the ultrasound energy is accumulated. Once the bubble size reaches to a critical maxima, it becomes unstable and collapses. This bubble collapse is called as cavitation and it rapidly releases an energy with a heating and cooling rates of $> 10^{10}$ K/Sec, temperatures of ~ 5000K and pressures of ~ 1000 bar. These hot spots create such extreme conditions not only within the bubble but also in nearby vicinity (~200nm).

In actual, only a fraction of input energy is transformed in to cavitation. The creation of cavities and their collapsing intensity is dependent over large number of parameters. The cavitation process and resulting extreme pressure and temperature conditions are governed by acoustic frequency, acoustic intensity, choice of liquid (vapor pressure, viscosity, and chemical reactivity), and temperature and gas atmosphere.

The sonochemical synthesis has been widely used for organic synthesis [85] and nanomaterials synthesis [86]. The employment of sonochemical technique for MOF synthesis has the following prime objectives.

1. To operate a room temperature synthesis method which is fast, energy efficient and environmentally friendly.
2. This is advantageous in the way that fast reaction will allow scale up production of MOFs.
3. To achieve the product of MOFs in the form of nanocrystalline particles which is quite an advantage for their further applications.

1.4 Post Synthesis modification of MOFs

The post synthetic modification is an area in which the functionalization of available space in metal organic framework is made. Although the development of new structures is a prime concern but still it is imperative to utilize the already known structures for useful properties. The MOF with the presence of many carbon centers for functionalization/modifications provide excellent opportunities to explore unique chemical properties [87].

The first known post synthetic modification is the one in which excess CH_3I in DMF at room temperature has connected the free pyridyl groups in to N-methyl pyridinium ions. The MOF, (IRMOF-3), has been modified by acetylating the amino group of 2-amino benzene-dicarboxylate through acetic anhydrite [88]. Salicyladehyde have been used to functionalize the free amino group in IRMOF-3 [89]. A combination of crotonic anhydride and acetic anhydride along with crotonic anhydride and Br_2 has been used to introduce tandem modifications in IRMOF-3 [90]. Similarly, a doubly-interpenetrating MOF structure was prepared by 4,4'-biphenyldicarboxylate

with an aldehyde group at the 2-position. This MOF was then reacted with 2,4-dinitrophenyl hydrazine to produce the hydrazine [91]. In some cases post synthesis modifications results in formation of new structures; such as a reaction between $NaBH_4$ and $[Zn(C_4H_3N_2O)]$ (ZIF-90) results in formation of alcohol functionalized pores [92] (Fig. 1.15).

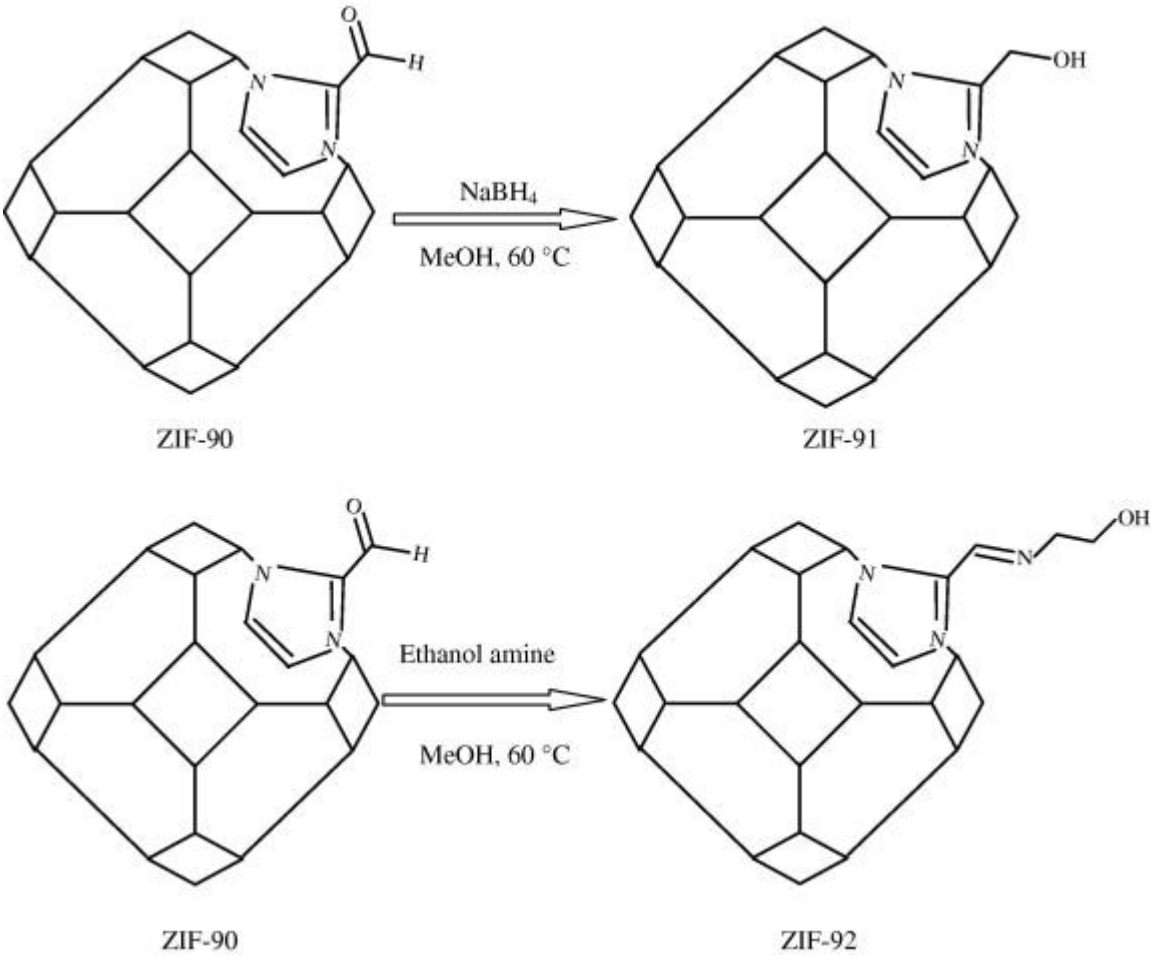

Fig. 1.15 Schematic of the post-synthetic modification reaction for the ZIF-90

1.5 Applications of MOFs

MOFs have been employed for a large number of industrial applications owing to their unique structures and high surface areas. Few of those applications are briefly described here.

1.5.1 Gas storage in MOFs

Gases are important for energy production. Gas storage needs storage tanks and special requirements such has employment of high pressure and multi stage compressors. Such methods are highly expensive for practical uses and there is a need for them to be substituted by simple and cheaper solutions. MOFs due to easy synthetic procedures, high surface area, wide opportunities for functionalization and tunable pore structures have shown outstanding performance for such applications. Few of such applications are described here.

1.5.1.1 Hydrogen storage in MOFs

Hydrogen (H_2) is considered as a possible ideal source of energy due to its large gravimetric heat of combustion (120 MJ kg^{-1}). However, due to its low density in the gaseous state (0.08 kg m^{-3}), its storage at ambient temperature and pressure is difficult. Low volumetric storage density of H_2 hinders its use as a fuel and therefore effective storage materials need to be explored. MOFs due to their high surface areas, light weight, open metal centers and specific week interactions have appropriate characteristics to be utilized for H_2 storage. More than 300 MOFs have been tested so far for their H_2 uptake capacity. Few prominent examples are MOF-177 (BET surface area ($\sim$ 5000 m^2 g^{-1}) and large pore volume (1.59 cm^3 g^{-1})), MOF-5 (BET surface area of 3800 m^2 g^{-1}), MOF-210, MIL-101, HKUST-1, NU-100, PCN-12, NOTT-102 and MOF-205 [93–95]. MOFs with open metal sites provide high surface area which facilitates stronger interaction between the metal ion nodes and H_2 molecules. This is the principal reason behind the high H_2 uptake in these promising class of materials.

1.5.1.2 CO_2 storage in MOFs

The rising level of atmospheric CO_2 is considered as major threat towards living beings. The emission from coal, oil and natural gas due to rapid industrial development is mostly responsible for the rising CO_2 level in the atmosphere. Zeolites and activated carbon has been used previously for CO_2 adsorption but in recent times MOFs have picked up attention as potential adsorbents. Very high internal surface area with polar functional groups associated with pores provides grounds for high CO_2 uptake capacity in MOFs. MOF-210 is the highest surface area (10450 m^2 g^{-1}) MOF known to date, has the CO_2 uptake value of 2400 mg g^{-1} (74.2 wt.%, 50 bar at 298 K) which exceeds that of any other porous material, such as MOF-177 or MIL-101(Cr) (60 and 56.9 wt.%, respectively)[32,96]. Other well-known MOFs are MOF-200, NU-100 (69.8 wt%, 40 bar at 298 K), Mg-MOF-74 (68.9 wt%, 36 bar at 278 K), MOF-5 (58 wt%, 10 bar at 273 K), and HKUST-1 (19.8 wt%, 1 bar at 298 K) which also show considerably higher CO_2 uptake.

1.5.1.3 CH_4 storage in MOFs

Methane is another potential fuel. The natural gas contains about 95% of methane. The MOFs employed for CH_4 adsorption are MOF-177 (adsorption capacity of 22 wt% at 298 K and 100 bar, HKUST-1 (15.7 wt% at 150 bar), MIL-101 (14.2 wt% at 125 bar), IRMOF-1 [228 cm^3 (STP) g^{-1} at 298 K and ~ 36 bar] and Ni-MOF-74 [190 cm^3 (STP) g^{-1} (298 K, 35 bar)].

1.5.1.4 CO and NO storage in MOFs

CO and NO are considered as hazardous gases and their separation from gaseous mixtures is of a paramount importance. MOFs with pores compatible with the kinetic diameter of these gases could be useful for this purpose. So far, the capture of CO in MOFs has not been achieved experimentally; it is believed that the interaction between the CO dipole and the open metal sites

of MOFs are the dominating factor for the sorption performance. In order to achieve better selectivity, some chemical modification needs to be adopted into these porous materials. On the other hand, for selective capture of NO, MOFs such as Cu-SIP-3, Zn(TCNQ-TCNQ)(bipy) [97] and Ni- and Co-MOF-74 have been successfully used.

1.5.2 MOFs as magnetic materials

Magnetism in solids is of considerable interest due to its widespread applications in electromagnetism, devices and sensing. MMOFs magnetic metal organic frameworks) have been developed through the use of paramagnetic 3*d* transition metal nodes along with suitable organic linkers. The MOFs based on V, Cr, Mn, Fe, Co, Ni and Cu have contributed significantly to developing porous molecular magnets [2,98–102]. The porous nature of MOFs combined with magnetic properties find interesting applications for air separation. Framework structure having layered geometry with shorter distance between metal nodes is also a contributing factor for magnetism in MOFs. Radicals associated with certain organic linkers also have properties to generate magnetism effects. Also metal-radical combined approaches have been used to synthesize a variety of magnetic metal-organic materials [103–105].

1.5.3 MOFs as sensors

The use of MOFs as luminescent materials have their potential application in small-molecule sensors [106,107], pH sensors [108], light concentrators for photovoltaic devices, antennae in photo-sensitive bioinorganic compounds and high-technology optics. MOF materials are advantageous because of their hybrid nature, which includes inorganic metal ions, organic linkers and also guest molecules. Lanthanide metal ions such as Eu, Tb, Dy, Sm, Nd, Gd, Er and Yb are

widely used for the synthesis of luminescent MOFs, due to their electronic transitions from *d* to *f* shells, with accompanying photon emission. The luminescent properties of transition-metal MOFs only come from the linkers. Naphthalene, anthracene, pyrene, perylene and stilbene types of ligands are most commonly used for luminescent MOF synthesis [109–111].

1.5.4 MOFs for drugs delivery

MOFs of MIL series function for drug delivery. These frameworks can absorb anti-tumor and anti-AIDS active agents (busulfan, azidothymidine triphosphate, doxorubicin and cidofovir) and release them again inhuman organs like the liver. The storage capacity depended on the pore size, pore functionalization and the MIL-particle size. For example, 40 mass% of doxorubin could be stored in (aminoterephthalato) iron (III) (MIL-101-NH2) [112].

II. Characterization of Metal Organic Frameworks

The Characterization methods applied during this research work are described in this section. X-ray diffraction (XRD), scanning electron microscopy (SEM), X-ray photoelectron spectroscopy, thermo gravimetric analysis (TGA) and Fourier transform infra-red (FT-IR) spectroscopy were used for the synthesized MOFs.

2.1 X-ray diffraction (XRD)

X-ray diffraction is the best technique for observing crystallinity in MOF. XRD is a very useful tool for identification of crystalline phase(s) and estimation of phase fractions. Ideally, the sample analyzed with XRD should contain a large number of randomly oriented, small crystals. The X-rays are therefore diffracted from different (hkl)-planes simultaneously according to Bragg's law:

$$\lambda = 2d_{hkl} \cdot \sin\theta \qquad (2.1)$$

Where λ is the wavelength, d_{hkl} is the distance between the (hkl)-planes and θ is the diffraction angle between the incoming beam and the (hkl)-planes. The resulting XRD pattern can be regarded as a fingerprint of a crystalline phase. The relative diffraction intensities and positions of peaks are compared with known samples. This comparison gives a fair identification of crystalline phase. In case if patterns are not match able then it indicates that a new phase is achieved. Various features of a XRD pattern reveal different information (Fig. 2.1). Such as (1) Unit cell dimensions can be accurately determined from the position of the diffraction peaks (2) The relative intensities of the diffraction peaks give information about the type of atoms and their

positions in the crystal (3) The degree of crystallinity in a sample can also be estimated from XRD.

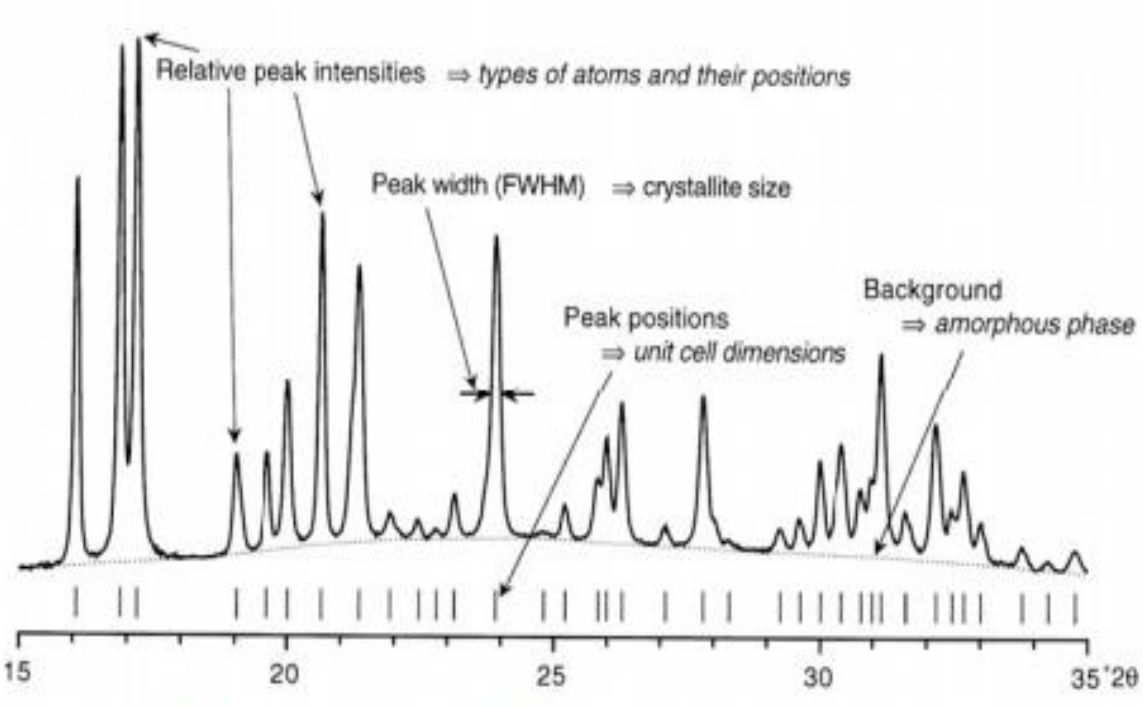

Fig. 2.1 The information from XRD pattern[113]

If the samples crystals are needle like or plate type, it is better that sample should be ground carefully before examination. It will avoid preferred orientation which would otherwise give rise to wrong relative intensities. The peak widths indicates about the size of the crystallites. Small crystallites can cause broadening of the peaks. A high background in an XRD pattern indicate the presence of an amorphous phase. XRD diffraction is also associated with overlap problem. This means that two or more unique reflections are superimposed at the same position (2θ angle). The intensity of overlapped peaks is the sum of all those reflections. The XRD data for MOFs in this thesis work was collected by using Rikagu D/MAX 2200H, Bede model200 X-ray diffractometer. The measurements were performed using a Cu-K_α radiation source of

wavelength λ=1.5406Å and the diffraction intensity were recorded in 2θ range of 2-60˚with a step of 0.02˚.

2.2 Scanning electron microscopy

The scanning electron microscope (SEM) is a tool which is widely used in number of industries and laboratories for investigating the microstructures of metallic and non-metallic materials. In a SEM, an electron beam is generated from an electron gun and directed over a surface to create its image. The electrons in the beam interact with the sample surface. With the interaction of these primary electrons, two types of scattered electrons are generated from the surface

1. The in-elastic collision of primary electrons with the surface produces secondary electrons of low energy from sample surface. Of these secondary electrons, only those who are generated from top (1-2nm) surface of sample can escape whereas the remaining get reabsorbed in the sample itself.

2. Primary electrons that maintain their energy and velocity during change of direction, as in elastic scattering, are called backscattered electrons (BSEs). The BSEs have high energies (≥50 eV) and leave the surface from different depths of the sample. Both SEs and BSEs are used in the imaging but the BSEs can also provide additional information about the elemental content of a sample.

For this work over MOFs, the SEM measurements were performed on JEOL, JEM1200EX II set up equipped with field emission gun.

2.3 Fourier transform infra-red spectroscopy (FT-IR)

Fourier Transform-Infrared Spectroscopy (FTIR) is an analytical technique used to identify organic (and in some cases inorganic) materials. This technique measures the absorption of infrared radiation by the sample material at characteristic wavelength. The infrared absorption bands identify molecular components and structures. When a material is irradiated with infrared radiation, the molecules of materials are excited to higher vibrational state.

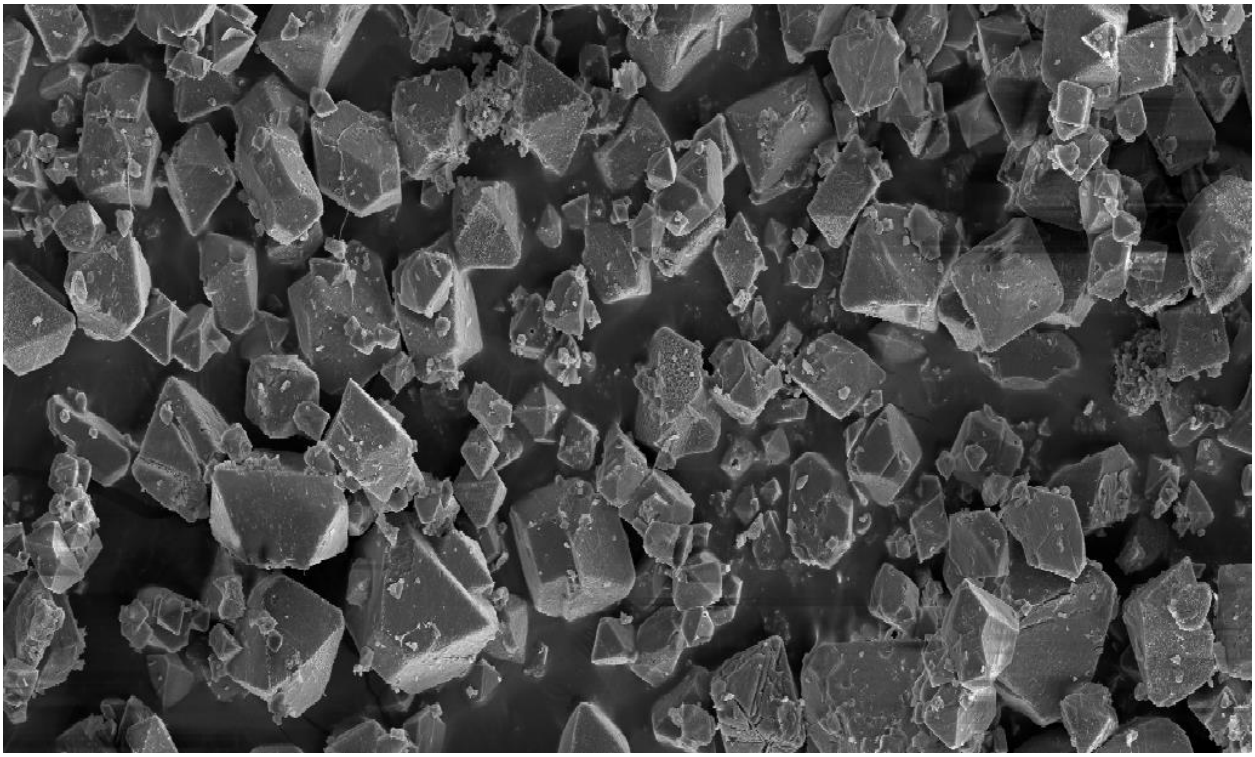

Fig. 2.2 SEM image of ultrasonically synthesised Cu-BTC

The wavelength of light absorbed by a particular molecule is a function of the energy difference between the ground and excited vibrational states. The wavelengths that are absorbed by the sample are characteristic of its molecular structure. Samples may be in liquid, solid or gaseous

form. The FTIR spectrometer uses an interferometer. A detector measures the intensity of transmitted or reflected light as a function of its wavelength. The signals obtained from the detector are analyzed with a computer using Fourier transforms to obtain infrared spectrum. The FTIR spectra are usually presented as plots of intensity versus wavenumber (in cm^{-1}). Wavenumber is the reciprocal of the wavelength. The intensity can be plotted as the percentage of light transmitted or absorbed at each wavenumber. The identification of a material is made by comparing its spectrum with an authenticated spectra of same known material. The identification is obtained by matching the polymers and other constituent in sample. The Absorption bands in the range of 1500-4000 wavenumbers are typically due to functional groups (e.g., -OH, C=O, N-H, CH_3, etc.) [114]. The region from 400-1500 wavenumbers is referred to as the fingerprint region. Absorption bands in this region are generally due to intramolecular phenomena.

FT-IR can also be used for quantification as well. The concentration of a compound can be determined from the area under the curve in characteristic regions of IR spectrum. Concentration calibration is obtained through a standard curve from spectrum of known concentrations.

FT-IR has applications:

1. Identification of foreign materials such as particulates, fibers and residues.
2. Identification of bulk material compounds.
3. Identification of constituents in multilayered materials.
4. Quantification of silicone and ester as contamination on various materials.

.

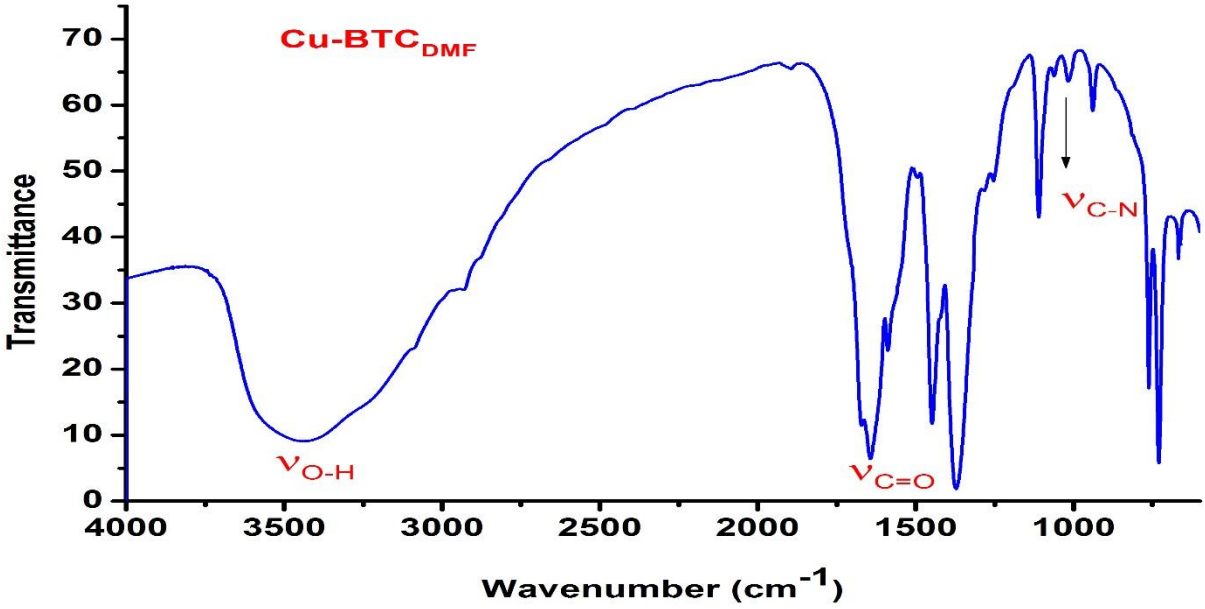

Fig. 2.3 FT-IR graph for ultrasonically synthesized Cu-BTC

For the work in this thesis, FT-IR has been employed for identification of various organic bonding in MOF structures. FT-IR spectra were collected on a BRUKER IFS66/S Fourier transform IR spectrophotometer in KBr disks at room temperature. A typical FT-IR spectra collected during this research work is shown as Fig. 2.3.

2.4 Nitrogen sorption isotherms

In order to measure the extent of permanent porosity in a porous solid such as MOF, gas adsorption technique is used. The gas adsorption technique measures the specific surface area and pore size distribution of powdered or solid materials. For this usually nitrogen, krypton and argon gases are used. The samples are dried, evacuated and cooled to a temperature of 77K, the temperature of liquid nitrogen prior to measurement. At this temperature inert gases such as

nitrogen, argon and krypton will physically adsorb on the surface of the sample. This adsorption process can be considered to be a reversible condensation or layering of molecules on the sample surface during which heat is evolved. Nitrogen gas is ideal for measuring surface area and pore size distribution.

The adsorption measurement is represented as adsorption isotherm. An adsorption isotherm is usually recorded as volume of gas adsorbed (cc/g @ STP) versus relative pressure (i.e., sample pressure / saturation vapor pressure). Using relative pressure to construct the isotherm eliminates changes in pressure from small changes in temperature. A small change in temperature changes the saturation vapor pressure considerably. The use of relative pressure is convenient and is scaled from 0 to 1. A relative pressure of 1 represents a completely saturated sample, i.e., all of the available surface structure is filled with liquid-like gas. The resulting adsorption isotherm from N_2 adsorption is also known as BET (after Brunauer, Emmett and Teller) isotherm. The BET isotherm gives the volume of gas needed to form a monolayer on the surface of the sample.

Single or multiple point BET equation is used to measure specific surface area of sample. The actual surface area can be calculated from knowledge of the size and number of the adsorbed gas molecules. Nitrogen is used most often to measure BET surface, but if the surface area is very low, argon or krypton may be used as both give a more sensitive measurement, because of their lower saturation vapor pressures at liquid nitrogen temperature.

An example of an isotherm of Cu-BTC Is shown in Figure 2.4. Nitrogen adsorption and desorption isotherms were measured at 77 K on a Micrometrics ASAP 2020 system.

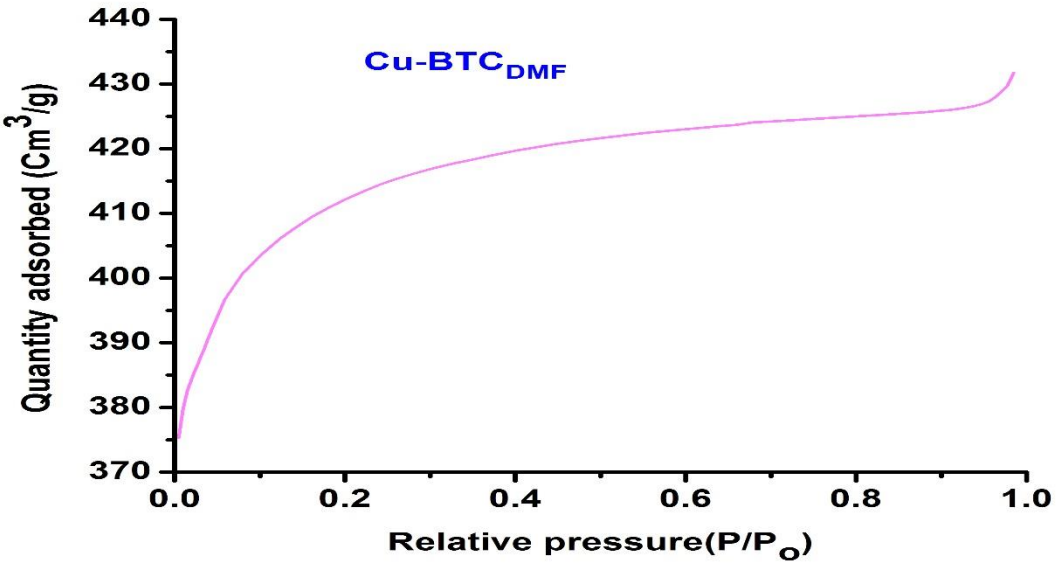

Fig. 2.4 N_2 adsorption isotherm for Cu-BTC

2.5 Thermo gravimetric analysis

The thermal stability and decomposition of MOFs are studied by thermo gravimetric analysis (TGA). The sample weight is measured as the temperature is increased with a continuous heating rate (2−5 °C/min) in an oxidizing (oxygen) or inert (nitrogen or argon) atmosphere. It is important, as always, to calibrate the instrument and to saturate the system with particular chosen atmosphere. The resulting thermogram shows sample remaining weight as a function of temperature in various steps. At first there is a release of uncoordinated water and solvent from the pores/channels of material. This is followed by release of crystal water (coordinated water molecules) and finally the loss of the linkers resulting in decomposition of the MOF. The amount of released crystal water and water/solvent occupying the pores can be calculated from these steps. Information about framework composition obtained from single crystal structure refinement can be of great help during these calculations. The results are compared with those from CHN elemental analysis.

In general, MOFs have relatively low thermal stability. From TGA curves it appears that certain MOFs remain stable up to the temperatures of about 300−400 °C. However, it is more useful if TGA results are validated by in situ XRPD.

The TGA thermograms for this thesis work were obtained from SDT2960 (DTA-TGA) analyzer where MOF samples were heated from room temperature to 600°C at heating rate of 5°C/min under nitrogen atmosphere. An example of thermogram of Ni-BTC is shown here (Fig. 2.5).

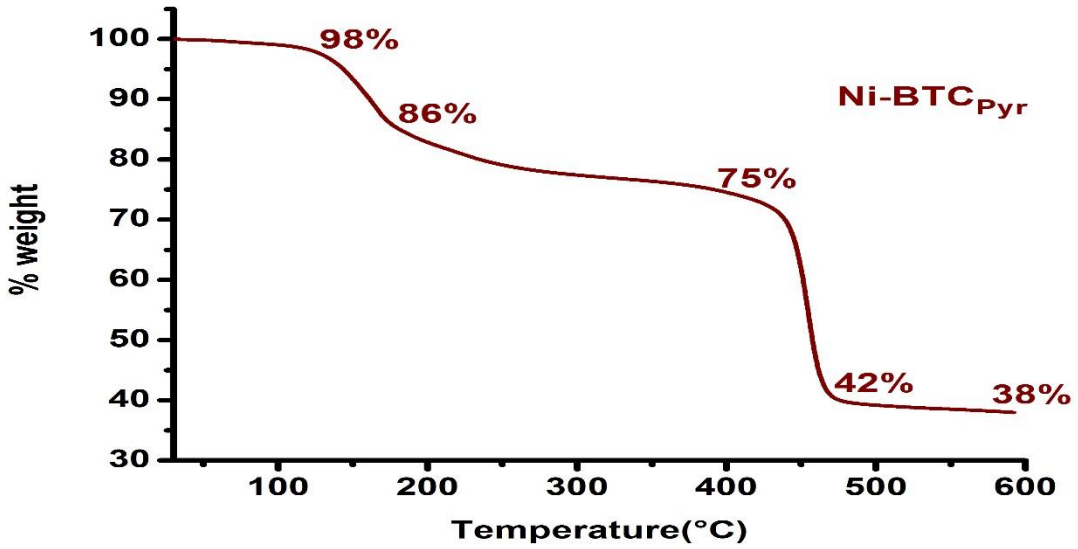

Fig. 2.5 TGA curve for Ni-BTC

2.6 X-ray photoelectron spectroscopy

X-ray photoelectron spectroscopy (XPS) is a surface-sensitive quantitative spectroscopic technique which measures:

1. Elemental composition of the surface (top 0-10nm).
2. Empirical formula of pure materials.
3. The surface contaminations.

4. Chemical and electronic state of surface elements.
5. Uniformity of elemental composition on the top surface.
6. Depth profiling to read the compositional uniformity inside the sample

XPS spectra are obtained by irradiating a material with a beam of X-rays. This irradiation is accompanied with simultaneous measurement of total number of escaping electrons from the top surface along with their individual kinetic energies. XPS requires high vacuum. It can detect all elements from atomic number (Z) of 3 and above [115].

An XPS spectrum is a plot of the number of electrons detected against the binding energy of electrons. Each element produces a characteristic set of XPS peaks at specific binding energy values that directly identify each element that exists in or on the surface of the material. The number of detected electrons in each of the characteristic peaks is directly related to the amount of element within the XPS sampling volume. XPS detects only those electrons that have actually escaped from the sample into the vacuum of the instrument, and reach the detector. In order to escape from the sample into vacuum, a photoelectron must travel through the sample.

For the present thesis work, XPS analysis were done with theta probe AR-XPS system, Thermo Fisher Scientific (UK). XPS measurements were made with mono chromatic Al-K_α X-ray source of 15kv, 150w. An example of XPS data plot for Ni-BTC is shown here (Fig. 2.6).

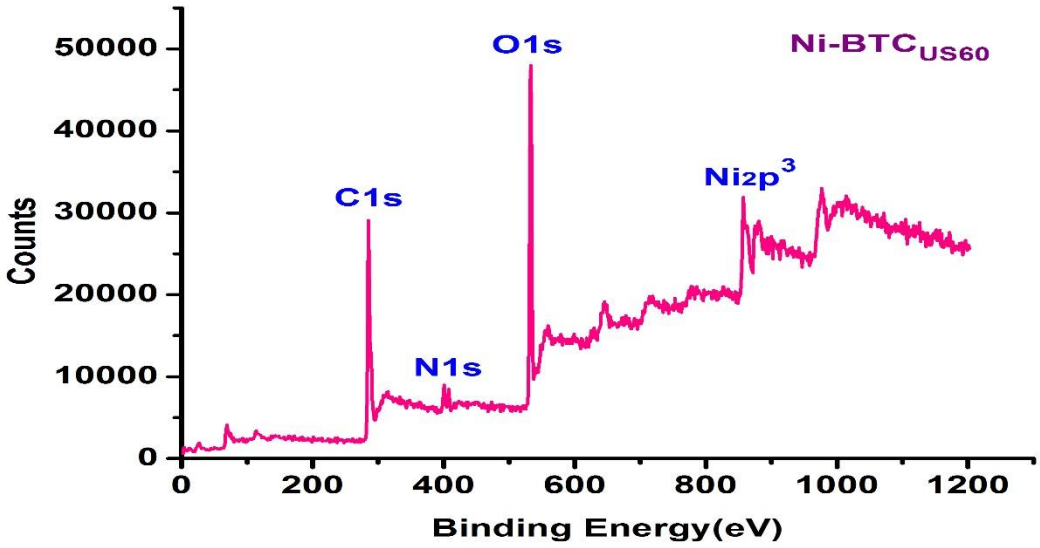

Fig. 2.6 XPS curve for Ni-BTC

III. Synthesis of porous Cu-BTC with ultrasonic treatment: Effects of ultrasonic power and solvent condition

3.1 Introduction

Metal organic frameworks (MOFs) are a new class of porous 3-D structures, which have attained a remarkable attention over the recent few years for certain applications such as gas storage, gas separation, catalyst materials [116–125], gas carrier for nano-sized materials [126] and drug delivery [127,128]. There high surface areas and unique pore structures are key properties for such applications. Cu-BTC (BTC= 1,3,5-benzenetricarboxylic acid), is a well-established MOF for hydrogen gas storage, gas storage and heterogeneous catalysis [129–134].

Cu-BTC resembles a paddle wheel complex built from Cu^{+2} ions and 1, 3, 5-benzenetricarboxylic acid (H_3BTC). It has three dimensional face centered cubic crystal structure with two different pore sizes [135]. Larger pores are in square cross section with 0.9nm diameter whereas smaller pores approximate a tetrahedral slot with 0.5nm diameter. Initially reported [31] Cu-BTC was synthesized by solvothermal process at 180°C.

The drawbacks associated with solvo-thermal process are long reaction time (12 hours or more) and consumption of large amount of solvents used during operation. In contrast to it, novel developments such as ultrasonic irradiation, microwave heating and mechanochemical techniques have also been successfully employed for synthesis of Cu-BTC [83,136–140]. Fast crystallization in porous materials has been induced through microwave heating [141]. Employment of microwave assisted hydrothermal process for synthesis of Cu-BTC reduced the reaction time to few minutes with high phase purity and yield [137], but high reaction temperature and pressure are still needed. Compared with traditional techniques, sonochemical method is more convenient

and easily controlled. The ultrasound methods for synthesis of Cu-BTC reported so far, has employed typical organic solvents (DMF/EtOH/H_2O or EtOH/H_2O) for complete dissolution of reactants prior to sonication. Thus there is an ample scope of investigation for usage of alternative solvents, their performance under various operating conditions and overall effect on product yield.

In this work we report Cu-BTC synthesis by using combinations of organic and inorganic solvents. As for our knowledge, the solvent combinations of DMF/H_2O, NaOH/EtOH/H_2O, NH_4OH/EtOH/H_2O and Pyr/EtOH/H_2O has never been reported so far during ultrasonic synthesis of Cu-BTC. The experiments were conducted with the addition of three bases such as NaOH, NH_4OH and pyridine. It was anticipated that addition of a base will deprotonate the carboxylic acid. The deprotonation is the starting point towards the MOF formation. the anions generated by the deprotonation effects are then capable of attracting the metal ions to complete the reaction. From our experiment with DMF/H_2O, we recorded an appreciably high surface area (1434 m^2/g) MOF product. In previously reported ultrasonic and microwave assisted synthesis, either $Cu(NO_3)_2.3H_2O$ or $Cu(OAc)_2.H_2O$ has been used as metal precursor. We have experimented with $CuCl_2.2H_2O$ instead. The comparison of synthesis with various solvent combinations revealed that product yield and physicochemical properties (morphology, surface area, pore volume and particle size) varied with each solvent.

3.2 Experimental

3.2.1 Materials and methods

All materials including $CuCl_2.2H_2O$ (99.5%, Alfa Aesar), 1,3,5-Benzenetricarboxylic acid (H_3BTC) (99%, Alfa Aesar), N, N-Dimethylformamide (DMF) (99.8%, Alfa Aesar), Ethyl alcohol (94-96%, Alfa Aesar), NaOH (pellets 98%, Alfa Aesar), NH_3 water (Daejung chem.) and

Pyridine (99.5%, Daejung chem.) were used as received. We experimented for four Cu-BTC yields resulting from DMF/H_2O, DMF/EtOH/H_2O, 0.5MNaoH/EtOH/H_2O, 0.5M NH_4OH/EtOH/H_2O and 0.5M pyridine/EtOH/H_2O as solvents. The details of solutions prepared before sonication are described as under:

3.2.1.1 Cu-BTC$_{DMF}$

0.5mmol of H_3BTC and 0.125M solution of $CuCl_2.2H_2O$ were dissolved in 30ml DMF.

3.2.1.2 Cu-BTC$_{DMF+EtOH}$

0.5mmol of H_3BTC and 0.125M solution of $CuCl_2.2H_2O$ were dissolved in a mixed solution of DMF and Ethyl alcohol. DMF and Ethyl alcohol were in a molar ratio of 1:2.

3.2.1.3 Cu-BTC$_{NaOH}$

0.5mmol of H_3BTC and 0.125M solution of $CuCl_2.2H_2O$ were dissolved in a mixed solution of 0.5M NaOH, de-ionized water and Ethyl alcohol in molar ratio of 2:4:11 respectively.

3.2.1.4 Cu-BTC$_{NH4OH}$

0.5mmol of H_3BTC and 0.125M solution of $CuCl_2.2H_2O$ were dissolved in a mixed solution of 0.5M NH_4OH and Ethyl alcohol in molar ratio of 2:3.

3.2.1.5 Cu-BTC$_{Pyr}$

0.5mmol of H_3BTC and 0.125M solution of $CuCl_2.2H_2O$ were dissolved in a mixed solution of 0.5M pyridine and Ethyl alcohol in molar ratio of 1:4.

Each sample solution was then irradiated through ultrasonic generator (VCX 750, Sonics & materials, Inc.) for 10, 20, 30, 60 and 120 minutes. The energy of ultrasound was kept at 40% of the maximum power (750W) for those reactions. Additionally, for observing the effect of applied sonication power level, sample solutions of Cu-BTC$_{DMF+EtOH}$ were also irradiated under 20%, 60% and 80% of the maximum power of ultrasonic generator. The probe

temperature was maintained below 40°C in all reactions. The solid products were allowed to settle down in solution as precipitates. After the removal of top solution, the solid products were then purified through 30 minutes sonication at low power (20%) in the presence of 20ml DMF. The purified products were then filtered and washed with de-ionized water (20ml×3) and Ethyl alcohol (20ml×3) repetitively. The precipitates were then dried for 12 hours at 100°C.

3.3 Results and discussion

From the initial hydrothermally prepared Cu-BTC at 180°C by Chui et al.[31], $Cu(NO_3)_2.2H_2O$ was a premier choice as starting material for most of solvo-thermal synthesis of this MOF. The optimal temperature for using $Cu(NO_3)_2.2H_2O$ without formation of any impurity is about 120°C [142]. In an another study[143], $Cu(OAc)_2.H_2O$ has been used as starting material for solvo-thermal synthesis at 70°C with high yield of Cu-BTC without impurities. In this work we have used $CuCl_2.2H_2O$ as metal precursor and successfully synthesized Cu-BTC through ultrasonic irradiation at ambient temperature and atmospheric pressure. The reaction of $CuCl_2.2H_2O$ with H_3BTC in various solvents solutions gave a Cu-BTC yield in a wide range of 24-86% (based on H_3BTC as limiting reagent). Compared with traditional hydrothermal and solvo-thermal methods for preparing same compound, by which product yields varied from 60% to 65% for various reaction times, high yields were obtained within a short period of time by using ultrasonic method at ambient temperature.

The presence of solvents in general, tends to increase the chemical activity of the reactants. It increases the mobility of reactants during the chemical reaction and the rate of mass transfer from reactants to product phases. The water of hydration present within salt also acts as internal solvent. Traditionally synthesis processes of Cu-BTC, either hydrothermal [31], ultrasonic [144],

microwave assisted [145,146] or mechanochemical [147], have employed typical solvent mixtures for efficient dissolution of metal precursor and carboxylate ligands prior to the treatment. In the present work, we have extended the solvent usage scope by including some inorganic solvents in ultrasonic synthesis of Cu-BTC. The synthesis was successfully accomplished with appreciable product yields. In addition to the previously reported [147,148] synthesis for Cu-BTC which used DMF/EtOH/H_2O as solvent, We have accomplished the process with four new solvent combinations.i.e. DMF/H_2O, NaOH/EtOH/H_2O, NH_4OH/EtOH/H_2O and Pyr/EtOH/H_2O. All reactant solutions were tested under ultrasonic irradiation at 40% of maximum power (750W) for 10, 20, 30, 60 and 120 minutes at ambient temperature and atmospheric pressure. For Cu-$BTC_{DMF+EtOH}$ with conventional solvent (DMF/EtOH/H_2O), the maximum yield of 86% has been obtained after 120 minutes of sonication (Table. 1). Cu-BTC_{DMF}, Cu-BTC_{NaOH} and Cu-BTC_{NH4OH} has yields of 73%, 33% and 81% respectively. Cu-BTC_{Pyr} did not show any increase in yield after 20 minutes of irradiation, and in fact, sonication of 30 minutes or more tend to dissolve the initial product into original reaction mixture.

The XRD patterns (Fig. 3.1) of Cu-BTCs were compatible with each other and matched with the one reported in literature [144]. The appearance of sharp peaks in XRD patterns was a testimony of good degree of crystallinity in synthesized product.

The vibrational spectral analysis of synthesized MOFs were compared (Fig. 3.2) and matched with those previously reported [149]. The bands at 950cm^{-1}, 1050cm^{-1}, 1660cm^{-1} and 3250-3500cm^{-1} represented N-CHO, C-N, C=O and O-H bonding in Cu-BTC.

The specific surface area and pore volumes are considered to be the important properties of metal organic frameworks because of their use in certain applications. For these characteristics, BET N_2 gas adsorption isotherms were measured

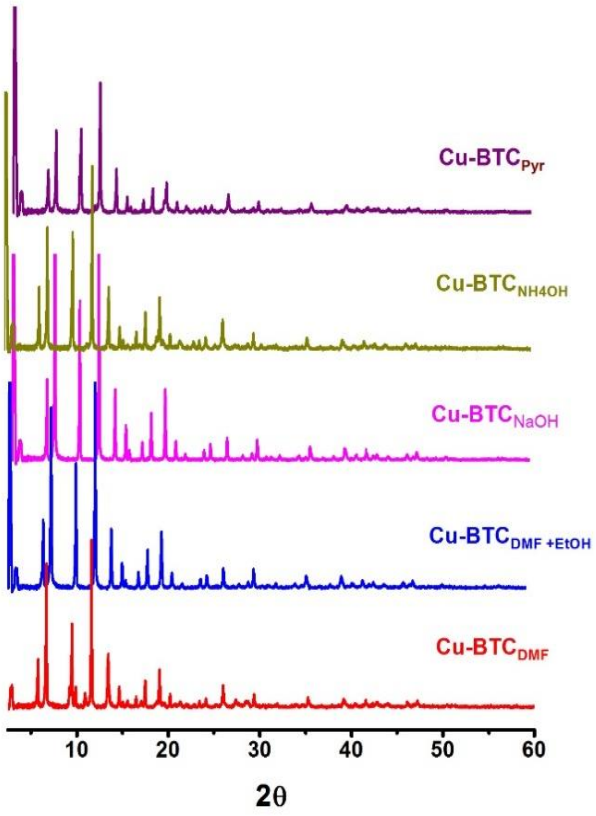

Fig. 3.1 XRD patterns of Cu-BTCs

.

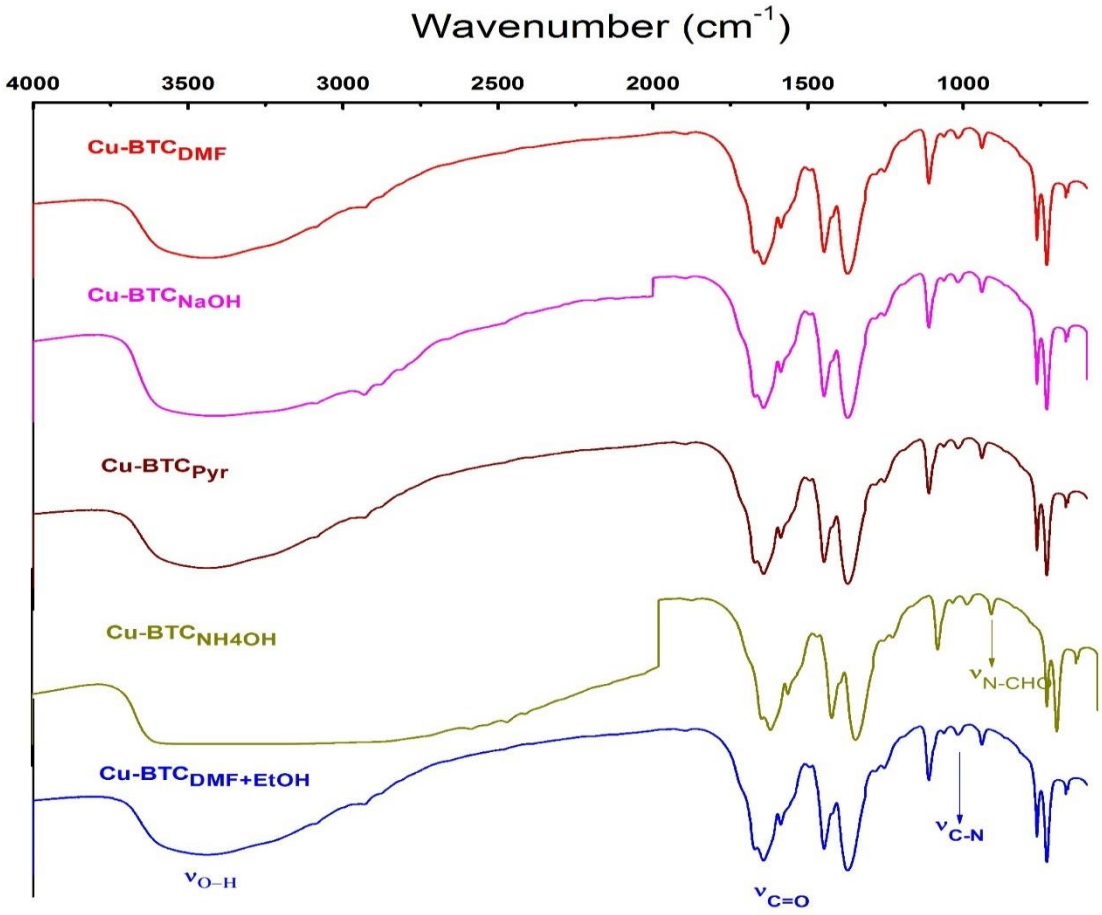

Fig. 3.2 FT-IR spectra of Cu-BTCs

The BET isotherms (Fig. 3.3) resembled type-I isotherm, with a clear evidence of steep rise in adsorption at high relative pressure (P/P_O). That confirmed the nanoporous nature of synthesized powder. We have achieved extremely high surface area (1434 m^2/g) while using DMF/H_2O as solvent in one of our experiment. As per our knowledge, this surface area value is higher than so far previously reported [147,148] Cu-BTC synthesize by room temperature ultrasonic treatment. The surface areas of 1434m^2/g, 1401m^2/g, 1185m^2/g, 925.6m^2/g and 791m^2/g

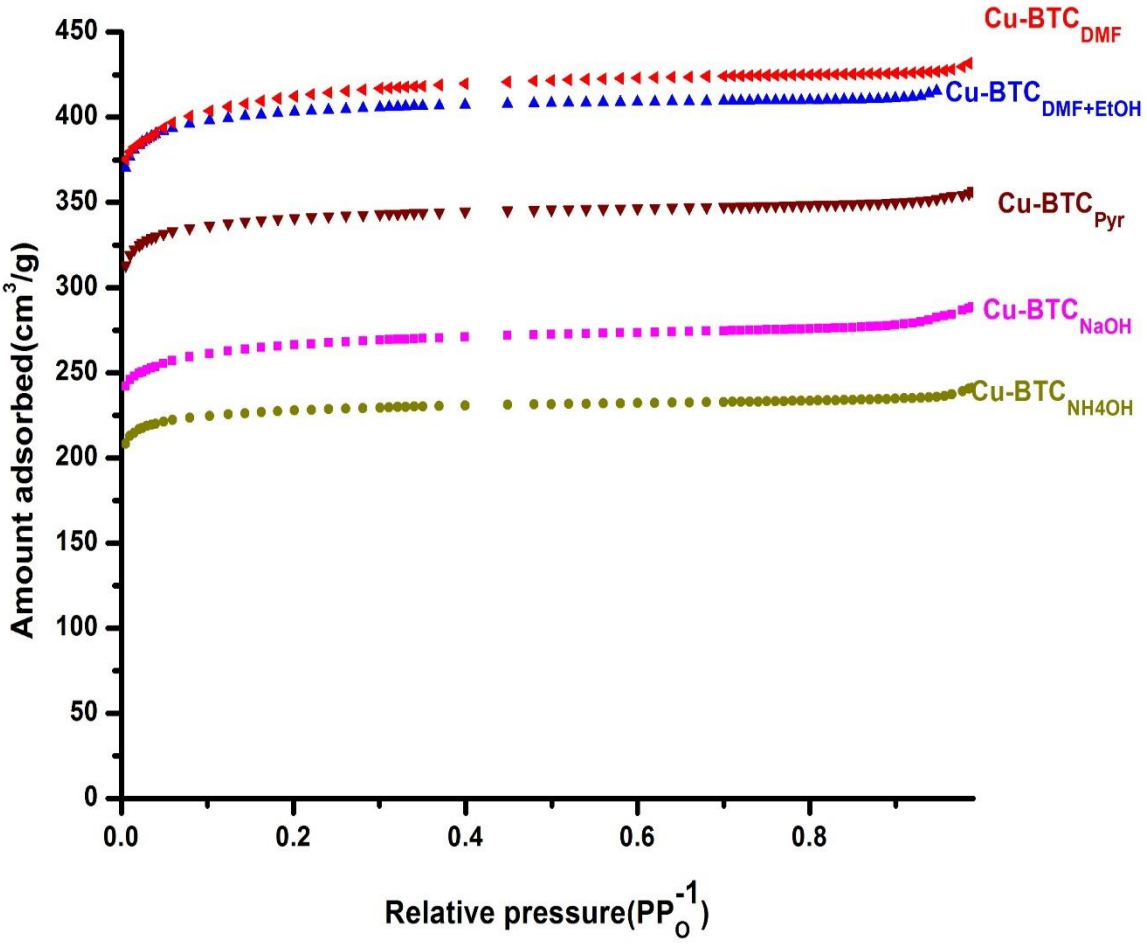

Fig. 3.3 BET adsorption Isotherms for Cu-BTCs

were obtained for Cu-BTC_{DMF}, Cu-$BTC_{DMF+EtOH}$, Cu-BTC_{NaOH}, Cu-BTC_{NH4OH} and Cu-BTC_{Pyr} respectively. The micro pore volumes, particle sizes and surface areas are tabulated in Table 1. The order of the values of micro pore volume and particle size were quite logical and understandable since for a fixed sample test volume, both, typical porosity present inside a material and individual particle size would offer corresponding surface area of material.

The microstructures (Fig. 3.6) of the five MOF products were also found to be comparable with those reported before [139], which validated the fact that MOF product has been successfully synthesized from all of the solvents employed in this work.

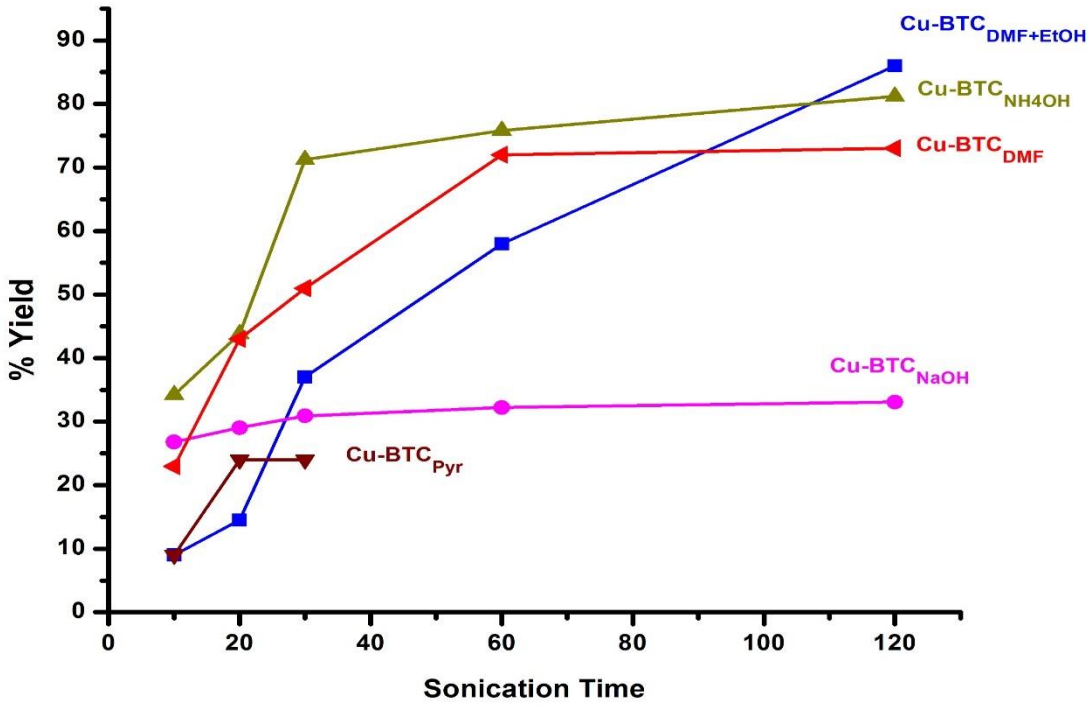

Fig. 3.4 variation of yield with sonication time

Ultrasonic radiation leads to acoustic cavitation. During cavitation process, mechanical activation through ultrasonic waves destroy the original attractive forces among the molecules in liquid phase [150]. The activation force provided by ultrasonic radiation to overcome the bonding energy provides impetus to reacting species for completion of successful reaction. Increased sonication time would provide more of such activation energy and such fact has been shown quite evidently in this work (Fig. 3.4). It has been observed that increased sonication time resulted in successive higher yield of Cu-BTCs when the reacting precursor solutions were treated for series of sonication times at 40% power.

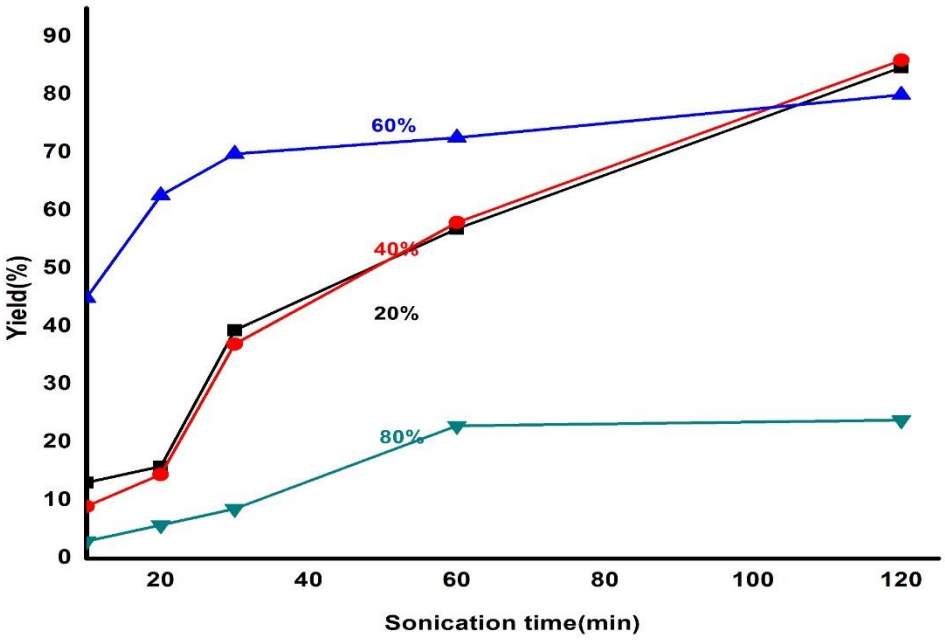

Fig. 3.5 variation in yield with sonication time at different operating power levels

With the fixed sonic power of 40%, the solvent effect on isolated crystal yields was tested with a variety of different solvent mixtures, and the results are shown in Fig. 2 and summarized in Table 1. With the increase in irradiation time for 10, 20, 30, 60 and 120 minutes at ambient temperature, water/ethanol/DMF condition resulted in the maximum yield of 86% after 120 minutes. Solvent systems with the addition of NH_4OH base led the yield reach quickly to 72% after 30 minutes then the increase slows reaching maximum of 81% yield after 120 minutes of treatment. Water/DMF condition results in increase in the yields reaching 73 % after 60 minutes then the trend saturates after that. Meanwhile the reaction condition with the addition of NaOH leads to the maximum yield of only 31% after 30 minutes then the trend slows after that. Addition of NH_4OH looks help produce initial crystal seeds effectively even under lower ultrasonic power conditions. that leads to the similar trends between 40% with NH_4OH and 60% without NH_4OH. Addition of NaOH was working negatively toward the formation of Cu-BTC. The condition with the addition of pyridine did not show any increase in yield after 20 minutes of irradiation, and in fact, sonication of 30 minutes or more made the crystals re-dissolved into the solution, probably because of non-chelating pyridine's participating into the metal organic frame work preventing the formation of three dimensional networks.

For evaluating the influence of applied sonication power, one of the reference solution for Cu-$BTC_{DMF+EtOH}$ has been examined for series of sonication times under varying ultrasonic power from generator. The corresponding yields results were found to be quite interesting (Fig. 3.5). Apparently the yields from 20% and 40% power levels are very much similar and almost replicate each other both at low (10 minutes) and high (120 minutes) sonication times. 80% power level

seemed to be a bit harsh for this process as the maximum product yield has found to be only 20% after 60 minutes of sonication and remained unchanged even after 120 minutes. The 60% power level operation appeared to be the most consistent in terms of product yield, here the variation in yield with sonication was quite steady.i.e. 44% (product yield) after 10 minutes to 80% after 120 minutes. Thus for a short sonication time (10-30 minutes), 60% power level sonication operation gave the best output. Thermo gravimetric analysis (Fig. 3.7) were done under N_2 atmosphere. Cu-BTC_{DMF} and Cu-$BTC_{DMF+EtOH}$ showed continuous mass loss of about 14% until 300°C. In between 300°C and 370°C, Cu-MOF structure collapsed and final masses of residue were found to be 37% and 38% respectively. Thermo gravimetric analysis graphs of Cu-BTC_{NaOH}, Cu-BTC_{NH4OH} and Cu-BTC_{Pyr} showed three distinct regions. Viz., (1) weight losses of 35%, 24% and 18% respectively at 100°C indicating the loss of moisture (2) weight losses of 13%, 12% and 7% in the region between 100°C and 300°C corresponds to the loss of water molecules from MOF and (3) between 300 °C and 375°C MOFs collapsed and organic linkers are buried. The final residues of three MOFs were 28%, 31% and 34% respectively at 600°C.

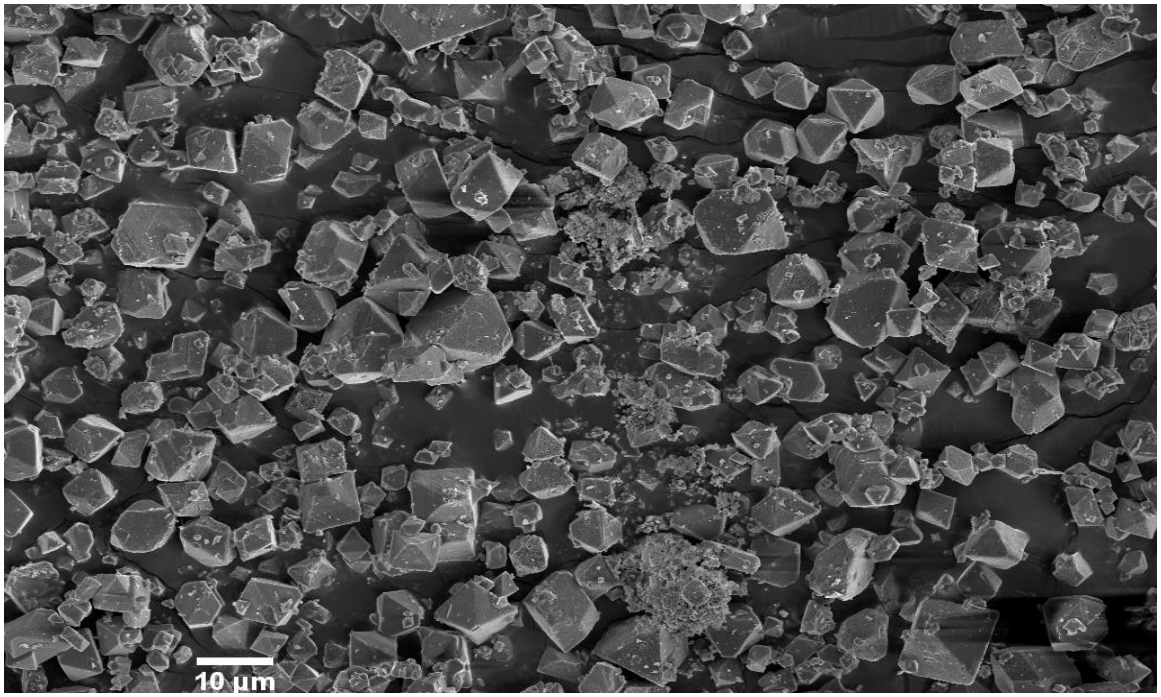

Fig. 3.6 (a) SEM image of Cu-BTC_{DMF}

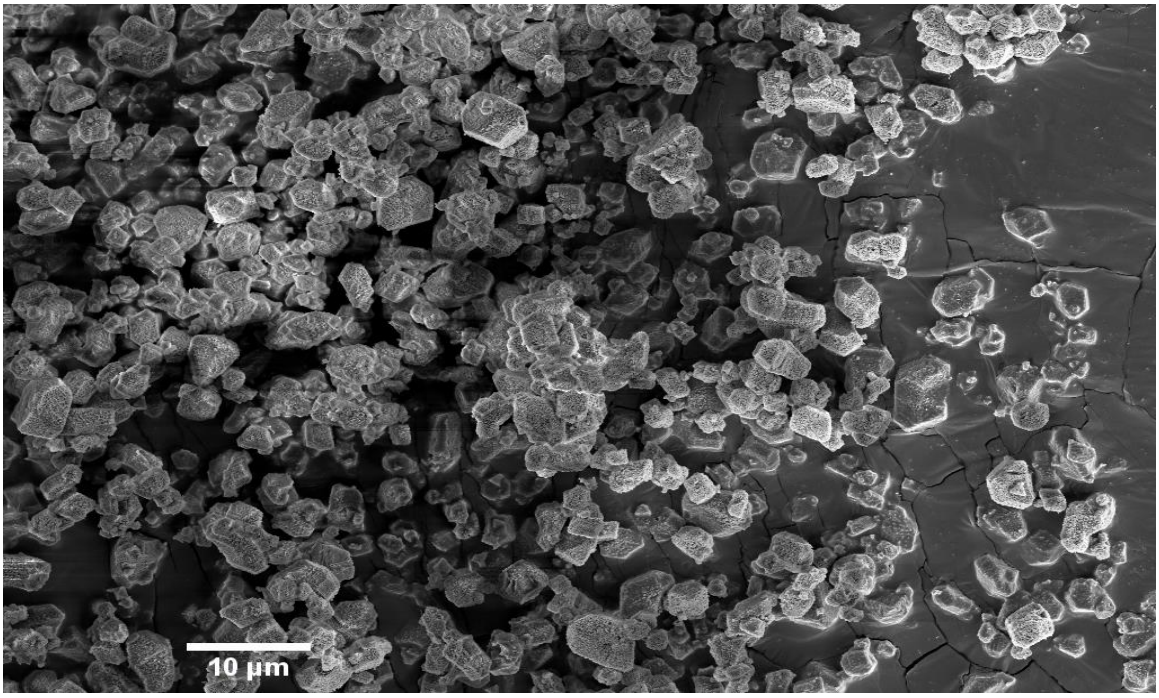

Fig. 3.6(b) SEM image of Cu-$BTC_{DMF+EtOH}$

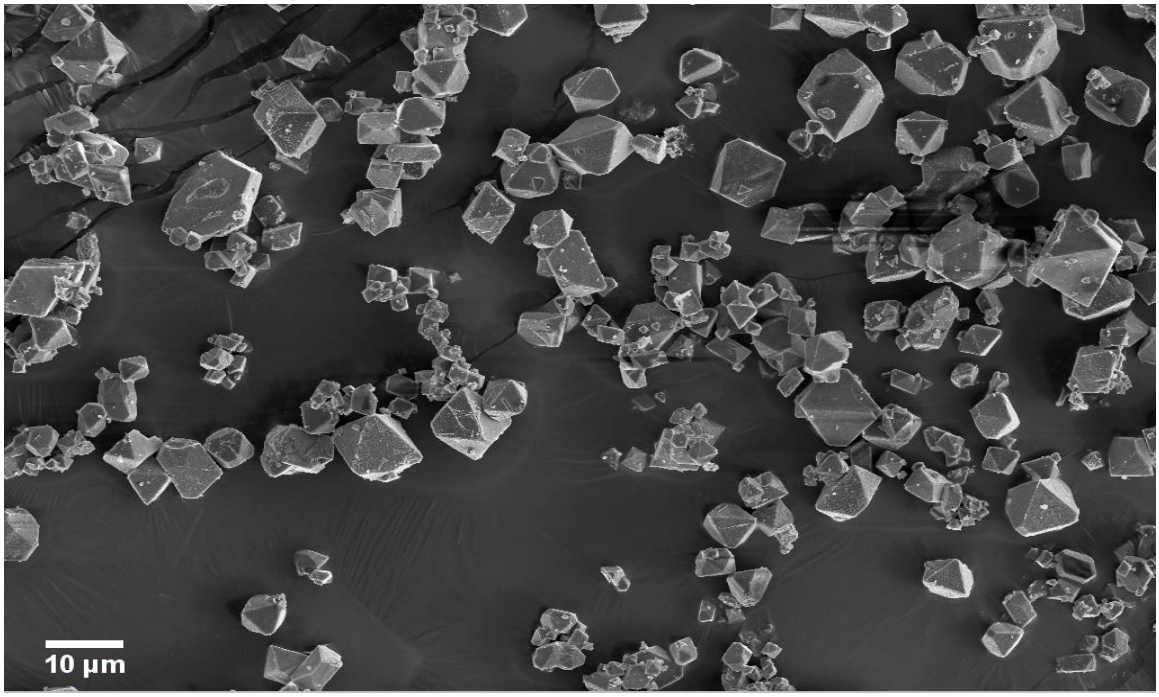

Fig. 3.6(c) SEM image of Cu-BTC_{NaOH}

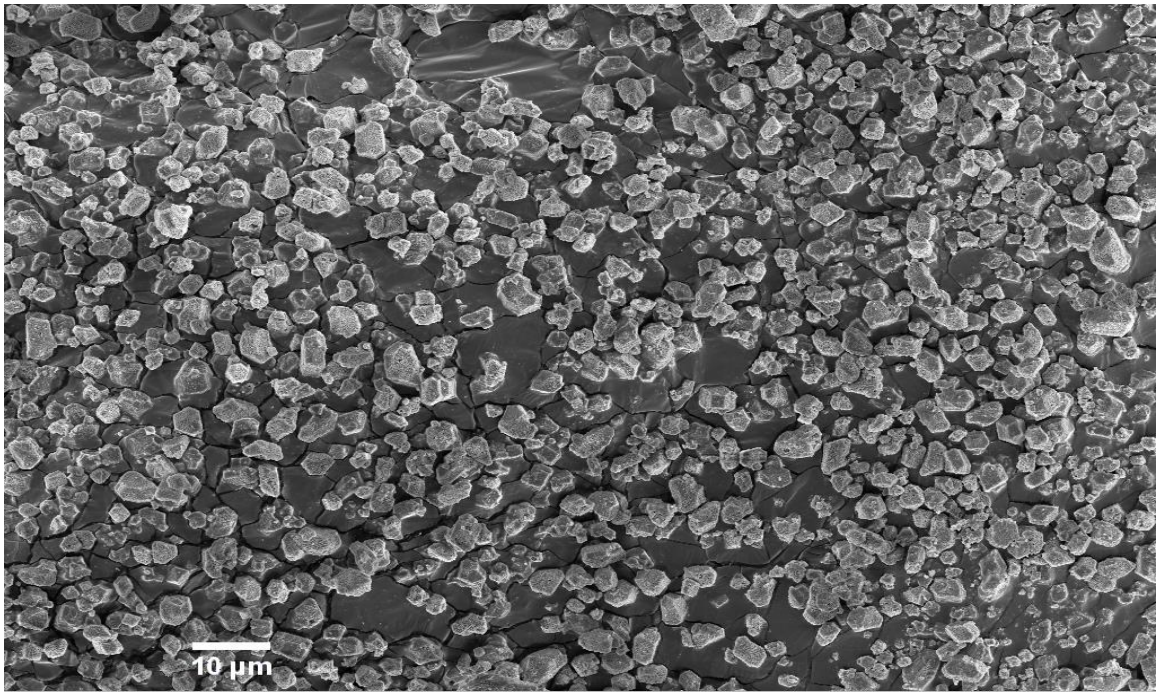

Fig. 3.6(d) SEM image of Cu-BTC_{NH4OH}

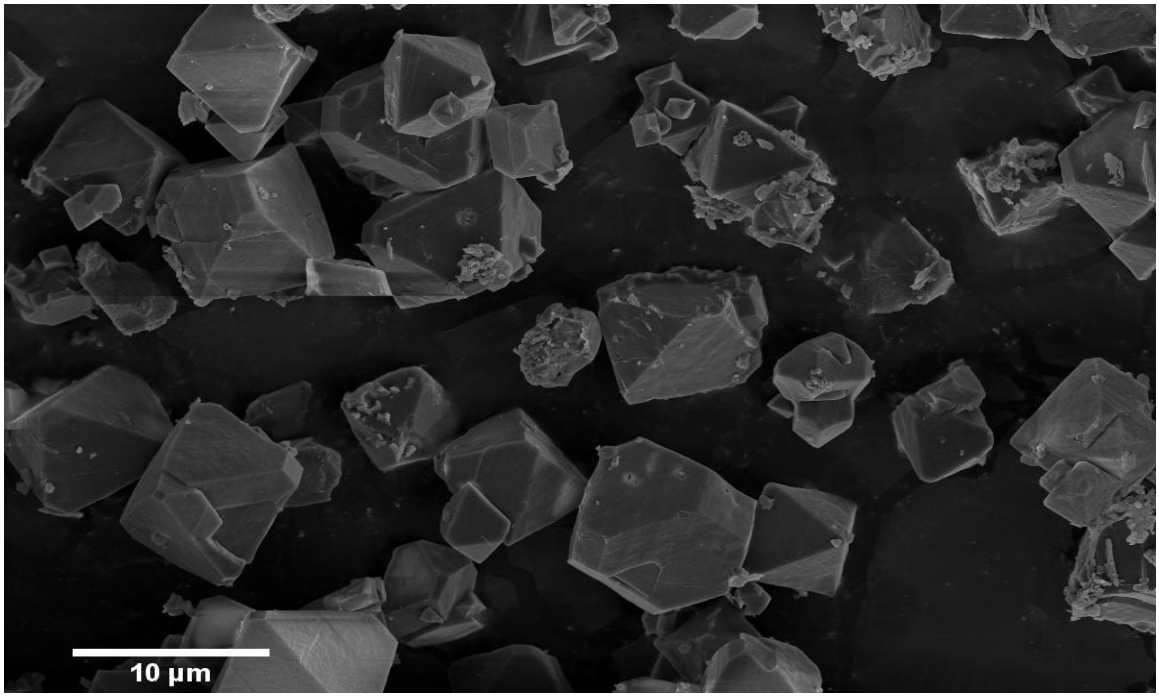

Fig. 3.6(e) SEM image of Cu-BTC_{Pyr}

Table 3.1. Reaction conditions and results for synthesis of Cu-BTC by ultrasonic irradiation at room temperature.

Cu-BTC	Solvent	pH	Time (minutes)	Yield (%)	S_{BET} (m^2/g)	Micro pore volume (cm^3/g)	Particle Size (nm)
Cu-BTC$_{DMF}$	DMF/H_2O	1.95	120	73	1434.62	0.6678	4.3258
Cu-BTC$_{DMF+EtOH}$	DMF/EtOH/H_2O	2.2	120	86	1401.762	0.4874	5.47
Cu-BTC$_{NaOH}$	NaOH/EtOH/H_2O	2.2	120	33	925.6	0.3446	6.7893
Cu-BTC$_{NH4OH}$	NH_4OH/EtOH/H_2O	2.2	120	81	791.973	0.3045	7.952
Cu-BTC$_{Pyr}$	Pyr/EtOH/H_2O	2.2	30	24	1185.06	0.4224	4.532

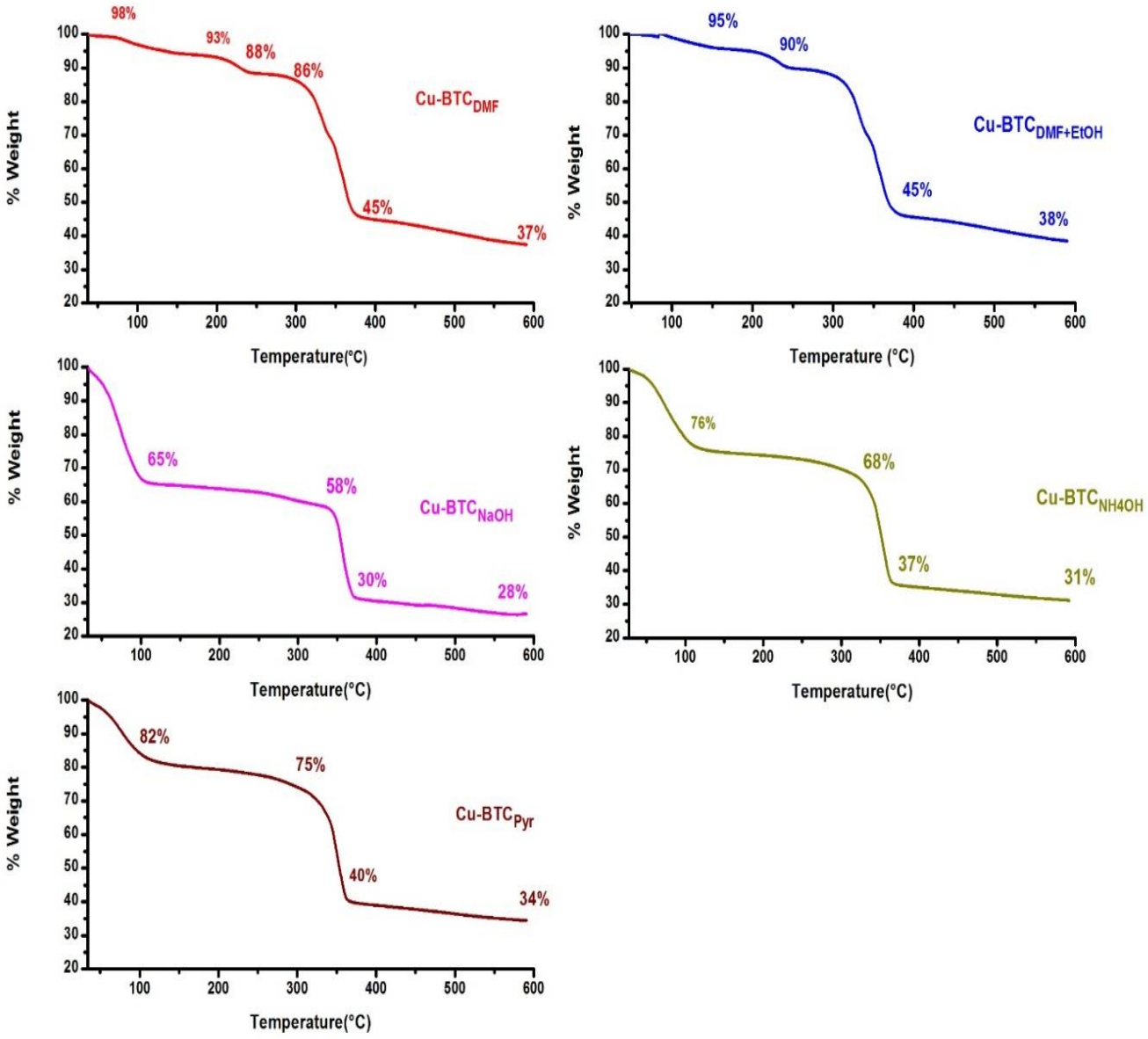

Fig. 3.7 Thermo gravimetric analysis of Cu-BTCs

IV. High yield synthesis of Ni-BTC metal –organic framework with ultrasonic irradiation: Role of polar aprotic DMF solvent

4.1 Introduction

In recent times, remarkable research has been focused on metal organic frame works (MOFs) [151]. The major portion of that research has been attributed towards their synthesis, structure analysis and potential applications such as gas adsorption [152–154], separation [155], catalysis [156], drug carriers [157], luminescence [158], polymerization [159], imaging [160], removal of hazardous materials [161,162], magnetism [163] and carriers of nanomaterials [164,165]. Traditionally MOFs has been synthesized by hydrothermal or solvo thermal processes at high temperature using conventional electric heating. To overcome the issues of prolong heating times at elevated temperature, new synthesis routes such as ultrasonic and microwave assisted heating has been effectively employed. These facile processes include ultrasonic synthesis of $Cu_3(BTC)_2$ [148], Fe-BDC [166], Ln-BTCs [167], $Zn_3(BTC)_2.12H_2O$ [168], $[Zn(BDC)(H_2O)]_n$ [169], MOF-5 [170]. Sonochemistry is the research area in which molecules undergo a reaction due to application of powerful ultrasonic radiation (20 kHz-10MHz). Compared with traditional techniques, sonochemical method is more efficient and easily controlled.

Ni-BTC is one of the class of hydrated 1-D hydrogen bonded porous solids $[M_3(BTC)_2.12H_2O(M=Co, Ni and Zn)]$ which has been initially synthesized through hydrothermal process and reported by O. M. Yaghi *et al* [171]. similarly B. Arstad *et al*.[172] has reported the solvo thermal synthesis of USO-2-Ni (Ni_2(dabco).4DMF.0.5H_2O) and USO-2-Ni-A (amine functionalized) in connection with its CO_2 capture potential. Ultrasound has also been employed for processing of Nickel based MOFs, for example nickel(II) metal organic frame

works with ligand $H_3L\{[Na_{16}(Ni_8L_{12})(H_2O)_{20}(H_3O)_4](CH_3CN)(H_2O)_{18.5}\}$ which were reported to be synthesized as precursor for the production of nickel oxide nano particles [173]. Enamul Haque *et al*.[174] has reported successful ultrasonic synthesis of nickel based CPO-27. Isostructural MOFs such as CPO-27(Co, Zn and Ni) have high concentrations of coordinatively unsaturated metal sites and 1D pore structure and had been deeply studied previously for the adsorption of gases such as hydrogen [175–177], methane [178] and CO_2 [179]. In the present work we have successfully synthesized a Ni based porous MOF through ultrasonic technique using 1, 3, 5-benzenetricarboxylic acid which has not been reported before. During the process, for fix reactants solution composition and sonication exposure, we have maneuvered the process parameters (applied ultrasonic power level and probe temperature) to figure out the optimal conditions for higher process yield. The MOF product yields, adsorption surface areas and surface compositions from three different applied ultrasound power levels has been obtained and compared.

4.2 Experimental

4.2.1 Materials and methods

All materials including $NiNO_3.6H_2O$ (99.5%, Alfa Aesar), 1,3,5-benzenetricarboxylic acid (H_3BTC)(99%, Alfa Aesar), N, N-Dimethylformamide (DMF) (99.8%, Alfa Aesar) and Ethyl alcohol (94-96%, Alfa Aesar) were used as received. For synthesis, each reactants mixture was prepared by combining metal precursor solution (2.91g of $NiNO_3.6H_2O$ dissolved in 30 ml DMF) and organic ligand solution (2.1 g of H_3BTC dissolved in 30 ml DMF). Sample solutions were then irradiated through ultrasonic generator (VCX 750, Sonics & materials, Inc.) for 120 minutes at 40%, 60% and 80% of maximum power level for various probe temperatures (50°C, 60°C, 70°C and 80°C). The pH of each solution was maintained at 2.1. After sonication, the product samples were placed at room temperature for complete separation and settlement of light

green precipitates in solution. After the removal of top solution through filtration, the solid precipitates were repeatedly washed with de-ionized water (20ml×3) and Ethyl alcohol (20ml×3). The precipitates were then completely dried by heating at 100°C for 12 hours.

4.3 Results and Discussion

The ultrasonic treatment of nickel nitrate hexahydrate with 1, 3, 5-benzenetricarboxylic acid (H_3BTC) in 1:1 molar ratio yielded green crystals. The process was performed at three different power levels with varying probe temperatures. Facile synthesis of Ni based MOFs have been reported [173,174] earlier while using different organic ligands but processing with this current combination of metal precursor and organic linker has remained so far unprecedented.

A variety of different solution mixtures of H_2O with DMF, H_2O with DMF/ethanol, and H_2O with ethanol under ultrasonic irradiation were previously tried to synthesize MOF crystals. However, all of the attempts to use polar-protic solvent systems (H_2O and/or ethanol) as part of the solvent under ultrasonic irradiation were not working for the formation of crystals.However, successful synthesis of a Ni-BTC MOF through ultrasonic treatment was achieved in two hours of ultrasonic treatment by using polar aprotic solvent N, N-Dimethylformamide (DMF) as a sole solvent. The synthetic process using ultrasound was performed at three different power levels of 40%, 60% and 80% with different reaction temperatures. Two reactants of$Ni(NO_3)_2.6H_2O$ and H_3BTC were completely dissolved in DMF separately prior to the ultrasonic treatment. Two solutions were then mixed and irradiated at 40%, 60% and 80% of maximum generator power with each solution temperatures of 50°C, 60°C, 70°C and 80°C for 2 hours. The isolated yield from each condition is tabulated in Table 1. The isolated yield is tending upward from 21% at 50°C-40% to 88% at 60°-80% as the applied power level was increased from 40% to 80%. From the yield point of view, a probe temperature of 60°C at each power level resulted in higher

numbers than the other temperature conditions, and the maximum yield (based on metal precursor) of 88% was observed from 80% power level at 60°C, which is a very high number compared to reported ~70% yields from conventional solvo-thermal methods (Table 4.1(a)).

Table 4.1(a) Ni-BTC yield with different power levels and probe temperatures combinations

Power level	Probe Temperature(°C)	yield%
40%	50	21
	60	29
	70	24
	80	26
60%	50	64
	60	78
	70	62
	80	78
80%	50	74
	60	88
	70	82
	80	84

A reported study on the accelerated rate of MOF crystal formation under ultrasonic treatment in terms of Arrhenius plot showed that the rate of both nucleation and crystal growth are caused by increased pre-exponential factor (A) instead of decrease in activation energy (E_a). In terms of activation energy, the addition of polar-protic solvents, like H_2O or ethanol, to the reaction mixture surrounds possible negative anions by hydrogen bonding which raises activation energy hampering the reaction between Ni cation and ligands, while DMF which is a polar aprotic solvent frees motion of negative anions toward the reaction with Ni cation. If the activation energy of the reaction is increased by ultrasonic treatment, it might be from the blockage of intervening polar-protic solvent between metal cation and ligands, preventing MOF crystal formation. However, it is not clear to explain why this effect happens more seriously under ultrasonic irradiation than conventional solvo-thermal reaction.The possible explanation of the increase in reaction rate

could be explained by any or all of theincrease in the heating rate, more uniform heating, and enhancement of the dissolution of precursor gel caused by ultrasonic irradiation to the solution.

The XRD patterns of Ni-BTC MOFs are shown in Fig. 4.1. XRD patterns are quite compatible to each other and sharpness of respective peaks is the evidence of inherent crystallinity. While the patterns taken from US_{40} and US_{60} show the same crystal structure, US_{80} forms different crystal structure under stronger agitation effect under higher power ultrasound. The XRD patterns were further examined through X'Pert HighScorePlus software. The Reitveld refinement was performed to obtain the approximate crystal structures of US_{40}, US_{60} and US_{80}. The structure parameters are reported in Table 4.2. The chemical formulas obtained from the elemental analysis measurements are: US_{40} and US_{60}: $C_{16}H_{41}O_7Ni_4N_{17}$ with C: 23.47%, H: 5.01%, O: 13.7%, N: 29.1%, Ni: 28.7%; US_{80}: $C_{26}H_{44}O_8Ni_2N_8$ with C: 47.73%, H: 6.16%, O: 17.94%, N: 15.7%, Ni: 16.45%.

The infra-red spectra of products were shown in Fig. 4.2. These Ni-BTCs show identical spectra with absorption band at 1438cm^{-1}, 1562cm^{-1} and 1625cm^{-1}. They show similar IR absorption patterns with Ni ion coordinated COO moiety in the range of 1350 – 1650 cm^{-1} and ν_{C-N} and ν_{CN-CHO} vibrational frequencies observed at 1055 cm^{-1} and 932 cm^{-1}indicating the presence of Ni coordinating to DMF molecules.

The multipoint BET surface surface areas (between P/P_o = 0.12 to 0.3) and pore volumes (at P/P_o = 0.992826292) of synthesized Ni-BTCs were measured by N_2gas adsorption isotherms. The BET isotherms resembles type-I isotherm. The sharp increase in adsorption capacity at the end stage of the curve is the evidence of multilayer formation of adsorbent. It makes an appreciable increase in adsorption as the relative pressure (P/P_O) value approaches unity (Fig. 4.3). Surface areas of 1000m^2/g, 980m^2/g and 960m^2/g were recorded for the MOF crystals from US_{60}, US_{80}

and US_{40} conditions. Surface areas, pore volumes for Ni-BTCs taken from US_{40}, US_{60}, and $US_{80}$are tabulated in Table. 4.3. The MOFs show good potential in terms of their physisorption, and properties such as pore size, pore volume and average particle size. Pore volumes of MOFs are reasonably ranged between 0.55 ~ 0.57 cm^3/g. For comparison with single crystal, the approximated unit cell volume obtained from Reitveld refinement and standard atomic volumes of the constituent elements in one formula unit were used to calculate the total free volume or total pore volume in unit cell. The pore volume per unit mass of unit cell was calculated and compared with experimentally measured pore volumes. The calculated pore volume of US_{80} (0.3953cm^3/g) is 29.4% less than the experimentally observed value (0.56cm^3/g), while US_{40} and US_{60} show the calculated pore volume (0.4671cm^3/g) of 15.07% and 18.05% less than experimental values of 0.55cm^3/g and 0.57cm^3/g, respectively.

In order to have an insight about surface compositions of MOFs particles, XPS analyses for the top 5nm surface layer were conducted, and the results are shown in Fig. 4. Peaks of Ni, C and O are vividly shown, and the results are summarized in Table 3.

The morphology of Ni-BTC was characterized by field emission SEM. SEM images of the MOF crystals are shown in Fig. 6. It shows that the products are composed of nano spheroidal structure with regulated particle sized of 0.5-0.8 μm.

The thermograms of synthesized MOFs were measured under N_2 atmosphere and the results are shown in Fig. 7.Thermo-grams show broadly losing weights of 45%, 50% and 53% from US_{40}, US_{60}, and US_{80} respectively until 400°C due to the slow loss of coordinated DMF in channel, and possibly some probably was captured during washing process. MOFs structures are to be broken at the temperatures of between 400°C and 450°C. The weights of residues at 600°C were 20%, 22% and 21% respectively from US_{40}, US_{60}, and US_{80}.

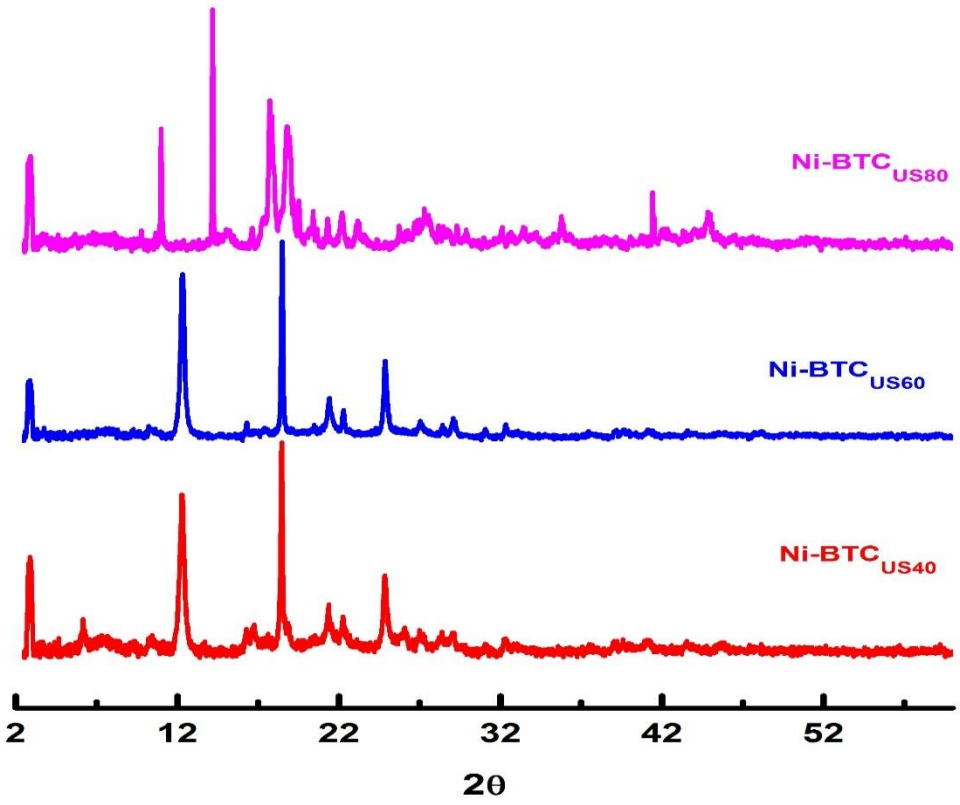

Fig. 4.1 XRD patterns of three Ni-BTCs

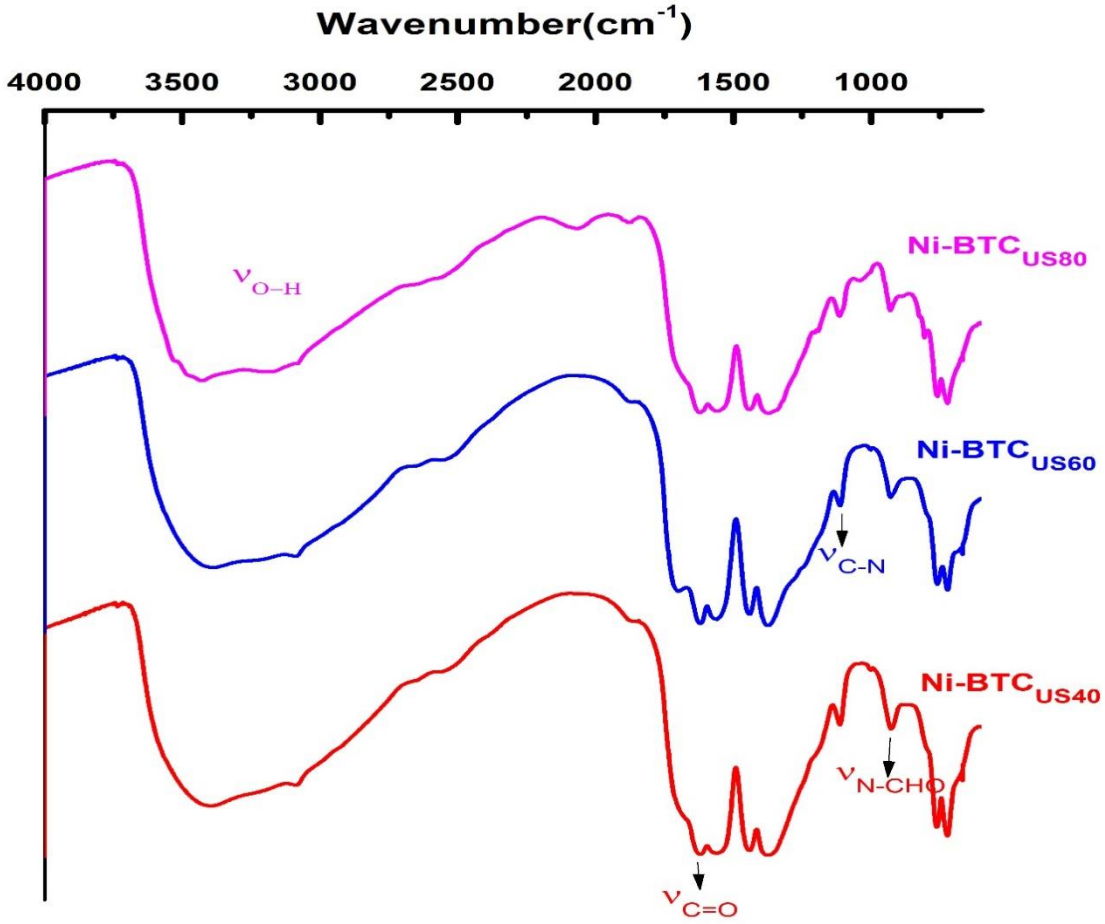

Fig. 4.2 FT-IR spectra of three Ni-BTCs

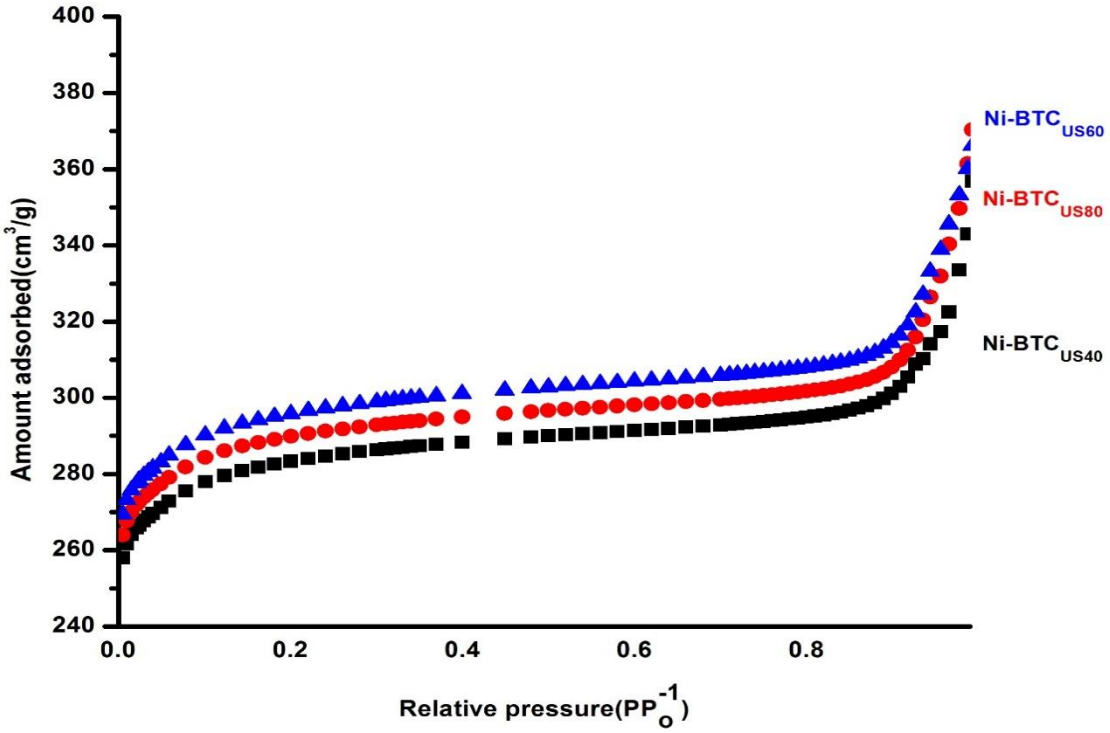

Fig. 4.3 Nitrogen adsorption isotherms of Ni-BTCs

Table 4.1(b) Comparison with selected synthesis routes

Ni-MOF	Synthesis Route	Time	% Yield	Reference
$Ni_3C_{18}H_{30}O_{24}$	Hydrothermal	24 hrs	Not mentioned	[30]
$Ni_3C_{18}H_{30}O_{24}$	Hydrothermal	48 hrs	71%	[41]
USO-2-Ni	Solvothermal	24 hrs	Not mentioned	[31]
USO-2-Ni-A	Solvothermal	24 hrs	Not mentioned	[31]
$\{[Na_{16}(Ni_8L_{12})(H_2O)_{20}(H_3O_4)](CH_3CN)(H_2O)_{18.5}\}$	Ultrasonic	1 hr	53.9%	[32]
$\{[Na_{16}(Ni_8L_{12})(H_2O)_{20}(H_3O_4)](CH_3CN)(H_2O)_{18.5}\}$	Reflux	2 hrs	57.3%	[32]
CPO-27 (Ni)	Ultrasonic	58min (Nucleation time)	Not mentioned	[33]
US_{80}	Ultrasonic	2 hrs	74%-88%	Present work
US_{60}	Ultrasonic	2 hrs	64%-78%	Present work
US_{40}	Ultrasonic	2 hrs	21%-29%	Present work

Table 4.2 Physical properties of Ni-BTC

Ni-BTC	SSA_{BET} (m^2/g)	Pore volume(cm^3/g)	Pore size(nm)	Particle size(nm)	XPS Surface composition
US_{40}	957.87	0.5464	2.1786	7.5683	C1s (57.16%)
					N1s (3.72%)
					$Ni2p_3$ (4.3%)
					OIs (34.81%)
US_{60}	1001	0.5685	2.200665	7.90096	C1s (54.96%)
					N1s (6.37%)
					$Ni2p_3$ (5.26%)
					OIs (33.41%)
US_{80}	978.37	0.5572	2.189915	8.2170	C1s (54.01%)
					N1s (6.08%)
					$Ni2p_3$ (5.42%)
					OIs (34.49%)

Table 4.3 Crystal structures and unit cell parameters of synthesized MOFs

	US_{40}	**US_{60}**	**US_{80}**
Chemical Formula	$C_{16}H_{41}O_7Ni_4N_{17}$	$C_{16}H_{41}O_7Ni_4N_{17}$	$C_{26}H_{44}O_8Ni_2N_8$
Molecular weight	817.8	817.8	713.4
Crystal system	Monoclinic	Monoclinic	Monoclinic
Space group	C12/C1	C12/C1	C12/C1
Space group No.	15	15	15
a (Å)	20.2304	20.2304	8.546
b (Å)	13.2202	13.2202	30.263
c (Å)	13.9978	13.9978	15.6278
α	90°	90°	90°
β	116.50294°	116.50294°	118.305°
γ	90°	90°	90°
Density (g/cm^3)	1.6212	1.6212	1.33
V (Å)^3	3350.289	3350.289	3558.53
Z	8	8	8
RIR	1.1945	1.1945	0.79

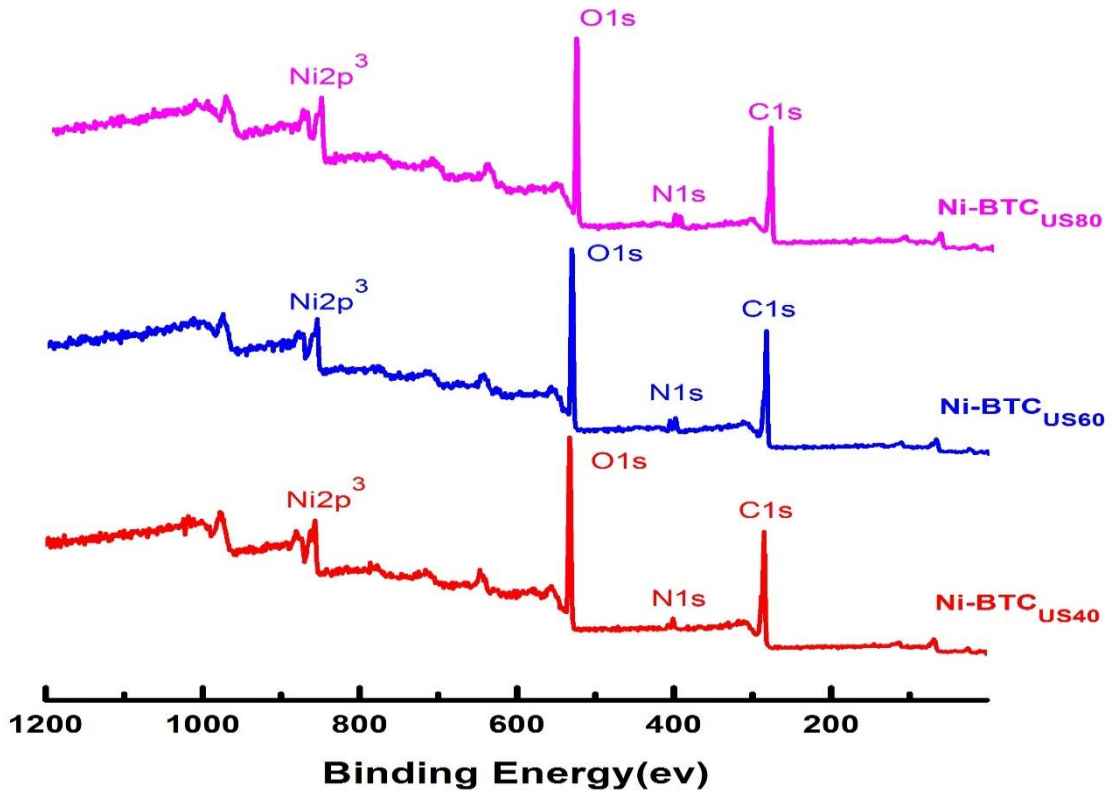

Fig. 4.4 Surface composition of Ni-BTCs from XPS

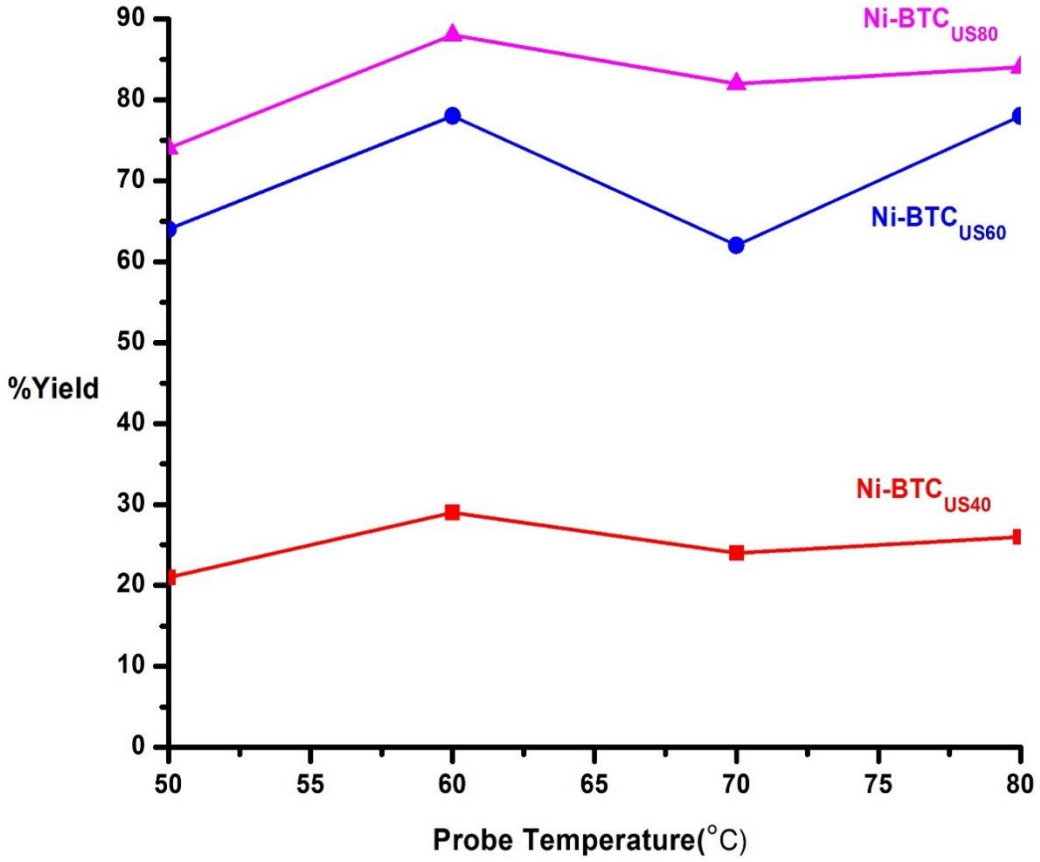

Fig. 4.5 Process yield at three different power levels with variation of probe temperature

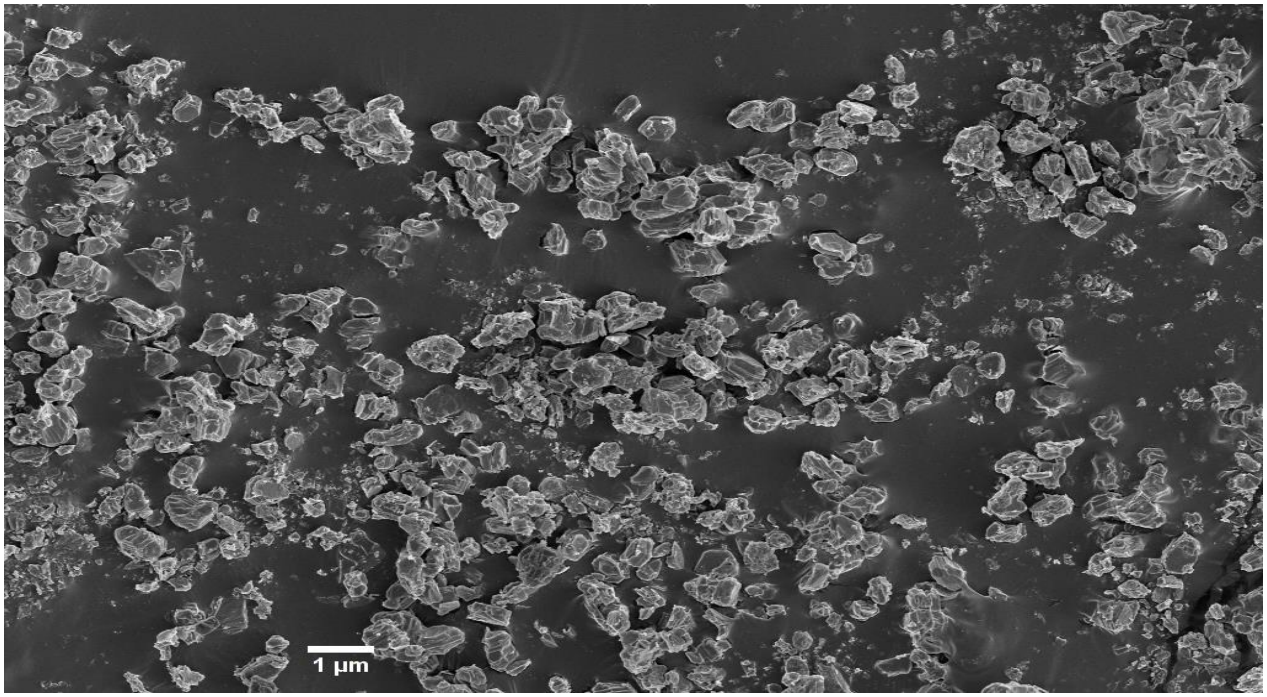

Fig. 4.6(a) SEM image of Ni-BTC$_{US40}$

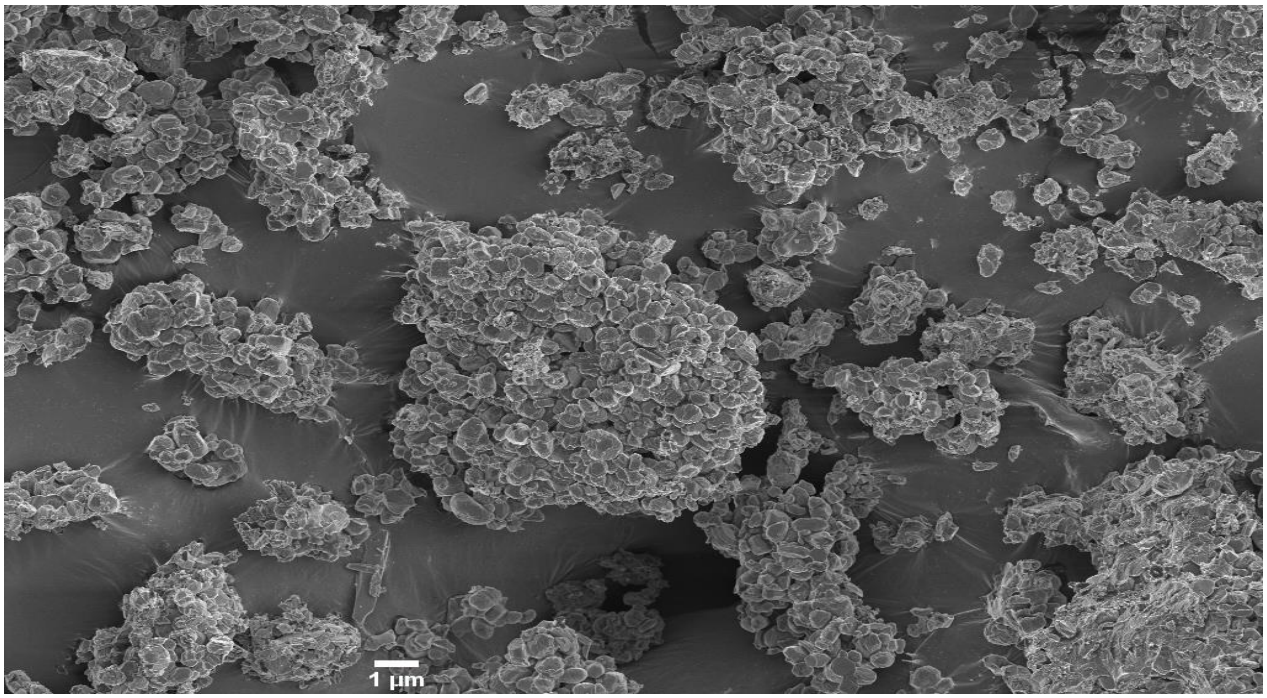

Fig. 4.6(b) SEM image of Ni-BTC$_{US60}$

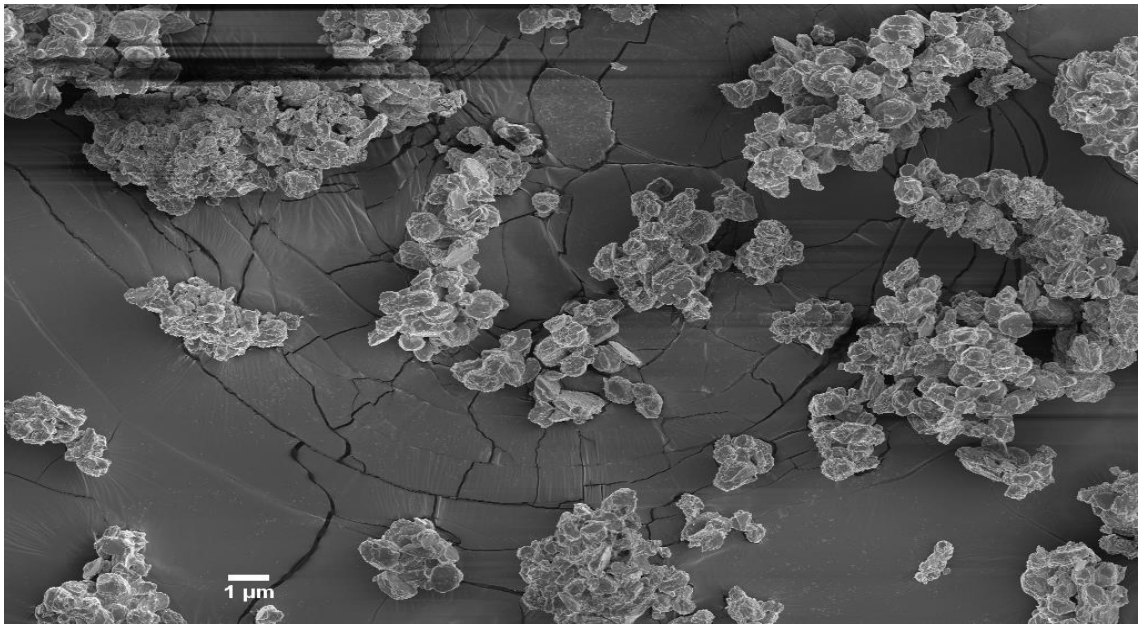

Fig. 4.6(c) SEM image of Ni-BTC_{US80}

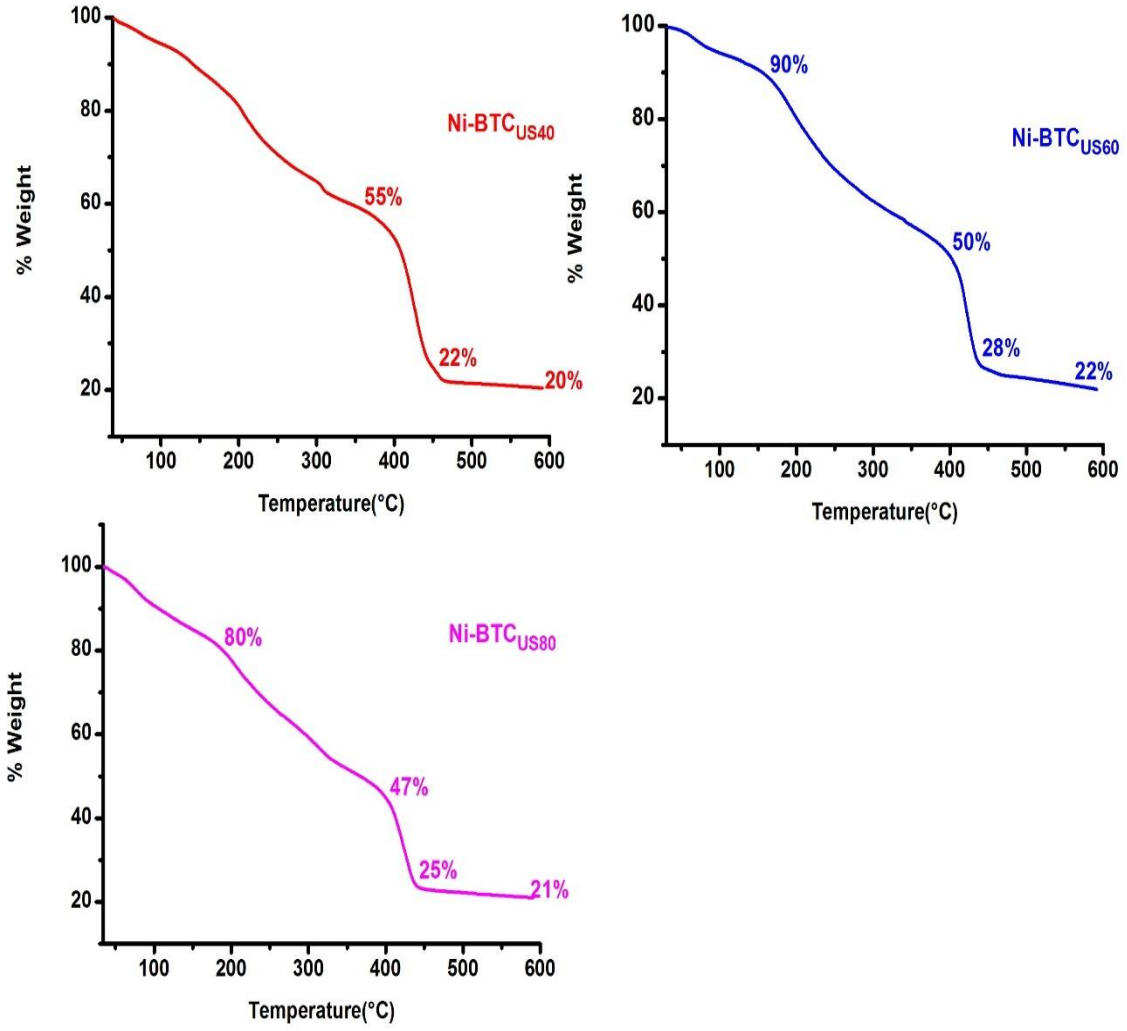

Fig. 4.7 Thermo gravimetric analysis of Ni-BTCs

V. Scope of various solvents and their effects-Solvothermal Synthesis of Ni-BTC

5.1 Introduction

Coordination polymers (CPs) and metal– organic frameworks (MOFs) represent one of the most attractive research areas of coordination chemistry. The combination of metal ions and organic linkers provides various possibilities for the fabrication of materials with different structure and functionality. These have wide potential application in the fields of gas adsorption and storage, separation, sensors and catalysis [180–185]. These crystalline, highly porous solids can possess ultra-high Brunauer-Emmett-Teller (BET) surface areas (~7000 m^2/g) [95,186–188]. Due to their modular nature and structural tunability, MOFs has also found in applications such as light harvesting [189–193], sensing [194], optical luminescence[195,196], ionic conductivity[197–199], nonlinear optical behavior[200] and as precursors for the synthesis of nano-materials with interesting properties[201–207].

A huge variety of MOFs has been synthesized and reported so far with synthesis techniques such as Hydrothermal, solvo thermal, microwave assisted heating, mechanochemical, electrochemical and more recently ultrasonic processes. Ni-BTC as a part of this long chain of MOFs, has been initially reported by O. M. Yaghi *et al*.[171]. DUT-9 [208] constructed by btb linkers (btb = benzene 1, 3, 5-tribenzoate) and $\{Ni_5(\mu_3\text{-}O)_2(O_2C)_6\}$, porous paddle-wheel structures using different combination of metal/organic linker/base/solvents via high through put synthesis [209] and CPO-27(Ni) [174] are few other noticeable contributions for Ni based porous solids.

In the present work we have opted for solvo thermal synthesis of Ni-BTC. The unique and interesting aspect here in this work is that we have employed seven different solvents such as Dimethylformamide (DMF), Ethyl alcohol (EtOH), Sodium hydroxide (NaOH), Ammonium

hydroxide (NH_4OH), Pyridine (Pyr), Aniline (Anl) and Trimethlyamine (TMA) in separate synthesis. The results in terms of process yields, surface properties, surface compositions and morphologies are reported and then based on these properties, we have attempted to draw a comparison among the potential of these solvents.

5.2 Experimental

5.2.1 Materials and methods

All materials including $NiNO_3.6H_2O$ (99.5%, Alfa Aesar), 1, 3, 5-Benzenetricarboxylic acid (H_3BTC)(99%, Alfa Aesar), N, N-Dimethylformamide (DMF) (99.8%, Alfa Aesar), Ethyl alcohol (94-96%, Alfa Aesar), NaOH (pellets 98%, Alfa Aesar), NH_3 water (Daejung chem.), Aniline (99.5%, Daejung chem.), Trimethylamine (TMA) (99%, Alfa Aesar)and Pyridine (99.5%, Daejung chem.) were used as received. We have synthesized seven Ni-BTC yields from combination of these solvents. All reactant solutions prepared had pH (2-2.15). The details of synthesis are as under:

5.2.1.1 Ni-BTC$_{EtOH}$

5.82g of $NiNO_3.6H_2O$ in 40ml de-ionized water whereas 2.1g of H_3BTC in 40ml EtOH were dissolved separately. The two solutions were then mixed and loaded in Teflon liner assembly.

5.2.1.2 Ni-BTC$_{NaOH}$

For Ni-BTC_{NaOH}, 5.82g of $NiNO_3.6H_2O$ in 40ml de-ionized water whereas 2.1g of H_3BTC in a mixture of DMF (27ml) and 0.2M NaOH (13ml) were dissolved separately. The solutions were then mixed and loaded in Teflon liner assembly.

5.2.1.3 Ni-BTC$_{NH4OH}$

For Ni-BTC$_{NH4OH}$, 5.82g of $NiNO_3.6H_2O$ in 40ml de-ionized water whereas 2.1g of H_3BTC in a mixture of DMF (24ml) and 0.2M NH_4OH (16ml) were dissolved separately. The solutions were then mixed and loaded in Teflon liner assembly.

5.2.1.4 Ni-BTC$_{Anl}$

For Ni-BTC$_{Anl}$, 5.82g of $NiNO_3.6H_2O$ in 40ml de-ionized water whereas 2.1g of H_3BTC in a mixture of DMF (26ml) and 0.2M Aniline (14ml) were dissolved separately. The solutions were then mixed and loaded in Teflon liner assembly.

5.2.1.5 Ni-BTC$_{Pyr}$

For Ni-BTC$_{Pyr}$, 5.82g of $NiNO_3.6H_2O$ in 40ml de-ionized water whereas 2.1g of H_3BTC in a mixture of DMF (26ml) and 0.2M Pyridine (14ml) were dissolved separately. The solutions were then mixed and loaded in Teflon liner assembly.

5.2.1.6 Ni-BTC$_{TMA}$

For Ni-BTC$_{TMA}$, 5.82g of $NiNO_3.6H_2O$ in 40ml de-ionized water whereas 2.1g of H_3BTC in a mixture of DMF (25ml) and 0.2M TMA (15ml) were dissolved separately. The solutions were then mixed and loaded in Teflon liner assembly.

5.2.1.7 Ni-BTC$_{DMF}$

5.82g of $NiNO_3.6H_2O$ in 40ml de-ionized water whereas 2.1g of H_3BTC in 40ml DMF were dissolved separately. The two solutions were then mixed and loaded in Teflon liner assembly.

Each of these solutions were heated at 160°C for 48 hours in a convection oven. The Teflon liner assembly was then furnace cooled to room temperature. The solutions were filtered and precipitates were washed with de-ionized water (20ml×3) and Ethyl alcohol (20ml×3) repetitively. The precipitates were dried for 12 hours at 100°C. On a dry weight

basis, yields of57%, 72%, 75%, 73%, 34%, 74% and 73% were recorded for Ni-BTC_{DMF}, Ni-BTC_{EtOH}, Ni-BTC_{NaOH}, Ni-BTC_{NH4OH}, Ni-BTC_{Anl}, Ni-BTC_{Pyr} and Ni-BTC_{TMA} respectively (Table 5.1).

Table 5.1 Physical properties of Ni-BTCs

Compound	$SSA_{BET}(m^2/g)$	Pore-volume (cm^3/g)	Pore size(nm)	Particle size (nm)	%Yield	XPS-Surface composition
Ni-BTC_{Anl}	8.96	0.023037	10.32549	672.3247	34	C1s (56.4%)
						N1s (2.39%)
						Ni2p3 (7.99%)
						O1s (33.22%)
Ni-BTC_{NH4OH}	845.83	0.506290	2.39786	7.1042	73	C1s (56.46%)
						N1s (1.36%)
						Ni2p3 (6.65%)
						O1s (35.43%)
Ni-BTC_{DMF}	710	0.423	2.3241	11.846	57	C1s (52.43%)
						N1s (2.88%)
						Ni2p3 (7.83%)
						O1s (36.86%)
Ni-BTC_{TMA}	787.3	0.46165	2.28545	10.70969	73	C1s (51.44%)
						N1s (2.77%)
						Ni2p3 (8.67%)
						O1s (37.12%)
Ni-BTC_{NaOH}	1.8692	0.013535	28.96389	3209.8862	75	C1s (57.98%)
						N1s (1.45%)
						Ni2p3 (7.1%)
						O1s (33.48%)
Ni-BTC_{Pyr}	687.8	0.4119	2.3352	12.17234	74	C1s (57.75%)
						N1s (1.29%)
						Ni2p3 (6.23%)
						O1s (34.73%)
Ni-BTC_{EtOH}	587.5	0.36175	2.38535	13.64675	72	C1s (57.96%)
						N1s (1.57%)
						Ni2p3 (6.66%)
						O1s (33.81%)

5.3 Results and discussion

Ni-BTC was obtained by solvo-thermal reaction of $NiNO_3.6H_2O$ and 1, 3, 5-benzenetricarboxylic acid in 2:1 molar ratio. Seven different organic and inorganic solvents including Dimethylformamide (DMF), Ethyl alcohol (EtOH), Trimethylamine (TMA), Aniline (Anl), Pyridine (Pyr), Ammonium hydroxide (NH_4OH) and Sodium hydroxide (NaOH) have been employed. Ni-BTC product from each solvent has characteristic %yield, surface area, surface composition and morphology. High process yields (up to 75%) have been recorded. Ni-BTC_{NH4OH} has the highest recorded surface area of 845 m^2/g. of the seven MOF products synthesized in this work, Ni-BTC_{Anl} and Ni-BTC_{NaOH} has meso-porous nature with lowest recorded surface areas of 8.96m^2/g and 1.8692m^2/g respectively. However the other five; Ni-BTC_{NH4OH}, Ni-BTC_{Pyr}, Ni-BTC_{DMF}, Ni-BTC_{EtOH} and Ni-BTC_{TMA} has shown good potential in terms of their N_2 gas physiosorption and properties such as pore size, pore volume and average particle size (Table 5.1).

The addition of NaOH and aniline seemed to reduce the surface areas of MOFs. Most probably the solvent removal technique was not effective for the removal of solvents from those Ni-BTCs.

The lesser yield from aniline solution may be attributed to the fact that non-chelating aniline participating in the MOF formation which prevented the MOF production or possible redissolution of the product.

The conventional solvents such as DMF, EtOH and their combination such as DMF/EtOH showed good solubility and promoted cleaner process yield. The other two bases: NH_4OH and pyridine seemed to show good deprotonation effect and resulted in appreciable yields of Ni-BTCs.

The XRD patterns are shown in Fig. 5.1. Interestingly all of the XRD patterns show all different diffraction patterns meaning they are formed with different crystal structures. MOF of Ni-BTC_{Anl} with extremely low BET surface area does not show clear diffraction patterns. The FT-IR spectra of all of the synthesized MOFs are shown in Fig. 5.2. They show similar IR absorption patterns with Ni ion coordinated COO moiety in the range of 1350 – 1650 cm^{-1} [210], and ν_{C-N} and ν_{CN-CHO} vibrational frequencies observed at 1103 cm^{-1} and 936 cm^{-1} indicating the presence of Ni coordinating to DMF molecules. The top 5nm surface compositions of MOFs were measured through XPS analysis (Fig. 5.4). The X-ray photoelectron spectroscopy demonstrated the appearance of C1s, $Ni2p_3$ and O1s peaks which is the testimony for the presence of fundamental elements in this metal organic framework. Furthermore, the nitrogen content N1s on surface found to be very low which showed good purity level of products.

The surface morphology through SEM images (Fig. 5.5) of the MOF powders suggested that Ni-BTC_{Anl} has granular structure (Fig. 5.5(a)) whereas the other Ni-BTCs has predominantly rod like particle morphology with varying particle size for each and every MOF. The process yields, in general, were found to be on higher side as compared to the conventional hydrothermal/ solvo-thermal yields of 50-65%. Here the bulk of process runs (5 out of 7) has recorded yields in range of 73-75% (Fig. 5.6). Which is considered to be fairly high for solvo-thermal synthesis. Thermo gravimetric analysis (Fig. 5.7) were performed under N_2 atmosphere. Each of the thermo gram of Ni-BTCs has three distinct regions at different temperature ranges. Initial weight losses until decomposition were attributed to the loss of moisture and solvent molecules. The structures of Ni-BTC_{DMF} and Ni-BTC_{TMA} decomposed at 300°C whereas the structures of Ni-BTC_{EtOH}, Ni-$BTC_{Pyr,}$ Ni-BTC_{NaOH}, Ni-BTC_{NH4OH} and Ni-BTC_{ANL} were appeared to be dissolved in the temperature range of 400-425°C. The final residues weights were in the range of 31-39% at 600°C.

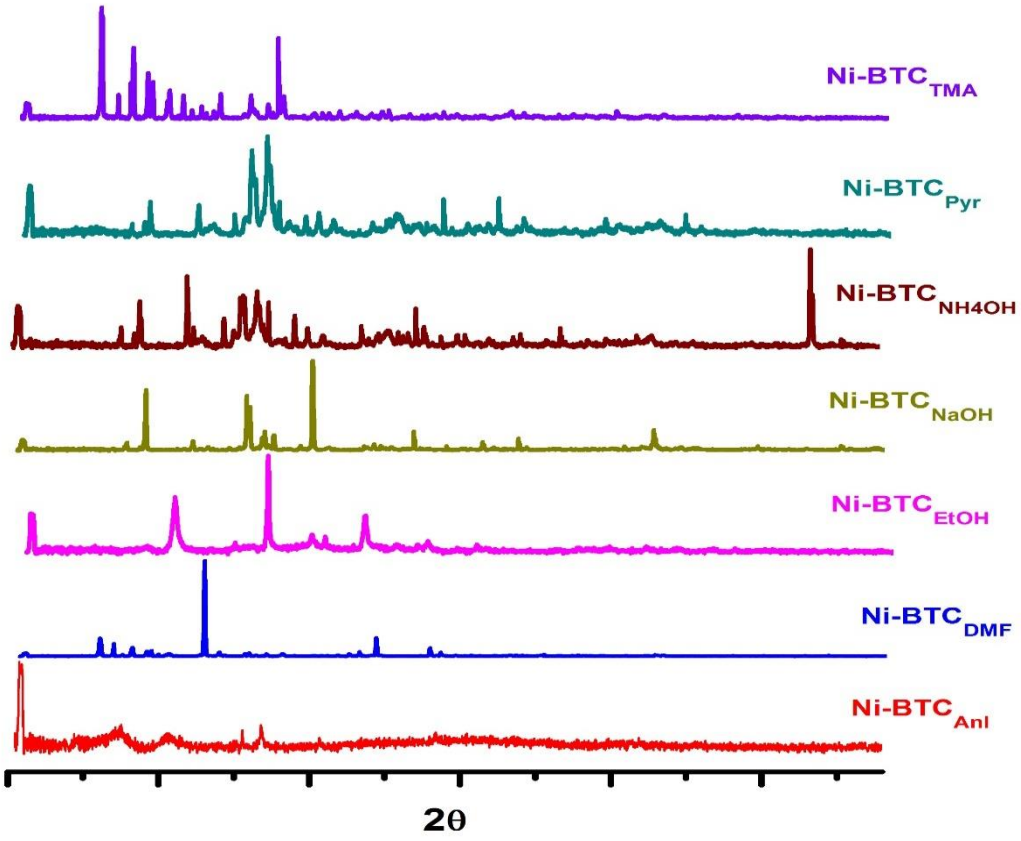

Fig. 5.1 XRD patterns of Ni-BTCs

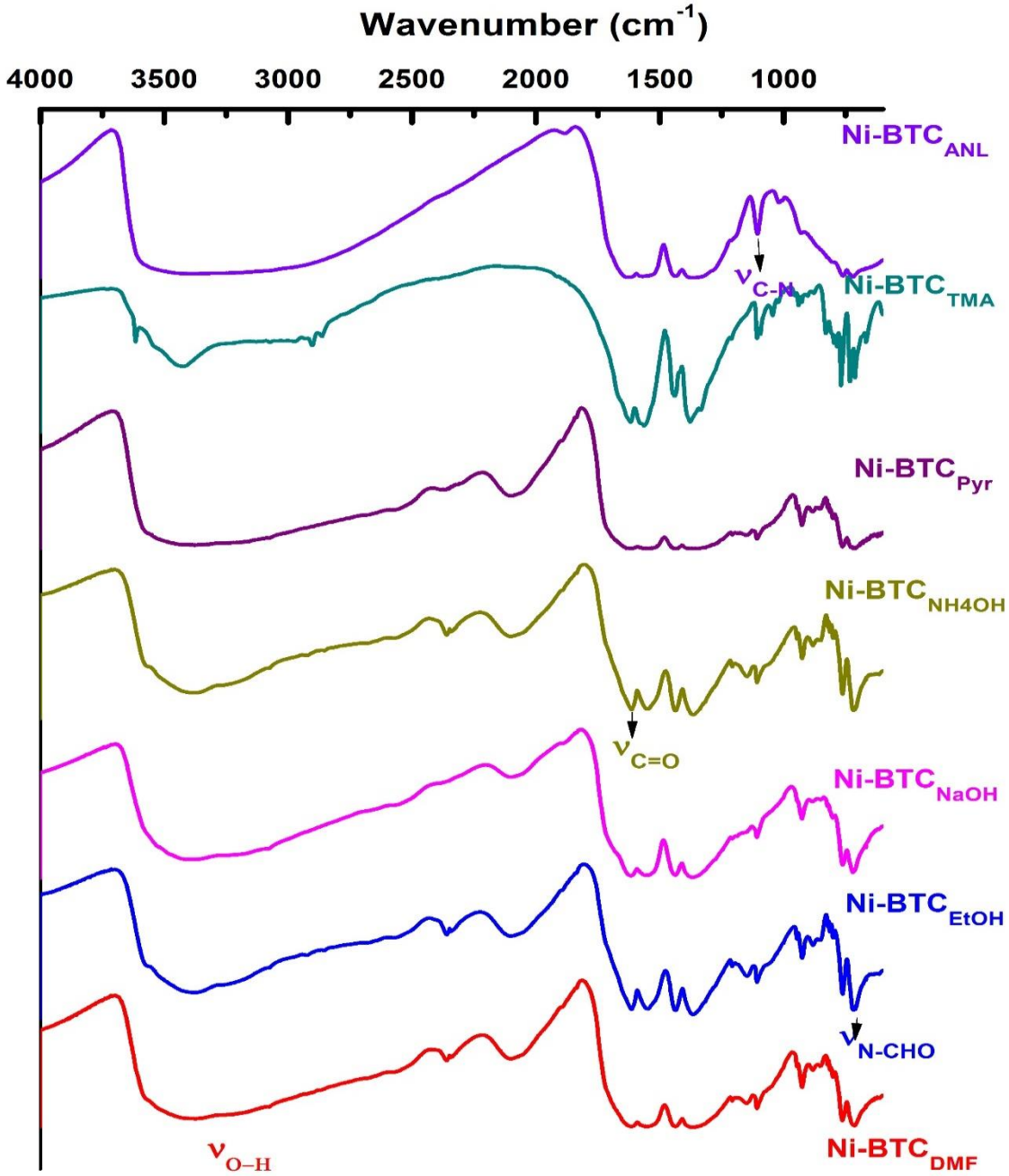

Fig. 5.2 FT-IR Spectra of Ni-BTCs

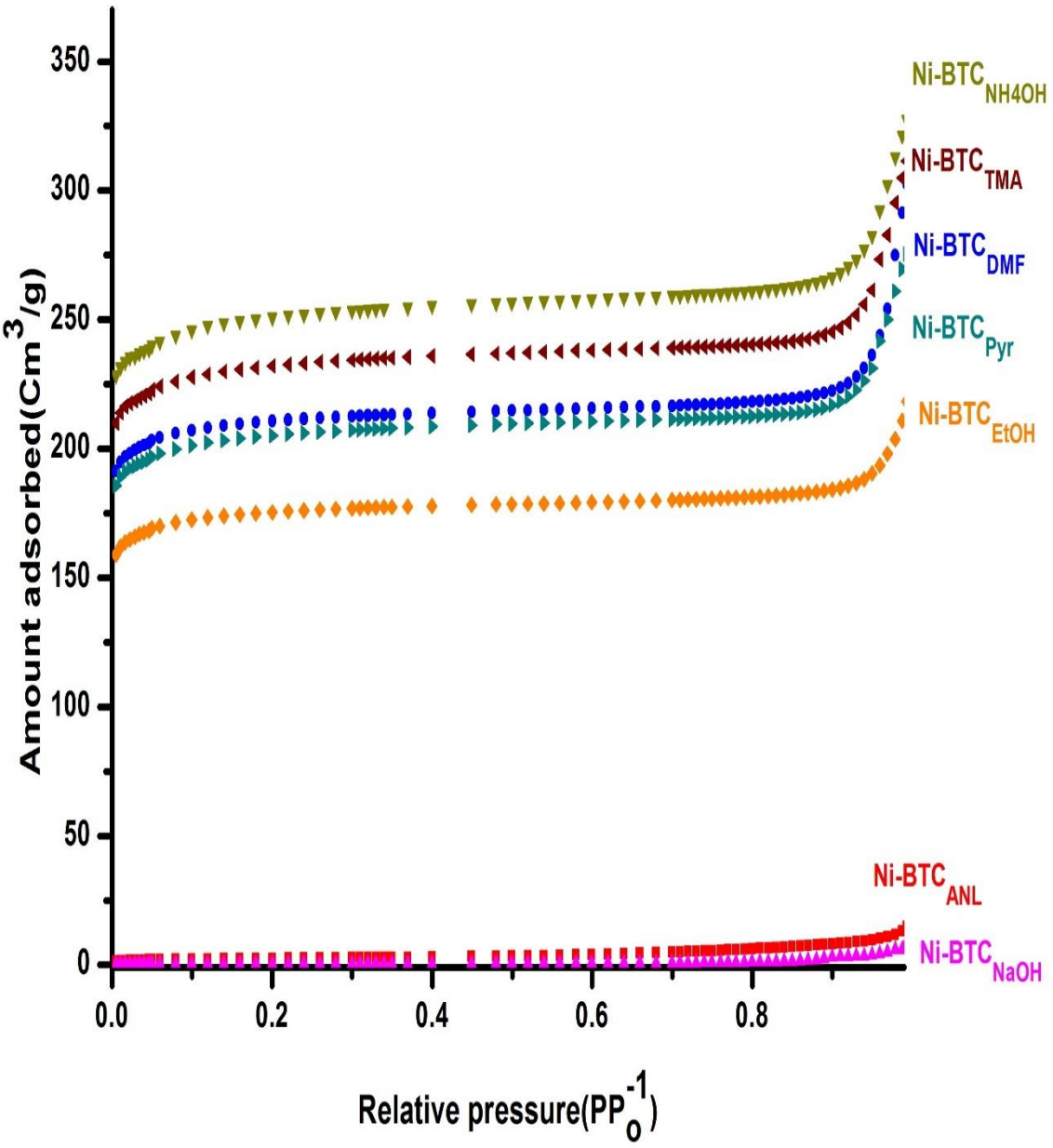

Fig. 5.3 BET adsorption isotherms of Ni-BTCs

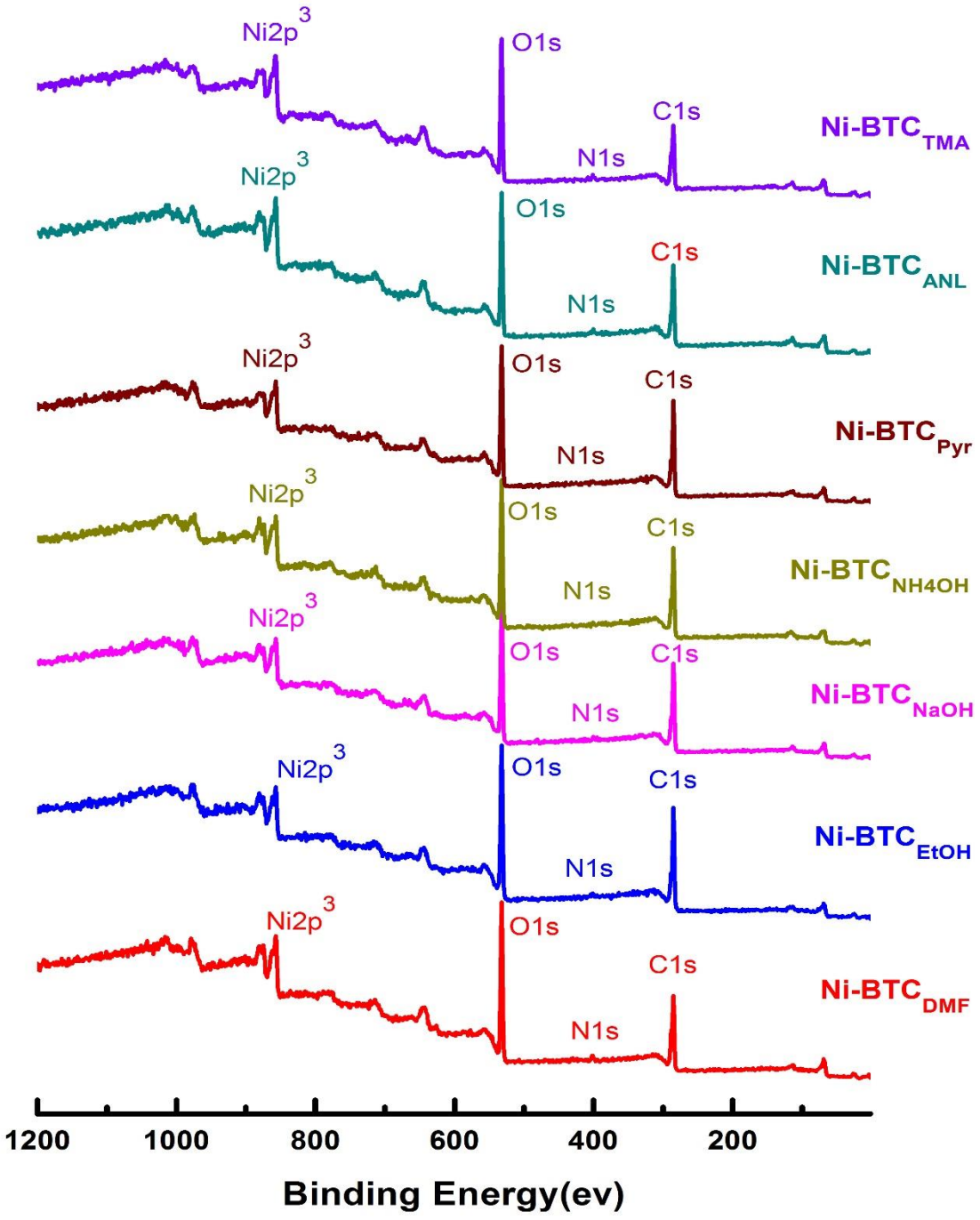

Fig. 5.4 XPS analysis graphs of Ni-BTCs

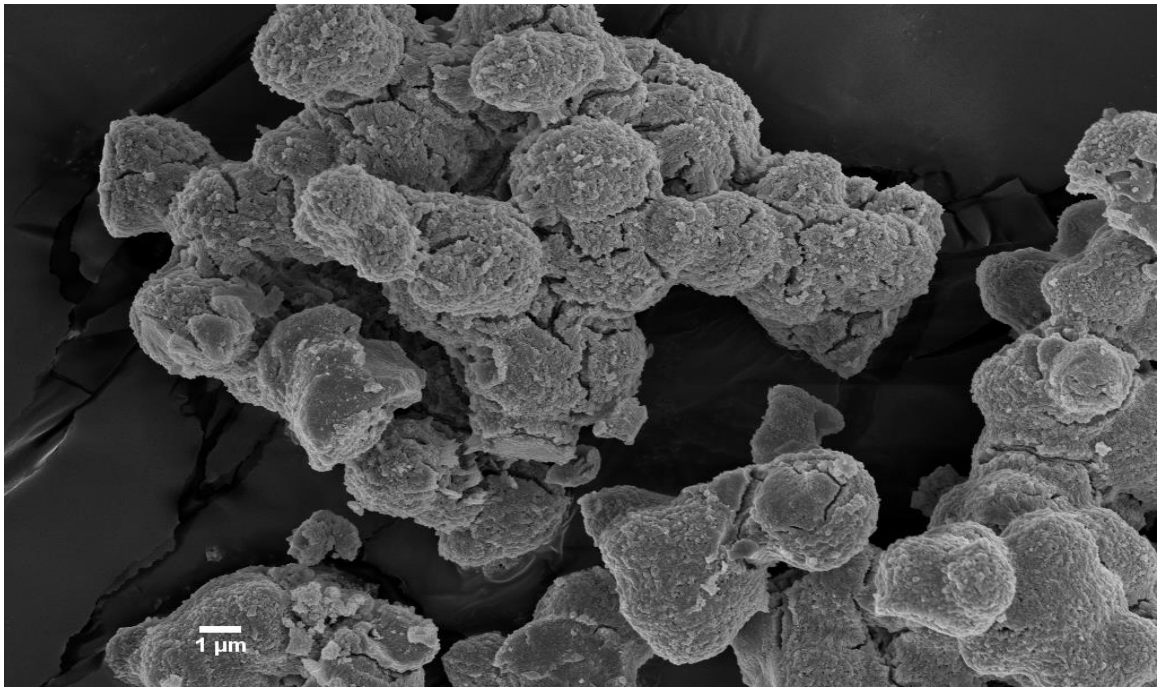

Fig. 5.5 (a) SEM image of Ni-BTC_{Anl}

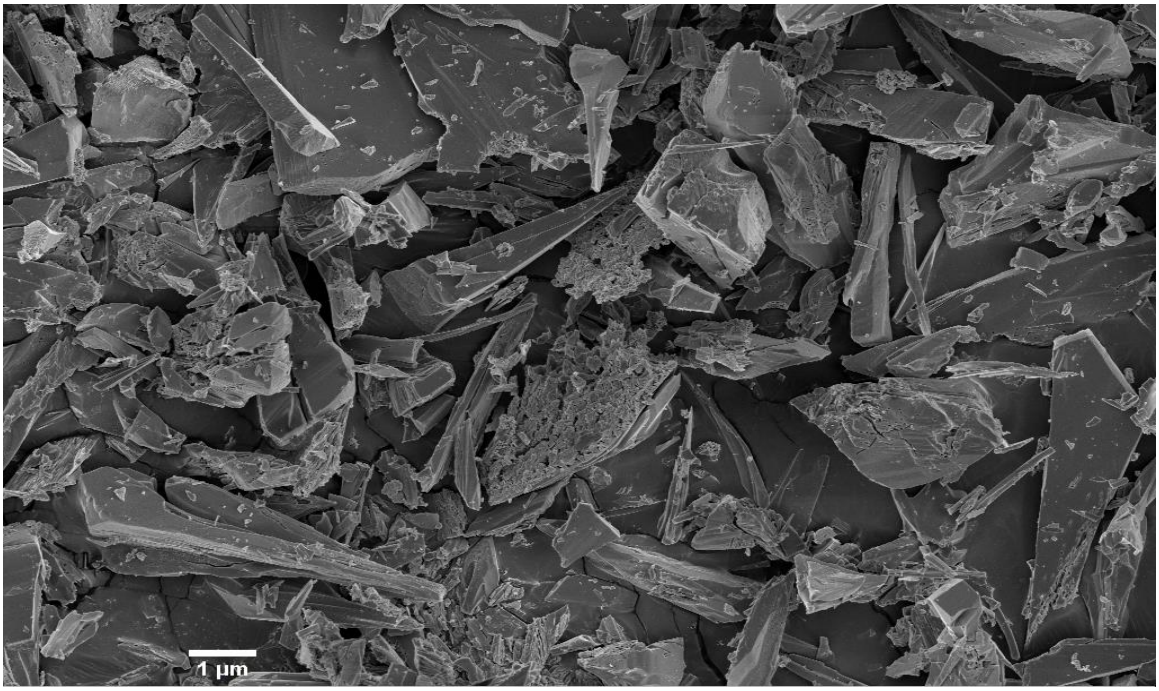

Fig. 5.5 (b) SEM image of Ni-BTC_{DMF}

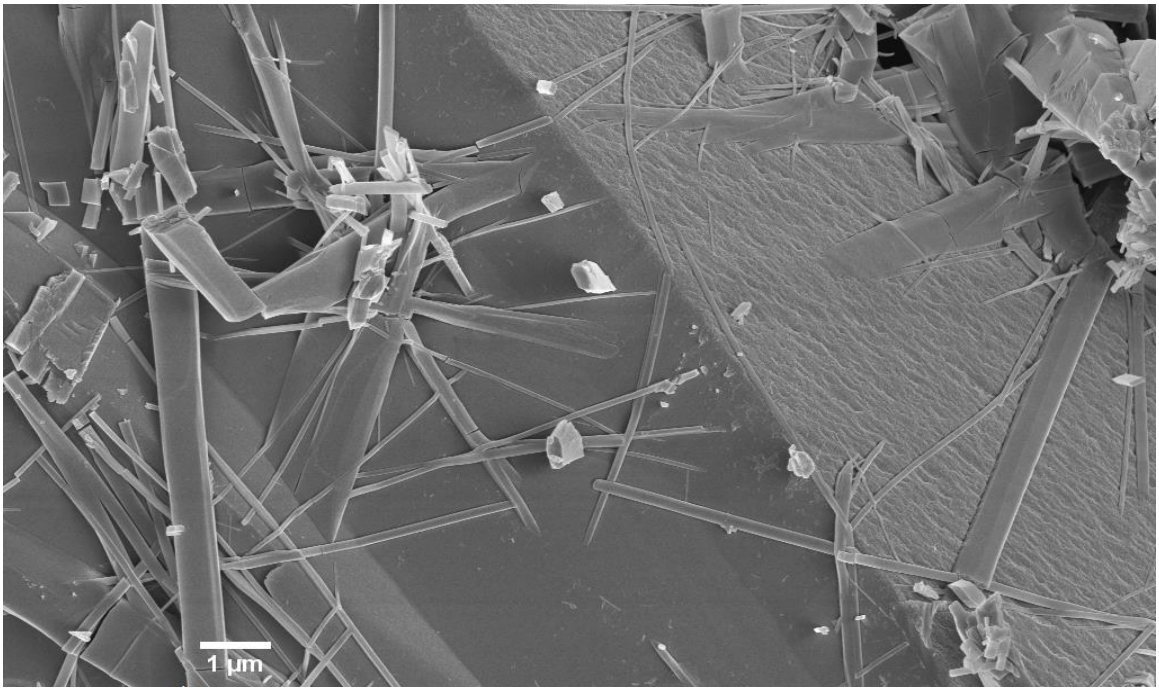

Fig. 5.5 (c) SEM image of Ni-BTC_{EtOH}

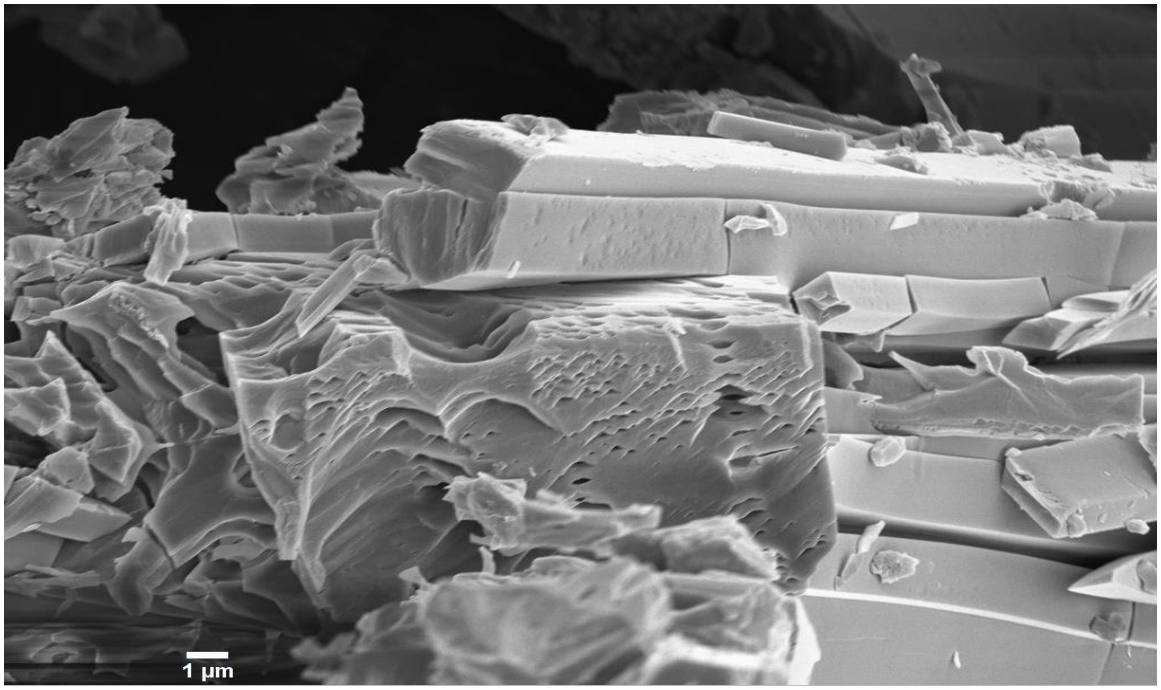

Fig. 5.5(d) SEM image of Ni-BTC_{NaOH}

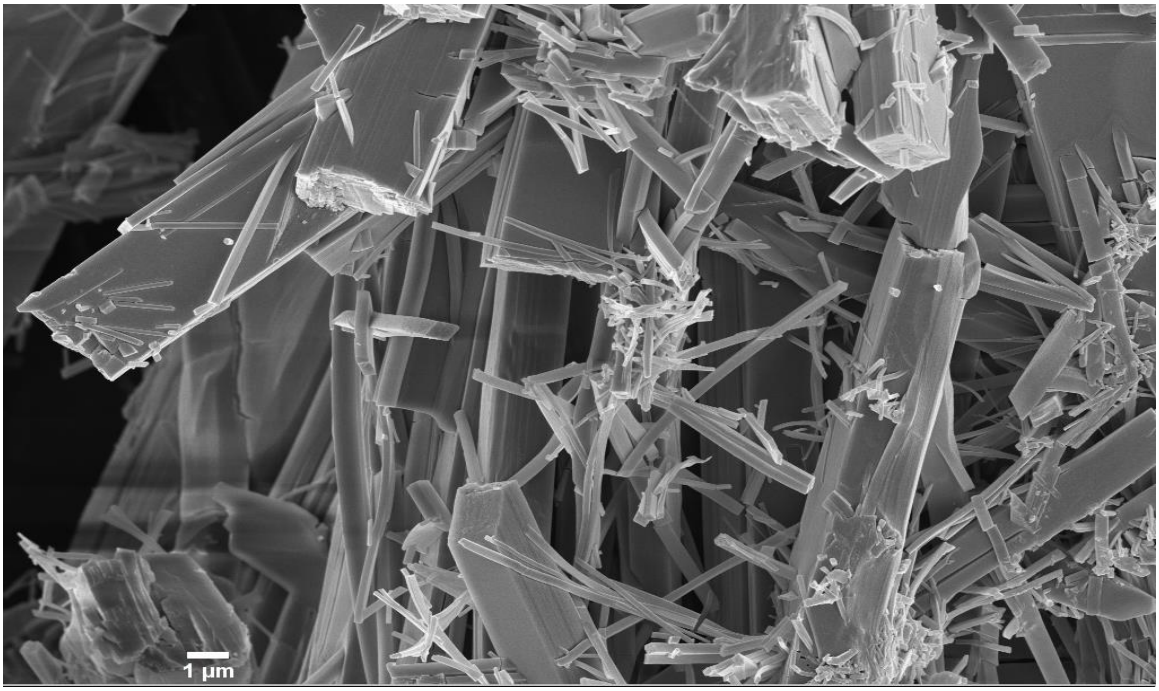

Fig. 5.5 (e) SEM image of Ni-BTC_{NH4OH}

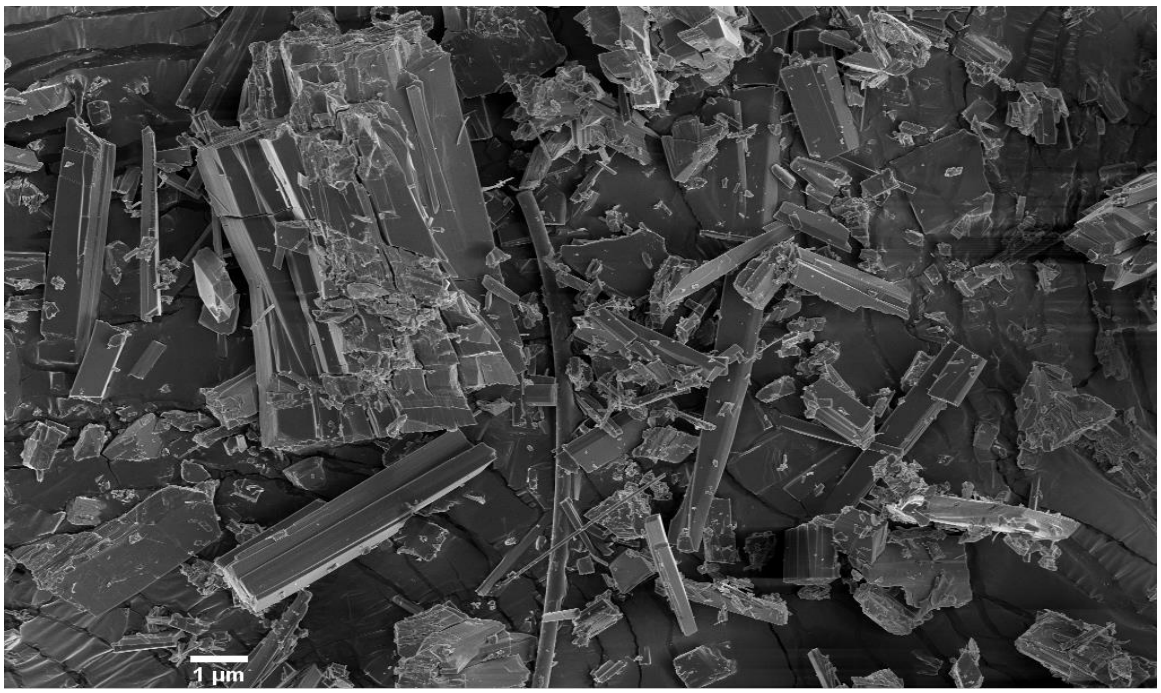

Fig. 5.5 (f) SEM image of Ni-BTC_{Pyr}

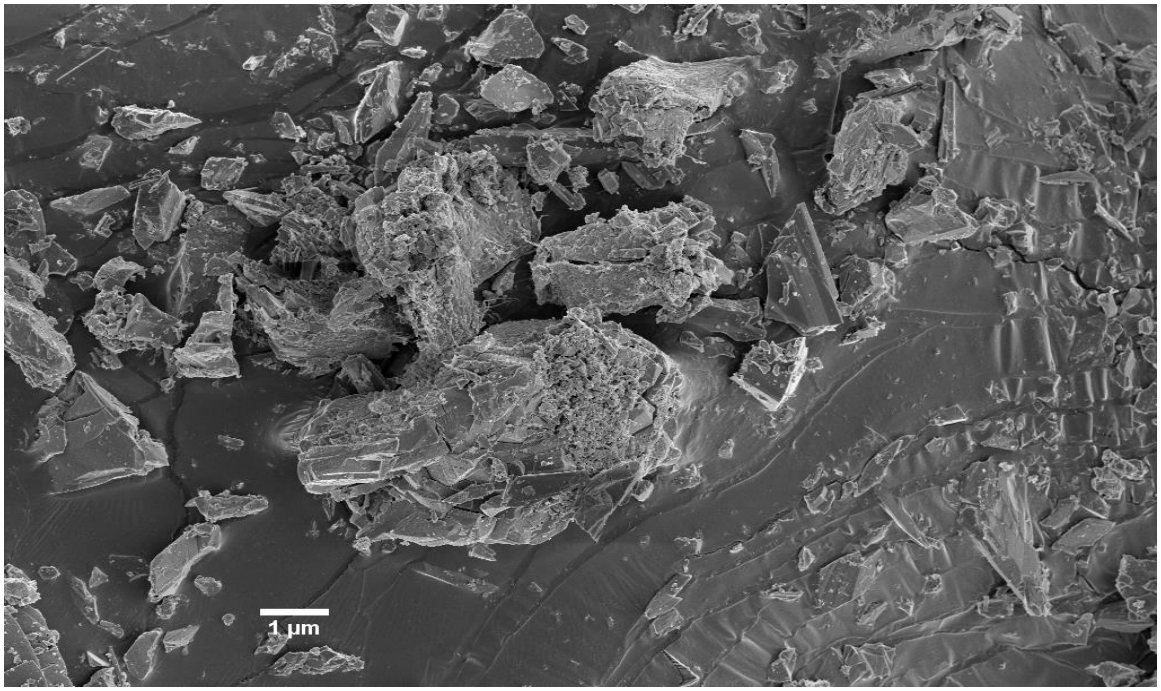

Fig. 5.5 (g) SEM image of Ni-BTC_{TMA}

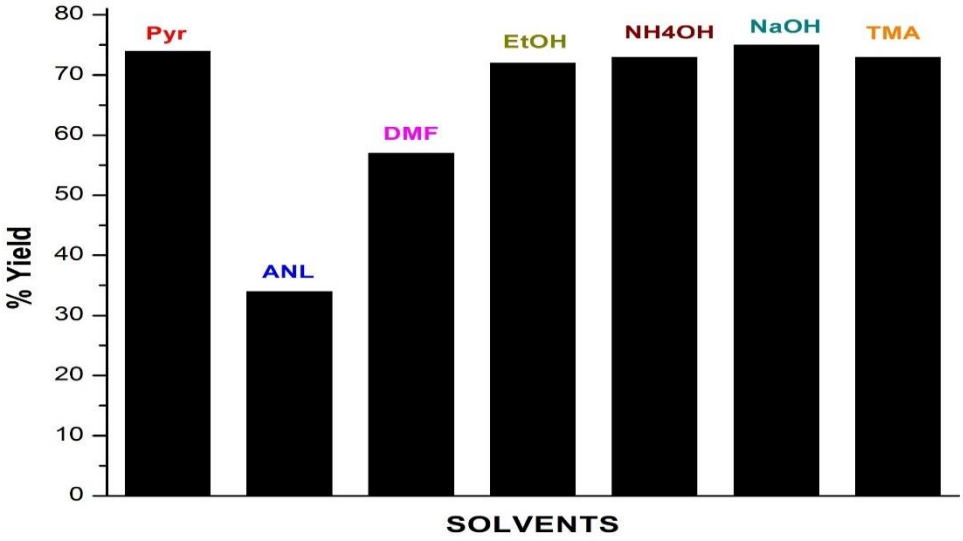

Fig. 5.6 % yield attained with different solvents

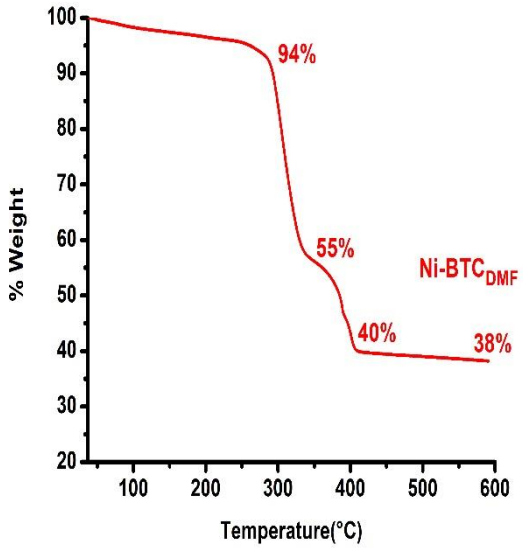

(a)

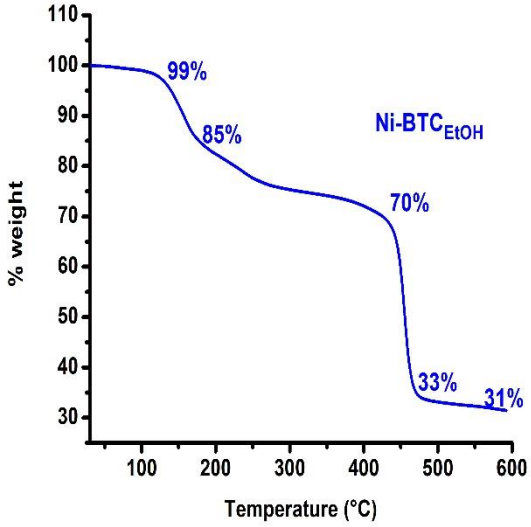

(b)

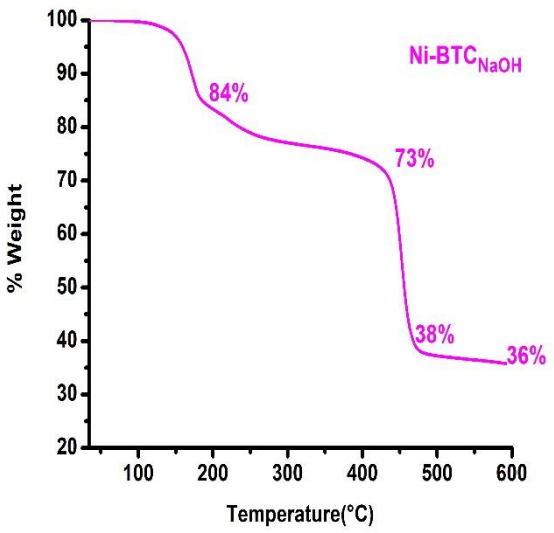

(c)

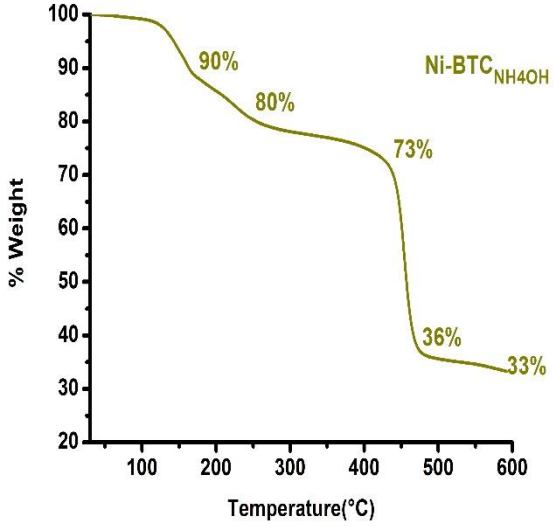

(d)

Fig. 5.7 Thermo gravimetric analysis of (a) Ni-BTC$_{DMF}$ (b) Ni-BTC$_{EtOH}$ (c) Ni-BTC$_{NaOH}$ and (d) Ni-BTC$_{NH4OH}$

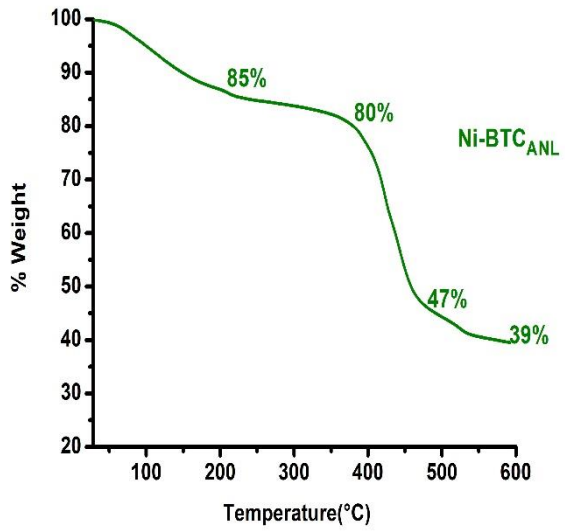

(e)

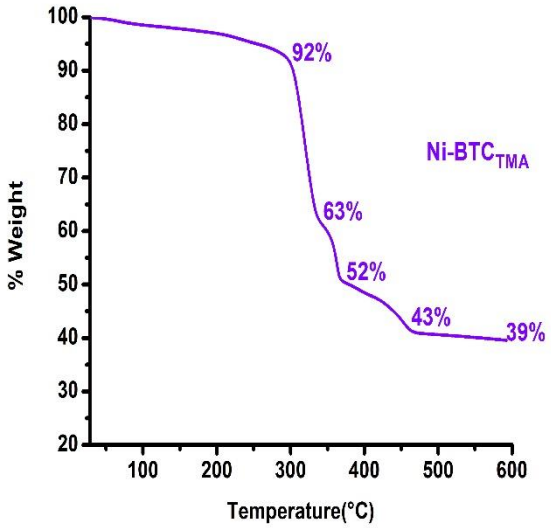

(f)

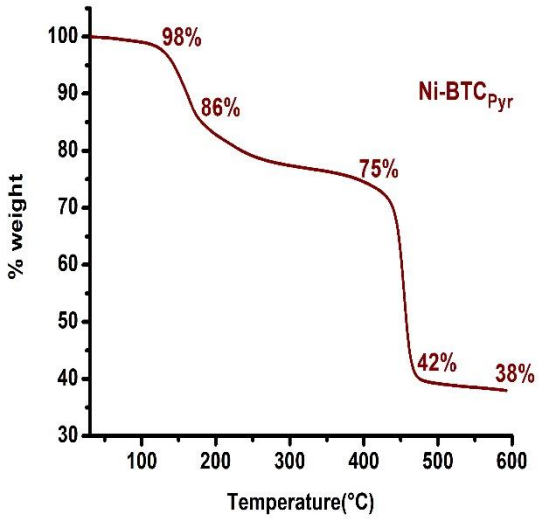

(g)

Fig. 5.7 Thermo gravimetric analysis of (e) Ni-BTC$_{Pyr}$ (f) Ni-BTC$_{TMA}$ and (g) Ni-BTC$_{Anl}$

VI. Hydrothermal synthesis of Fe based MOFs with process economy approach

6.1 Introduction

Porous metal–organic frameworks (MOFs) are considered to be an important class of advanced functional materials due to their unique coordination structures, variant configuration and potential applications [118,159,211]. The features of MOFs such as exceptionally high porosities, with regular pores and extremely high surface areas, well-defined crystalline structures, and more accessible bulk volume are hallmark which have attracted the attention of both academia and industry [212]. The crystalline iron (III) trimesate (MIL-100(Fe)) has three dimensional cubic structure with two types of meso-cages (25–29Å) accessible through micro-porous windows (5–9Å). MIL-100(Fe) is also known as a cheap and biocompatible material. Considering its physicochemical properties and non-toxicity, MIL-100(Fe) can be a good candidate as a new adsorbent and catalyst.

Here we have adopted a solvent less synthetic approach for Fe-BTC powder. We conducted synthesis process at 130˚C for 8 hours and were able to obtain noticeable MOF yield. Another unique feature of this study was the application of detailed diffraction indexing for diffraction patterns of as prepared and heat treated (200˚C) MOF powders. This application not only validated the crystalline nature of powders but also gave an insight for any possible susceptibility of material to oxidize at higher temperature.

6.2 Experimental

6.2.1 Materials and methods

The chemicals including iron chloride hexahydrate ($FeCl_3.6H_2O$) and trimesic acid ($C_6H_3(COOH)_3$) were purchased from sigma Aldrich and used without further purification. A mixture

of $FeCl_3.6H_2O$ (2.43g) with $C_6H_3(COOH)_3$ (0.83g) was dissolved in 30ml de-ionized water, stirred for 30 minutes, then loaded in Teflon liner and heated at 130˚C in autoclave for 8 hours. After hydrothermal treatment mixture was cooled down to room temperature. The recovered orange slurry for Fe-BTC was then centrifuged at 3500 rpm. A 30-45 minutes centrifuging was enough to separate out the clear solution from powder product residue. The powder was then washed with de-ionized water. After drying at room temperature, an orange Fe-BTC product was obtained.

6.3 Characterization

The crystallinity and phase purity of synthesized MOF was analyzed using X-ray diffractometer (Rikagu D/MAX 2200H, Bede model200). The X-ray diffraction (XRD) measurement was performed using a Cu-K_α radiation source of wavelength λ=1.5406Å and the diffraction intensity were recorded in 2θ range of 5-80˚with a step of 0.02˚. The particle sizes of synthesized powders were calculated by using the Debye-Scherrer (DS) equation (6.1), as shown below:

$$\boldsymbol{D = \frac{K\lambda}{\beta \cos \theta}} \qquad \textbf{(6.1)}$$

Where "*D*" is crystallite size, "λ" is the radiation wavelength (1.5406 Å), "β" is the full width half maximum (FWHM) for diffraction peak, "θ" is the diffraction angle. "k" is the shape factor and an average value for "k" was assumed as 0.9. The FT-IR spectra were collected on a BRUKER IFS66/S Fourier transform IR spectrophotometer in KBr disks at room temperature. The scanning electron microscopy (SEM) observations were done on JEOL, JEM1200EX II set up equipped with field emission gun. The measurements of N_2 adsorption were performed on a Quanta chrome AUTOSORB-1-MP apparatus at −196°C, and the specific surface areas of the investigated samples

were calculated using the multiple-point Brunauer–Emmett–Teller (BET) method. The samples were out gassed under vacuum at 150°C for 12 h, prior to the adsorption measurements.

6.4 Results and Discussion

The XRD pattern of Fe-BTC powder in as prepared and heat treated (at 200˚C) forms (Fig. 6.1(a) &(b)) in major portion, matched with the simulated one in literature [213,214] which confirmed that Fe-BTC has been successfully synthesized. The relative peaks at 2θ Bragg reflection values of 9˚, 10˚, 12˚, 15˚, 19˚, 20˚, 24˚ and 28˚ were obtained. The Bragg's equation (6.2) gives relationship between various diffraction lines and inter planer distance [215].

$$\lambda = 2dsin\theta \qquad (6.2)$$

A developed mathematical expression (6.3)

$$sin^2\,\theta/\lambda^2 = (h^2+k^2+l^2)/4a^2 \qquad (6.3)$$

has been employed for detailed indexing of diffraction pattern (Table 6.1). Here (*h k l)* values defined the positional co-ordinates of diffraction peaks and "a" is lattice parameter. The value of "a" for Fe-BTC calculated from equation (3) was 19.6Å. The relative positioning of peaks and corresponding (*h k l*) values confirmed the cubic nature of the synthesized Fe-BTC powder. There appeared to be no difference in structure of powder after heating it at 200˚C as the diffraction peaks are always at the same positions that suggested its compactness at higher temperature. The

FT-IR spectra (Fig. 6.2) indicated C=O vibration band at 1710-1720 cm^{-1} [216]. The absorption bands in the range of 1400-1600cm^{-1} and 600-780cm^{-1} owed to C-H bond stretching. The wide band in the range of 3300-3600 cm^{-1} suggested the presence of water molecules owed to O-H stretching. The adsorption isotherm for Fe-BTC exhibited the hysteresis loop similar like type I isotherm [217–219] (Fig. 6.3), typical for adsorbent of 1.5-100nm. The adsorption curve showed an initial increase (55%) in uptake at exposure of material to N_2 gas molecules. This uptake then became steady with increase in relative adsorption pressure as the pores are filled with monolayer and thereafter point of inflection occurred near the completion of first monolayer.

The BET surface area assessed from N_2 adsorption at -196 °C was 885cm^2/g which is much less as compared to those reported in literature [220–222]. The discrepancy may be due to the relative pressure range difference (P/P_0) under which the measurements have been made. The product yield was around 48% based on stoichiometric calculations. The size of crystal as calculated by using XRD pattern and equation (1) was 39nm.

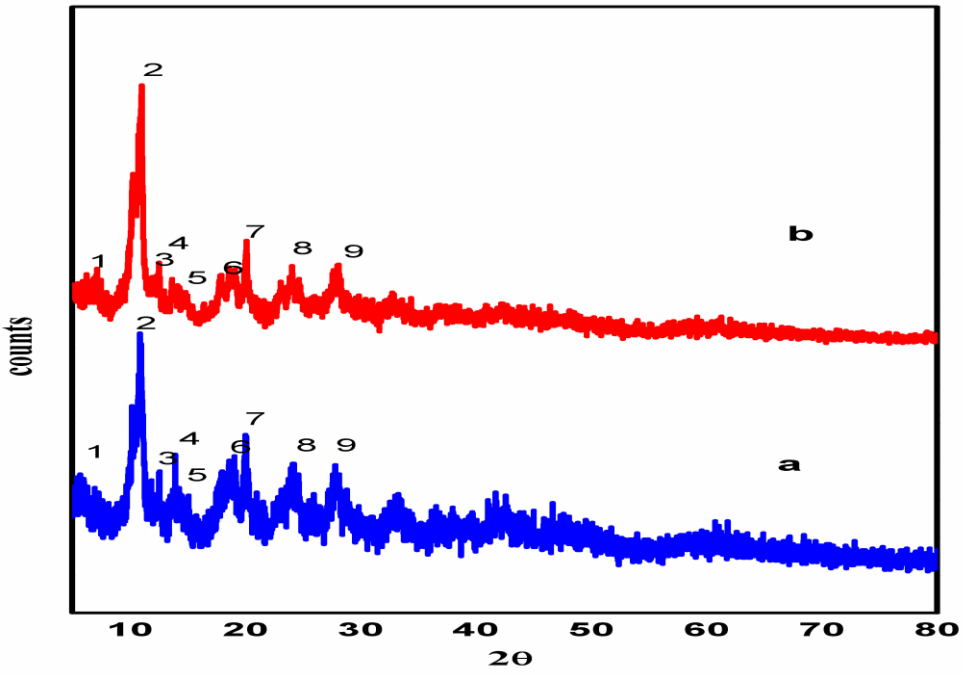

Fig. 6.1(a &b) XRD pattern for Fe-BTC

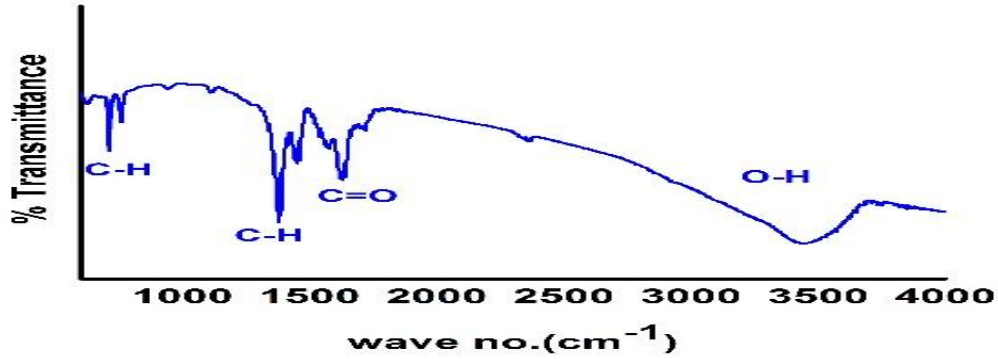

Fig. 6.2 FT-IR for Fe-BTC

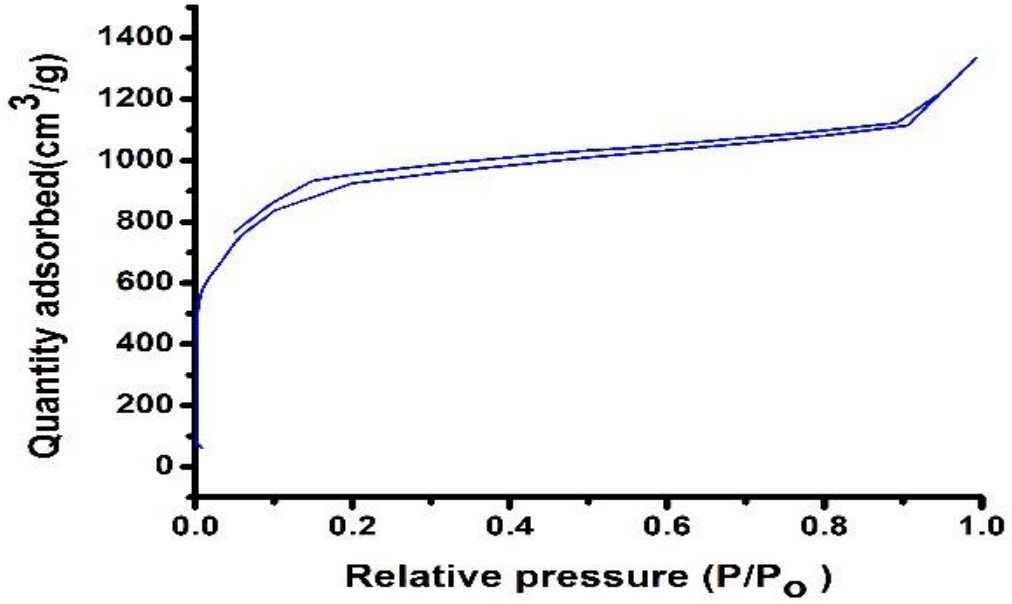

Fig. 6.3 Adsorption isotherm for Fe-BTC

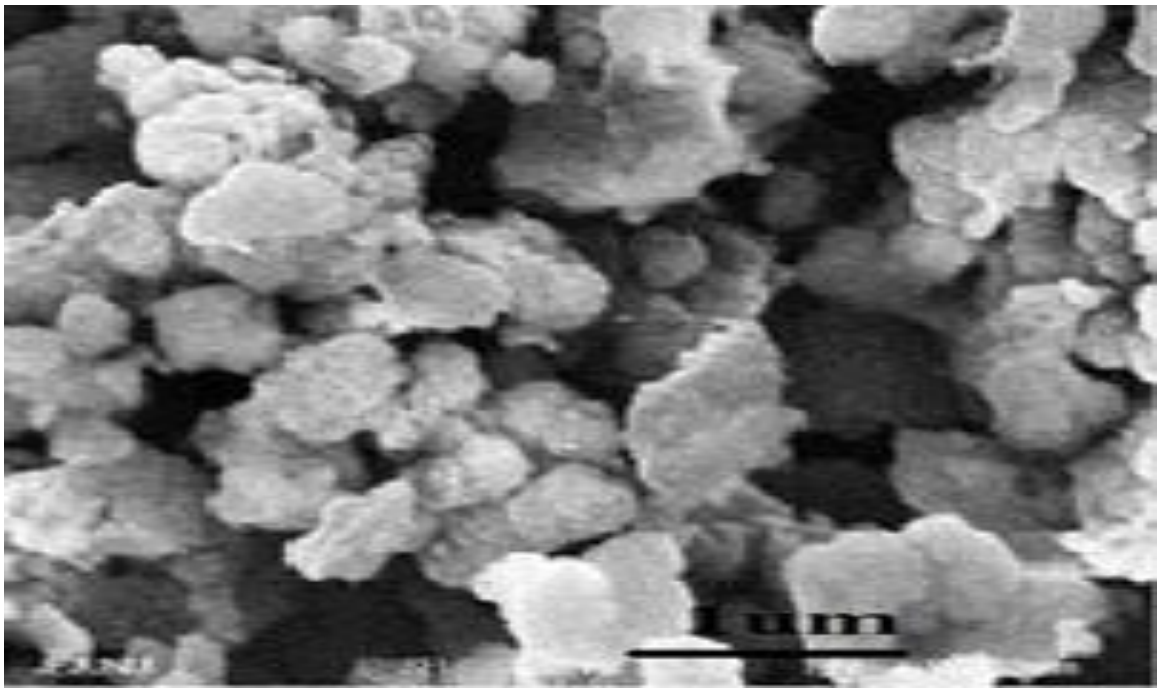

Fig. 6.4 Micro structure of Fe-BTC

Table 6.1 Indexing of Diffraction pattern for Fe-BTC

Peak No.	**1**	**2**	**3**	**5**	**6**	**7**	**8**	**9**
2θ	9	10	12	15	19	20	24	28
d	0.982	0.884	0.737	0.59	0.467	0.443	0.37	0.318
(h k l)	(100)	(010)	(110)	(111)	(200)	(210)	(211)	(310)

VII. Cost effective and low energy consuming hydrothermal synthesis of Ni based MOF

7.1 Introduction

Porous metal–organic frameworks (MOFs) are an important class of advanced functional materials. These materials have unique coordination structures and variant configurations due to which MOFs have wide range of applications [151,159,211]. The features of MOFs such as exceptionally high porosities, with regular pores and extremely high surface areas, well-defined crystalline structures, and more accessible bulk volume are hallmark which have attracted the attention of both academia and industry [223].

Ni-BTC is one such an example of MOF which is known to belong to M (BTC) (M = Cr, Fe, Ni, Cu, Mo). It has iso-structural relationship along with permanent porous structure. Hydrothermal and solvo-thermal synthesis has been reported by O. M. Yaghi *et al.*[224] and Casey R. Wade *et al.*[225]. There has been significant research going on for micro- and mesoporous materials as adsorbents for heat transfer applications in closed systems such as thermally driven adsorption chillers and heat pumps [226,227]. For a cooling application, the choice of the adsorbent/adsorptive working pair is key factor. The best pair choice is determined by the amount of heat that can be extracted from the evaporator per adsorption cycle. In general, the present generation of adsorption chillers use silica gels as adsorbent. The key problem with silica gel adsorbents for these applications is that most of the water adsorption occurs at too high relative pressures. However in recent times nickel based MOF (ISE-1) [228] has been reported which have good adsorption properties such as consistent water loading capacity over large number of

adsorption cycles. This metal organic framework is less hydrophilic than silica gel and readily releases water molecules at low desorption temperature.

The hydrothermal processes employed earlier had the drawback of high operating temperatures (180˚C) and longer reaction times (12 hours or sometimes more than that) along with consumption of large amount of solvents. Therefore an interest was there to investigate a hydrothermal process which is less time consuming and more economical.

Here we have adopted a low temperature synthetic approach for Ni-BTC powder. We conducted synthesis process at 130˚C for 8 hours and were able to obtain noticeable MOF yield. We applied diffraction indexing over diffraction patterns of as synthesized and heat treated Ni-BTC. This way we were able to gauge the crystalline nature of product in as synthesized condition and higher temperature stability at heat treatment temperature.

7.2 Experimental

7.2.1 Materials and Method

The chemicals including nickel nitrate hexahydrate ($Ni(NO_3)_2.6H_2O$) and trimesic acid ($C_6H_3(COOH)_3$) were purchased from sigma Aldrich and used without further purification. A mixture of $Ni(NO_3)_2.6H_2O$ (0.84g) with $C_6H_3(COOH)_3$ (0.42g) was dissolved in 30ml de-mineralized water, stirred for 30 minutes, then loaded in Teflon liner and heated at 130˚C in autoclave for 8 hours. After hydrothermal treatment solution was cooled down to room temperature. The solution was then filtered and green precipitates of Ni-BTC were recovered. The precipitates were then washed with de-ionized water and dried thoroughly.

7.3 Characterization

The crystallinity and phase purity of synthesized MOFs was analyzed using X-ray diffractometer (Rikagu D/MAX 2200H, Bede model200). The X-ray diffraction (XRD) measurement was performed using a Cu-K_α radiation source of wavelength λ=1.5406Å and the diffraction intensity were recorded in 2θ range of 5-80˚with a step of 0.02˚.

The particle sizes of synthesized powders were calculated by using the Debye-Scherrer (DS) equation (7.1), as shown below:

$$\boldsymbol{D = \frac{K\lambda}{\beta \cos\theta}} \qquad \textbf{(7.1)}$$

Where "*D*" is crystallite size, "λ" is the radiation wavelength (1.5406 Å), "β" is the full width half maximum (FWHM) for diffraction peak, "θ" is the diffraction angle. "k" is the shape factor and an average value for "k" was assumed as 0.9. The FT-IR spectra were collected on a BRUKER IFS66/S Fourier transform IR spectrophotometer in KBr disks at room temperature. The scanning electron microscopy (SEM) observation was done on JEOL, JEM1200EX II set up equipped with field emission gun. The measurement of N_2 adsorption was performed on a Quanta chrome AUTOSORB-1-MP apparatus at −196°C, and the specific surface area of the investigated sample was calculated using the multiple-point Brunauer–Emmett–Teller (BET) method. The sample was out gassed under vacuum at 150°C for 12 h, prior to the adsorption measurements.

7.4 Results and Discussion

Ni-BTC has been synthesized previously at room temperature [229] and by high temperature [209] using different solvents. In this work we have synthesized Ni-BTC by employing intermediate temperature of 130°C for 8 hours operation without using any conventional organic solvents. The process yield was 38% based on stoichiometric calculations and is 25% less than those reported [229]. There appeared to be a slight mismatch between the obtained XRD pattern of as prepared Ni-BTC (Fig. 7.1(a)) as compared to the one reported in literature[228].

Here the diffraction peaks were shifted to lower angles. The most commonly cited reasons [11] for such kind of discrepancy are changes in cell parameters typical for solid solutions, induced compressive stresses and to some extent equipment error. The diffraction peaks were observed at 2θ values of 4°, 10°, 13°, 15°, 18°, 20°, 22°, 24°, 25.5°, 28° and 30°, are tabulated along with their (*h k l*) and inter planner spacing values ”d” (Table. 7.1).

The calculated value of lattice parameter “a” for Ni-BTC was 44.1 Å. For heat treated sample, major comparable diffraction lines appeared on almost similar angles as were those for as prepared sample (Fig. 7.1(a) &1(b)), But in addition to those, there were a few additional peaks at 2θ values of 12°, 14°, 23° and 24.5°.

Those additional peaks might be a result of localized oxide formation within the MOF structure due to which diffraction pattern of heat treated sample gave somewhat distorted image. The observed FT-IR spectra of synthesized compound is shown in (Fig. 7.2) depicted C=O stretch at 1780cm^{-1}, O-H band between 1400 and 1600cm^{-1} and C-O stretch at 1200 and 1350cm^{-1}.

The adsorption isotherm for Ni-BTC (Fig. 7.3)) resembled typical type II category[230–232] which is a principle characteristics of solids with micro pores. The measured BET surface area was 137m^2/g. The crystal shape as revealed in microstructure (Fig. 7.4) was nano rods with high aspect ratio. The value of calculated crystal size was found to be 44nm.

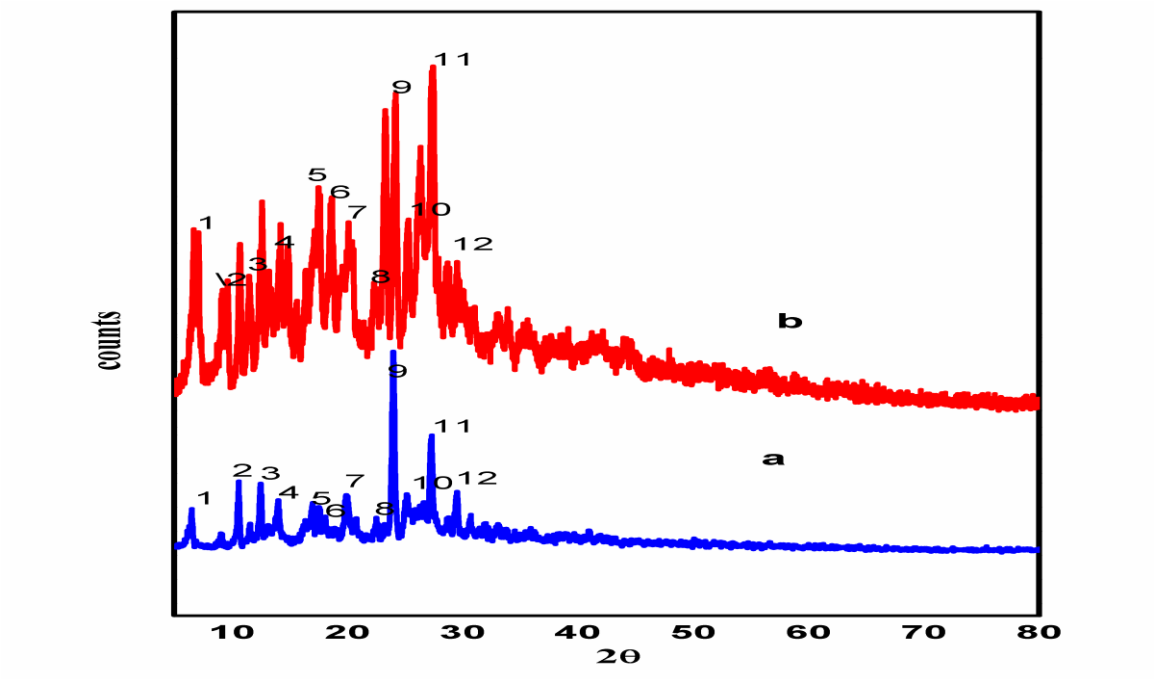

Fig. 7.1 XRD patterns of Ni-BTC

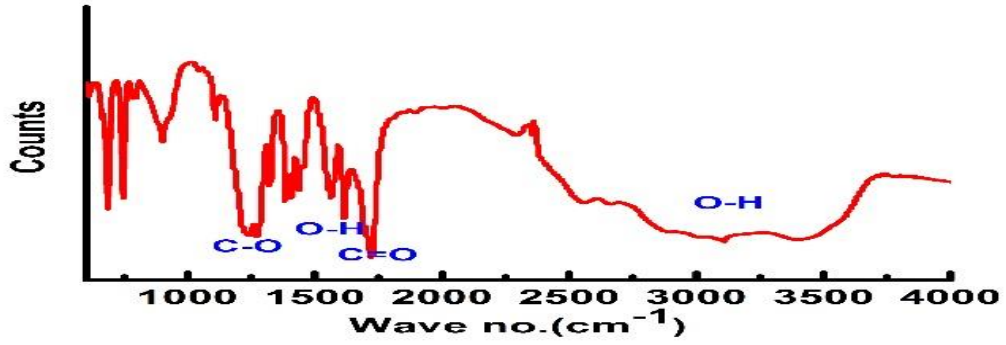

Fig. 7.2 FT-IR of Ni-BTC

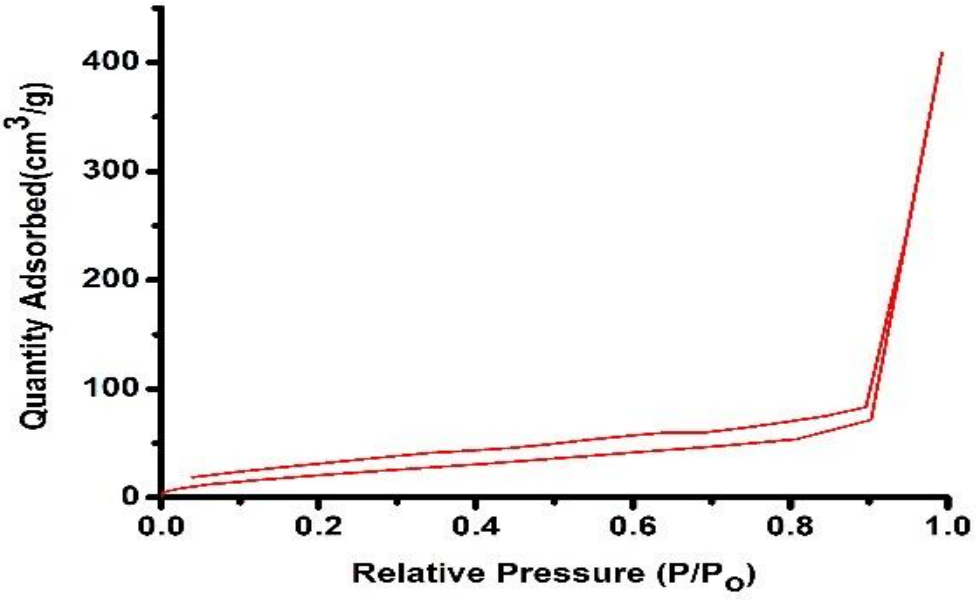

Fig. 7.3 Adsorption isotherm for Ni-BTC

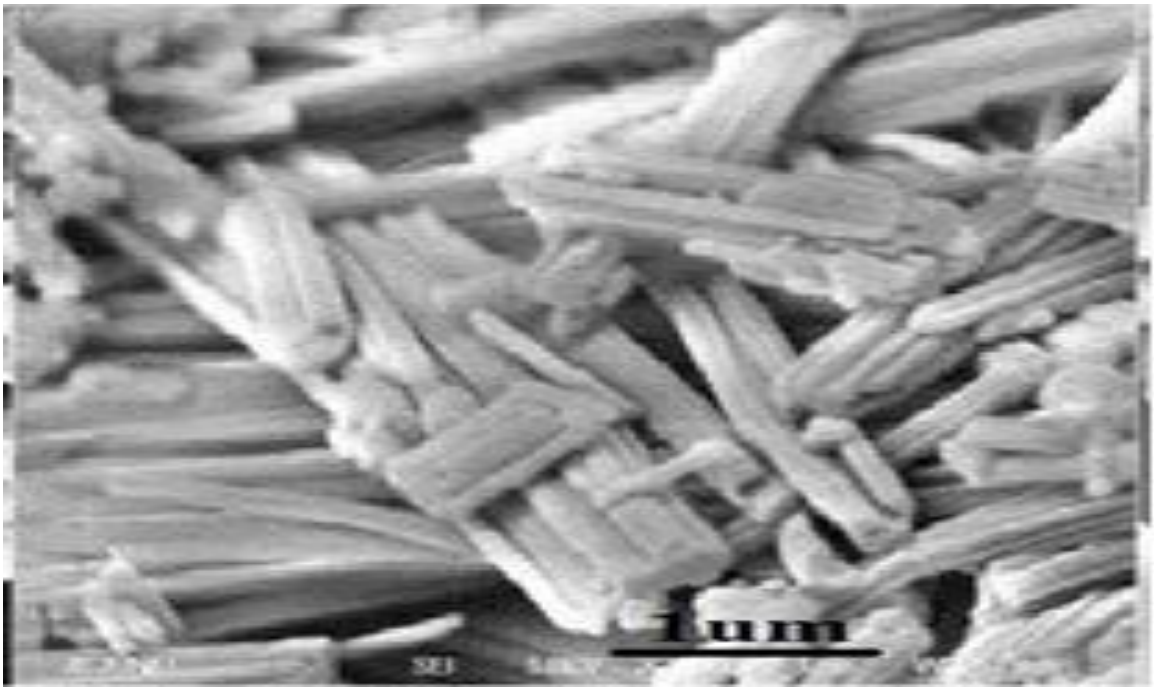

Fig. 7.4 Micro structure of Ni-BTC

7.1 Table Indexing of Diffraction pattern for Ni-BTC

Peak No.	**1**	**2**	**3**	**4**	**5**	**7**	**8**	**9**	**10**	**11**	**12**
2θ	4	10	13	15	18	20	22	24	25.5	28	30
d	2.207	0.884	0.68	0.59	0.492	0.422	0.404	0.37	0.35	0.318	0.298
(h k l)	(100)	(211)	(311)	(321)	(420)	(511)	(521)	(600)	(620)	(631)	(711)

VIII. Conclusions

This thesis work is based on three different synthesis of Copper and Nickel based MOFs.

First Cu-BTC, a copper based MOF was synthesized via ultrasonic treatment in the presence of some conventional and non-conventional solvents. It was demonstrated that the scope for the usage of solvents in synthesis of Cu-BTC is quite wide. In addition to conventional solvent combination of DMF/EtOH/H_2O, which has been used extensively in earlier reported synthesis, four new combinations of solvents have been examined successively. Extremely high BET surface areas of 1434m^2/g and 1401m^2/g were recorded for Cu-BTC_{DMF} and Cu-$BTC_{DMF+EtOH}$.

These are unprecedented so far from room temperature ultrasonic synthesis with short period of time. It was found that process yield enhanced progressively with sonication time due to prolong provision of activation energy to reactants in liquid state. The applied sonication power also has a strong bearing upon final product yield. Too much higher power tend to dissolve the product and resulted in decreased yield even after prolong sonication time. A change in ultrasonic power level from 20% to 40% has no effect on resultant process yields as the two outputs were found to be equal. Somewhat intermediate power level such as 60% seemed to befitting for a consistent process yield.

In another work, the ultrasonic synthesis route for Ni based porous solids, while using 1, 3, 5-benzenetricaroxylic acid has been successfully explored. The effects of three different power levels along with varying probe temperatures upon process has been demonstrated. Ni-BTC obtained with 60% power level showed highest porosity with lowest crystal size. Surface areas

and other adsorption properties of synthesized Ni-BTCs confirmed their porous nature. The process yield was found to vary with operating power level. Higher power level favored the process yield as we see a yield of up to 88% at 80% power level. In addition, a probe temperature of 60 °C was found to be the most appropriate operating conditions at any power level.

Ni-BTC was also synthesized by solvothermal process with combinations of organic and inorganic solvents. The product yields and physical properties were found to vary in each process. The major finding are summarized as;

1. A combination of NH_4OH and DMF as solvents resulted in a Ni based MOF with high surface area (845 m^2/g) along with high pore volume (0.5026 cm^3/g) and particle size of 7nm.

2. Appreciably high process yields were obtained in most of experimental results.

3. In general surface areas and physiosorption properties tend to vary in the order of Ni-BTC_{NH4OH}> Ni-BTC_{TMA}> Ni-BTC_{DMF} > Ni-BTC_{Pyr} >Ni-BTC_{EtOH} >Ni-BTC_{Anl} >Ni-BTC_{NaOH}.

In hydrothermal synthesis process for iron (Fe) based MOF, an intermediate process temperature (130°C instead of 170-180°C) and reduced reaction time (8 Hours instead of 12 Hours or more) has been used. This way conventional process parameters has been maneuvered.

We were able to accomplish the synthesis successfully under these new set conditions with recognizable product yield.

In a nutshell, this synthesis process at intermediate temperature and reduced operation time seemed to be cost effective and less energy consuming. Here we have also investigated the high temperature stability of this MOF by examining XRDs patterns of it's as prepared and heat treated samples. Fe-BTC product from the current work has shown compatibility and high temperature stability as there appeared to be no change in its diffraction pattern before and after heat treatment.

XI. Acknowledgements

These experimental works were supported by the National Research Foundation Korea (NRF) grants funded by the ministry of Science, ICT & Future Planning (No. 2009-0092786 & 2014R1A2A1A01006421.

X. References

[1] C. Janiak, Engineering coordination polymers towards applications.pdf, Dalt. Trans. (2003) 2781–2804. doi:10.1039/ b305705b.

[2] A.K. Cheetham, C.N.R. Rao, R.K. Feller, Structural diversity and chemical trends in hybrid inorganic-organic framework materials., Chem. Commun. (Camb). (2006) 4780–4795. doi:10.1039/b610264f.

[3] J.R. Long, O.M. Yaghi, The pervasive chemistry of metal-organic frameworks., Chem. Soc. Rev. 38 (2009) 1213–1214. doi:10.1039/b903811f.

[4] R.I. Walton, Subcritical solvothermal synthesis of condensed inorganic materials., Chem. Soc. Rev. 31 (2002) 230–238. doi:10.1039/b105762f.

[5] B. Wisser, A.-C. Chamayou, R. Miller, W. Scherer, C. Janiak, A chiral C3-symmetric hexanuclear triangular-prismatic copper(ii) cluster derived from a highly modular dipeptidic N,N′-terephthaloyl-bis(S-aminocarboxylato) ligand, CrystEngComm. 10 (2008) 461. doi:10.1039/b717207a.

[6] H. Thakuria, B. moni Borah, G. Das, ZnO Nanoparticles From a Metal-Organic Framework Containing ZnII Metallacycles, Eur. J. Inorg. Chem. 2007 (2007) 524–529.

[7] I. Senkovska, S. Kaskel, Solvent-Induced Pore-Size Adjustment in the Metal-Organic Framework [Mg3(ndc)3(dmf)4] (ndc = naphthalenedicarboxylate), Eur. J. Inorg. Chem. 2006 (2006) 4564–4569.

[8] H.-P. Jia, W. Li, Z.-F. Ju, Z. Jie, Synthesis, Structure and Magnetism of Metal-Organic Framework Materials with Doubly Pillared Layers, Eur. J. Inorg. Chem. 2006 (2006) 4264–4270.

[9] C.-Y. Sun, S. Gao, L.-P. Jin, Hydrothermal Syntheses, Architectures and Magnetic Properties of Six Novel MnII Coordination Polymers with Mixed Ligands., Eur. J. Inorg. Chem. 2006 (2006) 2411–2421.

[10] S.K. Ghosh, P.K. Bharadwaj, Infinite Chains of Quasi-Planar Hexameric Water Clusters Stabilized in a Metal-Organic Framework Built from CoII and Pyrazine- 2,3,5,6-tetracarboxylic Acid., Eur. J. Inorg. Chem. (2005) 4880–4885.

[11] C.N.R. Rao, S.N. and R. Vaidhyanathan, Metal Carboxylates with Open Architectures,

Angew. Chem., Int. Ed. 43 (2004) 1466–1496.

[12] A. Carton, A. Mesbah, L. Perrin, M. Francois, Poly[nickel(II)-µ2-benzene-1,4-dicarboxylate-µ2-Piperazine], Acta Crystallogr. Sect. E. 63 (2007) m948–m949.

[13] S.C. Manna, E. Zangrando, J. Ribas, N. Ray Chaudhuri, Cobalt(II)-(dpyo)-dicarboxylate networks: unique H-bonded assembly and rare bridging mode of dpyo in one of them [dpyo = 4,4'-dipyridyl N,N'-dioxide]., Dalton Trans. (2007) 1383–1391. doi:10.1039/b617278d.

[14] S. Banerjee, P.G. Lassahn, C. Janiak, A. Ghosh, Supramolecular architecture of cadmium(II)-terephthalate complexes having a tridentate or tetradentate Schiff base as blocking coligand, Polyhedron. 24 (2005) 2963–2971. doi:10.1016/j.poly.2005.06.038.

[15] H.-X. Zhang, B.-S. Kang, A.-W. Xu, Z.-N. Chen, Z.-Y. Zhou, A.S.C. Chan, et al., Supramolecular architectures from the self-assembly of trans-oxamidato-bridged dicopper(II) building blocks and phenyldicarboxylates, J. Chem. Soc., Dalt. Trans. 2001 (2001) 2559–2566.

[16] K.-Y. Choi, K.-M. Chun, K.-C. Lee, J. Kim, Synthesis and characterization of nickel(II) complexes of hexaazamacrotetracyclic ligand containing organic ligands., Polyhedron. 21 (2002) 1913–1920.

[17] B.-L. Chen, K.-F. Mok, S.-C. Ng, M.G.B. Drew, Thiophene-2,5-dicarboxylic acid incorporated self-assembly of one-, two- and three-dimensional coordination polymers, New J. Chem. (1999) 877–883.

[18] C.S. Hong, Y. Do, A Magnetically Coupled Three-Dimensional (Terephthalato)manganese(II) Network, Inorg. Chem. 36 (1997) 5684–5685.

[19] H.-K. Fun, S.S.S. Raj, R.-G. Xiong, J.-L. Zuo, Z. Yu, X.-Z. You, A three-dimensional network coordination polymer, (terephthalato)(pyridine)cadmium, with blue fluorescent emission, J. Chem. Soc., Dalt. Trans. 1999 (1999) 1915–1916.

[20] J. Cano, G. De Munno, J.L. Sanz, R. Ruiz, J. Faus, F. Lloret, et al., Ability of terephthalate (ta) to mediate exchange coupling in.pdf, J. Chem. Soc., Dalt. Trans. (1997) 1915–1923.

[21] B.M. and S. A. Bourne, J. Lu, A. Mondal, M.J. Zaworotko, No Title, Angew. Chem., Int. Ed. 40 (2001) 2111–2113.

[22] B.-H. Ye, M.-L.T. and X.-M. Chen, Review on 2,2’-bipyridine- and carboxylate-ligands, Coord. Chem. Rev. 249 (2005) 545–565.

[23] R.L. LaDuca, Aliphatic and aromatic carboxylate divalent metal coordination polymers incorporating the kinked and hydrogen-bonding capable tethering ligand 4,4???-dipyridylamine, Coord. Chem. Rev. 253 (2009) 1759–1792. doi:10.1016/j.ccr.2009.01.025.

[24] K. Biradha, M. Sarkar, L. Rajput, Crystal engineering of coordination polymers using 4,4’-bipyridine as a bond between transition metal atoms., Chem. Commun. (2006) 4169–4179. doi:10.1039/b606184b.

[25] M. Fujita, M. Tominaga, A. Hori, B. Therrien, Coordination assemblies from a Pd(II)-cornered square complex, Acc. Chem. Res. 38 (2005) 369–378. doi:10.1021/ar040153h.

[26] M.-X. Li, Z.-X. Miao, M. Shao, S.-W. Liang, S.-R. Zhu, Metal-Organic Frameworks Constructed from 2,4,6-Tris(4-pyridyl)-1,3,5-triazine, Inorg. Chem. 47 (2008) 4481–4489.

[27] H. Chevreau, T. Devic, F. Salles, G. Maurin, N. Stock, C. Serre, Mixed-linker hybrid superpolyhedra for the production of a series of large-pore iron(III) carboxylate metal-organic frameworks, Angew. Chemie - Int. Ed. 52 (2013) 5056–5060. doi:10.1002/anie.201300057.

[28] C. Kepert, Metal-organic framework materials., in: R. Bruce, DW; O’Hare, D and Walton (Ed.), Porous Mater., John Wiley & Sons, Ltd, 2011: pp. 1–67.

[29] G.L.& H.L. O. M. YAGHI, Selective binding and removal of guests in a microporous metal–organic framework, Nature. 378 (1995) 703–706.

[30] 2519–2526. 199 Shimizu, G. K. H. J. Solid State Chem. 2005, 178, Assembly of metal ions and ligands with adaptable coordinative tendencies as a route to functional metal-organic solids, J. Solid State Chem. 178 (2005) 2519–2526.

[31] S.S.Y. Chui, S.M.F. Lo, J.P.H. Charmant, A.G. Orpen, I.D. Williams, R EPORTS A Chemically Functionalizable Nanoporous Material, Science (80-.). 283 (1999) 1148–1150. doi:10.1126/science.283.5405.1148.

[32] G. Férey, C. Mellot-Draznieks, C. Serre, F. Millange, J. Dutour, S. Surblé, et al., A chromium terephthalate-based solid with unusually large pore volumes and surface area., Science. 309 (2005) 2040–2042. doi:10.1126/science.1116275.

[33] J.L.C. Rowsell, O.M. Yaghi, Metal-organic frameworks: A new class of porous materials, Microporous Mesoporous Mater. 73 (2004) 3–14. doi:10.1016/j.micromeso.2004.03.034.

[34] O.M. Eddaoudi, M.; Kim, J.; Rosi, N.; Vodak, D.; Wachter, J.; O'Keeffe, M.; Yaghi, Systematic design of pore size and functionality in isoreticular MOFs and their application in methane storage., Science (80-.). 295 (2002) 469–472.

[35] O.M. Yaghi, O.K. M, N.W. Ockwig, H.K. Chae, M. Eddaoudi, J. Kim, Reticular synthesis and the design of new materials, Nature. 423 (2003) 705–714. doi:10.1038/nature01650.

[36] J.T. Farha, O. K.; Eryazici, I.; Jeong, N. C.; Hauser, B. G.; Wilmer, C. E.; Sarjeant, A. A.; Snurr, R. Q.; Nguyen, S. T.; Yazaydin, A. Ö.; Hupp, Metal-organic framework materials with ultrahigh surface areas: is the sky the limit?, J Am Chem Soc. 134 (2012) 15016–15021.

[37] Y.O. Deng H, Grunder S, Cordova KE, Valente C, Furukawa H, Hmadeh M, Gándara F, Whalley AC, Liu Z, Asahina S, Kazumori H, O'Keeffe M, Terasaki O, Stoddart JF, Large-pore apertures in a series of metal-organic frameworks., Science (80-.). 336 (2012) 1018–1023.

[38] J.J. Low, A.I. Benin, P. Jakubczak, J.F. Abrahamian, S. a. Faheem, R.R. Willis, Virtual high throughput screening confirmed experimentally: Porous coordination polymer hydration, J. Am. Chem. Soc. 131 (2009) 15834–15842. doi:10.1021/ja9061344.

[39] Z. Ma, D.; Li, Y.; Li, Tuning the moisture stability of metal–organic frameworks by incorporating hydrophobic functional groups at different positions of ligands, Chem. Commun. 19 (2011) 7377–7379.

[40] G.K.H.S. Jared M. Taylor, Amir H. Mahmoudkhani, A Tetrahedral Organophosphonate as a Linker for a Microporous Copper Framework†, Angew. Chemie - Int. Ed. 46 (2007) 795–798.

[41] J. Liang, G.K.H. Shimizu, Crystalline Zinc Diphosphonate Metal − Organic Framework with Three-dimensional Microporosity, Inorg. Chem. 46 (2007) 10449–10451. doi:10.1021/ic701628f.

[42] S. Konar, J. Zoń, A. V Prosvirin, K.R. Dunbar, A. Clearfield, Synthesis and characterization of four metal-organophosphonates with one-, two-, and three-

dimensional structures., Inorg. Chem. 46 (2007) 5229–36. doi:10.1021/ic070132u.

[43] B. Liu, B.-L. Li, Y.-Z. Li, Y. Chen, S.-S. Bao, L.-M. Zheng, Lanthanide diruthenium(II,III) compounds showing layered and PtS-type open framework structures., Inorg. Chem. 46 (2007) 8524–8532. doi:10.1021/ic0621695.

[44] L.-M.Z. Yun-Sheng Ma, You Song, Nature of the LnIII–CoII magnetic interactions in compounds [Ln2Co3(C5H4NPO3)6] · 4H2O with open-framework structures, Inorganica Chim. Acta. 361 (2008) 1363–1371.

[45] M. Yun-Sheng, H. Li, J.J. Wang, S.S. Bao, R. Cao, Y.Z. Li, et al., Three-dimensional lanthanide(III)-copper(II) compounds based on an unsymmetrical 2-pyridylphosphonate ligand: An experimental and theoretical study, Chem. - A Eur. J. 13 (2007) 4759–4769. doi:10.1002/chem.200601786.

[46] S.R. Miller, G.M. Pearce, P. a. Wright, F. Bonino, S. Chavan, S. Bordiga, et al., Structural transformations and adsorption of fuel-related gases of a structurally responsive nickel phosphonate metal-organic framework, Ni-STA-12, J. Am. Chem. Soc. 130 (2008) 15967–15981. doi:10.1021/ja804936z.

[47] W.C. Martin P. Attfield, Carlos Mendieta-Tan, Zhanhui Yuan, Characterisation and properties of the n = 3 and n = 4 members of the Al2[O3PCnH2nPO3](H2O)2F2 framework aluminium alkylenediphosphonate series, Solid State Sci. 10 (2008) 1124–1131.

[48] C.N.R. Rao, J.N. Behera, M. Dan, Organically-templated metal sulfates, selenites and selenates., Chem. Soc. Rev. 35 (2006) 375–87. doi:10.1039/b510396g.

[49] H.-Y. Liu, H. Wu, J.-F. Ma, S.-Y. Song, J. Yang, Y.-Y. Liu, et al., Structural study of silver(I) sulfonate complexes with pyrazine derivatives., Inorg. Chem. 46 (2007) 7299–311. doi:10.1021/ic070147s.

[50] H. Hamaed, A.Y.H. Lo, L.J. May, J.M. Taylor, G.H. Shimizu, R.W. Schurko, Investigation of Silver-Containing Layered Materials and Their Interactions with Primary Amines Using Solid-State Ag-109 and N-15 NMR Spectroscopy and First Principles Calculations, Inorg. Chem. 47 (2008) 11245–11256. doi:Doi 10.1021/Ic801549p.

[51] A.H. Mahmoudkhani, G.K.H. Shimizu, Three guest-including coordination solids from a single crystallization: a discrete cage and open-channel networks from 1-d ladders and 1-d ribbons., Inorg. Chem. 46 (2007) 1593–602. doi:10.1021/ic0615123.

[52] S. Hu, K.H. He, M.H. Zeng, H.H. Zou, Y.M. Jiang, Crystalline-state guest-exchange and gas-adsorption phenomenon for a “soft” supramolecular porous framework stacking by a rigid linear coordination polymer, Inorg. Chem. 47 (2008) 5218–5224. doi:10.1021/ic800050u.

[53] F. Gándara, A. García-Cortés, C. Cascales, B. Gómez-Lor, E. Gutiérrez-Puebla, M. Iglesias, et al., Rare earth arenedisulfonate metal-organic frameworks: An approach toward polyhedral diversity and variety of functional compounds, Inorg. Chem. 46 (2007) 3475–3484. doi:10.1021/ic0617689.

[54] B.D. Chandler, J.O. Yu, D.T. Cramb, G.K.H. Shimizu, Series of Lanthanide-Alkali Metal-Organic Frameworks Exhibiting Luminescence and Permanent Microporosity, Chem. Mater. 19 (2007) 4467–4473. doi:10.1021/cm070930i.

[55] B.D. Chandler, G.D. Enright, K. a Udachin, S. Pawsey, J. a Ripmeester, D.T. Cramb, et al., Mechanical gas capture and release in a network solid via multiple single-crystalline transformations., Nat. Mater. 7 (2008) 229–235. doi:10.1038/nmat2101.

[56] V. Videnova-Adrabinska, Coordination and supramolecular network entanglements of organodisulfonates, Coord. Chem. Rev. 251 (2007) 1987–2016. doi:DOI 10.1016/j.ccr.2007.03.018.

[57] X.C. Huang, Y.Y. Lin, J.P. Zhang, X.M. Chen, Ligand-directed strategy for zeolite-type metal-organic frameworks: Zinc(II) imidazolates with unusual zeolitic topologies, Angew. Chemie - Int. Ed. 45 (2006) 1557–1559. doi:10.1002/anie.200503778.

[58] K.S. Park, Z. Ni, A.P. Côté, J.Y. Choi, R. Huang, F.J. Uribe-Romo, et al., Exceptional chemical and thermal stability of zeolitic imidazolate frameworks., Proc. Natl. Acad. Sci. U. S. A. 103 (2006) 10186–10191. doi:10.1073/pnas.0602439103.

[59] H. Hayashi, A.P. Côté, H. Furukawa, M. O’Keeffe, O.M. Yaghi, Zeolite A imidazolate frameworks., Nat. Mater. 6 (2007) 501–506. doi:10.1038/nmat1927.

[60] R. Banerjee, A. Phan, B. Wang, C. Knobler, H. Furukawa, M. O’Keeffe, et al., High-throughput synthesis of zeolitic imidazolate frameworks and application to CO2 capture., Science. 319 (2008) 939–943. doi:10.1126/science.1152516.

[61] B. Wang, A.P. Côté, H. Furukawa, M. O’Keeffe, O.M. Yaghi, Colossal cages in zeolitic imidazolate frameworks as selective carbon dioxide reservoirs., Nature. 453 (2008) 207–211. doi:10.1038/nature06900.

[62] P.F. Wu Tao, Xianhui Bu, Liu Rui, Zhien Lin, Jian Zhang, A New Zeolitic Topology with Sixteen-Membered Ring and Multidimensional Large Pore Channels, Chem. Eur. J. 14 (2008) 7771–7773.

[63] T. Wu, X. Bu, J. Zhang, P. Feng, New zeolitic imidazolate frameworks: From unprecedented assembly of cubic clusters to ordered cooperative organization of complementary ligands, Chem. Mater. 20 (2008) 7377–7382. doi:10.1021/cm802400f.

[64] K.S. Suslick, P. Bhyrappa, J.H. Chou, M.E. Kosal, S. Nakagaki, D.W. Smithenry, et al., Microporous porphyrin solids, Acc. Chem. Res. 38 (2005) 283–291. doi:10.1021/ar040173j.

[65] P.F. Nanfeng Zheng, Jian Zhang, Xianhui Bu, Cadmium−Porphyrin Coordination Networks: Rich Coordination Modes and Three-Dimensional Four-Connected CdSO4 and (3,5)-Connected hms Nets, Cryst. Growth Des. 12 (2007) 2576–2581.

[66] S. Muniappan, S. Lipstman, S. George, I. Goldberg, Porphyrin framework solids. Synthesis and structure of hybrid coordination polymers of tetra(carboxyphenyl)porphyrins and lanthanide-bridging ions, Inorg. Chem. 46 (2007) 5544–5554. doi:10.1021/ic0701099.

[67] E.-Y. Choi, P.M. Barron, R.W. Novotney, C. Hu, Y.-U. Kwon, W. Choe, A mixed-linker porphyrin framework with CdI2-type topology., CrystEngComm. 10 (2008) 824–826. doi:10.1039/B720035H.

[68] S.J. Narayanan, B. Sridevi, T.K. Chandrashekar, A. Vij, R. Roy, Sapphyrin supramolecules through C-H ⋯ S and C-H ⋯ Se hydrogen bonds-first structural characterization of meso-arylsapphyrins bearing heteroatoms, Angew. Chem., Int. Ed. 37 (1999) 3394–3397. doi:10.1002/(SICI)1521-3773(19981231)37:24<3394::AID-ANIE3394>3.0.CO;2-4.

[69] O.K. Farha, A.M. Spokoyny, K.L. Mulfort, M.F. Hawthorne, C.A. Mirkin, J.T. Hupp, Synthesis and Hydrogen Sorption Properties of Carborane Based Metal−Organic Framework Materials, J. Am. Chem. Soc. 129 (2007) 12680–12681. doi:10.1021/ja076167a.

[70] Y.-S. Bae, O.K. Farha, A.M. Spokoyny, C. a Mirkin, J.T. Hupp, R.Q. Snurr, Carborane-based metal-organic frameworks as highly selective sorbents for CO(2) over methane., Chem. Commun. (Camb). 0 (2008) 4135–4137. doi:10.1039/b805785k.

[71] M. Du, C.-P. Li, X.-J. Zhao, Metal-Controlled Assembly of Coordination Polymers with the Flexible Building Block 4-Pyridylacetic Acid (Hpya), Cryst. Growth Des. 6 (2005)

335–341.

[72] S.R. Halper, L. Do, J.R. Stork, S.M. Cohen, Topological Control in Heterometallic Metal−Organic Frameworks by Anion Templating and Metalloligand Design, J. Am. Chem. Soc. 128 (2006) 15255–15268.

[73] H. Ohi, Y. Tachi, S. Itoh, Supramolecular and Coordination Polymer Complexes Supported by a Tripodal Tripyridine Ligand Containing a 1,3,5-Triethylbenzene Spacer, Inorg. Chem. 43 (2004) 4561–4563.

[74] Y. Yoo, V. Varela-Guerrero, H.K. Jeong, Isoreticular metal-organic frameworks and their membranes with enhanced crack resistance and moisture stability by surfactant-assisted drying, Langmuir. 27 (2011) 2652–2657. doi:10.1021/la104775d.

[75] A. Rabenau, The Role of Hydrothermal Synthesis in Preparative Chemistry, Angew. Chemie Int. Ed. English. 24 (1985) 1026–1040. doi:10.1002/anie.198510261.

[76] C.-C. Wang, J. y. Ying, Sol−Gel Synthesis and Hydrothermal Processing of Anatase and Rutile Titania Nanocrystals, Chem. Mater. 11 (1999) 3113–3120.

[77] A. Lagashetty, V. Havanoor, S. Basavaraja, S.D. Balaji, A. Venkataraman, Microwave-assisted route for synthesis of nanosized metal oxides, Sci. Technol. Adv. Mater. 8 (2007) 484–493. doi:10.1016/j.stam.2007.07.001.

[78] H. Bux, F. Liang, Y. Li, J. Cravillon, M. Wiebcke, J. Caro, Zeolitic imidazolate framework membrane with molecular sieving properties by microwave-assisted solvothermal synthesis, J. Am. Chem. Soc. 131 (2009) 16000–16001. doi:10.1021/ja907359t.

[79] N. Stock, S. Biswas, Synthesis of Metal-Organic Frameworks (MOFs): Routes to Various MOF Topologies, Morphologies, and Composites, Chem. Rev. 112 (2012) 933–969.

[80] D. Mueller; Ulrich (Neustadt, DE), Puetter; Hermann (Neustadt, DE), Hesse; Michael (Worms, DE), Schubert; Markus (Ludwigshafen, DE), Wessel; Helge (Mannheim, DE), Huff; Juergen (Ludwigshafen, DE), Guzmann; Marcus (Muehlhausen, Method for electrochemical production of a crystalline porous metal organic skeleton material, WO2005/049892, 2005.

[81] V.V. and K.T. Boldyrev, Mechanochemistry of Solids : Past , Present , and Prospects, J. Mater. Synth. Process. 8 (2000) 121 – 132. doi:10.1023/A:1011347706721.

[82] G. Kaupp, Mechanochemistry: the varied applications of mechanical bond-breaking, CrystEngComm. 11 (2009) 388. doi:10.1039/b810822f.

[83] A.L. Garay, A. Pichon, S.L. James, Solvent-free synthesis of metal complexes, Chem Soc Rev. 36 (2007) 846–855. doi:10.1039/b600363j.

[84] M.K. Beyer, H. Clausen-Schaumann, Mechanochemistry: The mechanical activation of covalent bonds, Chem. Rev. 105 (2005) 2921–2948. doi:10.1021/cr030697h.

[85] J.-L. Fillion, H.; Luche, For a survey of sonochemical cycloaddition, in: J.-L. Luche (Ed.), Synth. Org. Sonochemistry, Plenum Press, New York, 1998: pp. 91–106.

[86] J.H. Bang, K.S. Suslick, Applications of ultrasound to the synthesis of nanostructured materials, Adv. Mater. 22 (2010) 1039–1059. doi:10.1002/adma.200904093.

[87] Y.F. Song, L. Cronin, Postsynthetic covalent modification of metal-organic framework (MOF) materials, Angew. Chemie - Int. Ed. 47 (2008) 4635–4637. doi:10.1002/anie.200801631.

[88] Z. Wang, S.M. Cohen, Postsynthetic covalent modification of a neutral metal-organic framework, J. Am. Chem. Soc. 129 (2007) 12368–12369. doi:10.1021/ja074366o.

[89] M.J. Ingleson, J.P. Barrio, J.-B. Guilbaud, Y.Z. Khimyak, M.J. Rosseinsky, Framework functionalisation triggers metal complex binding., Chem. Commun. (Camb). (2008) 2680–2682. doi:10.1039/b718367d.

[90] Z. Wang, S.M. Cohen, Tandem modification of metal-organic frameworks by a postsynthetic approach, Angew. Chemie - Int. Ed. 47 (2008) 4699–4702. doi:10.1002/anie.200800686.

[91] A.D. Burrows, C.G. Frost, M.F. Mahon, C. Richardson, Post-synthetic modification of tagged metal-organic frameworks., Angew. Chem. Int. Ed. Engl. 47 (2008) 8482–6. doi:10.1002/anie.200802908.

[92] W. Morris, C.J. Doonan, H. Furukawa, R. Banerjee, O.M. Yaghi, Crystals as molecules: Postsynthesis covalent functionalization of zeolitic imidazolate frameworks, J. Am. Chem. Soc. 130 (2008) 12626–12627. doi:10.1021/ja805222x.

[93] X.S. Wang, S. Ma, P.M. Forster, D. Yuan, J. Eckert, J.J. López, et al., Enhancing H2 uptake by “close-packing” alignment of open copper sites in metal-organic frameworks., Angew. Chem. Int. Ed. 120 (2008) 7373–7376.

[94] X. Lin, I. Telepeni, A.J. Blake, A. Dailly, C.M. Brown, J.M. Simmons, et al., High Capacity Hydrogen Adsorption in Cu(II) Tetracarboxylate Framework Materials: The Role of Pore Size, Ligand Functionalization, and Exposed Metal Sites, J. Am. Chem. Soc. 131 (2009) 2159–2171.

[95] O.K. Farha, A.Ö. Yazaydın, I. Eryazici, C.D. Malliakas, B.G. Hauser, M.G. Kanatzidis, et al., De novo synthesis of a metal-organic framework material featuring ultrahigh surface area and gas storage capacities., Nat. Chem. 2 (2010) 944–948. doi:10.1038/nchem.834.

[96] A.G. Wong-Foy, A.J. Matzger, O.M. Yaghi, Exceptional H2 saturation uptake in microporous metal-organic frameworks, J. Am. Chem. Soc. 128 (2006) 3494–3495. doi:10.1021/ja058213h.

[97] S. Shimomura, M. Higuchi, R. Matsuda, K. Yoneda, Y. Hijikata, Y. Kubota, et al., Selective sorption of oxygen and nitric oxide by an electron-donating flexible porous coordination polymer., Nat. Chem. 2 (2010) 633–637. doi:10.1038/nchem.684.

[98] A.K. Cheetham, C.N.R. Rao, Materials science. There’s room in the middle., Science. 318 (2007) 58–59. doi:10.1126/science.1147231.

[99] E. Coronado, G. Mínguez Espallargas, Dynamic magnetic MOFs., Chem. Soc. Rev. 42 (2013) 1525–39. doi:10.1039/c2cs35278h.

[100] M. Kurmoo, Magnetic metal–organic frameworks, Chem. Soc. Rev. 38 (2009) 1353–1379.

[101] H. Okawa, A. Shigematsu, M. Sadakiyo, T. Miyagawa, K. Yoneda, M. Ohba, et al., Oxalate-bridged bimetallic complexes {NH(prol)3}[MCr(ox) 3] (M = MnII, FeII, CoII; NH(prol)3+ = tri(3-hydroxypropyl)ammonium) exhibiting coexistent ferromagnetism and proton conduction, J. Am. Chem. Soc. 131 (2009) 13516–13522. doi:10.1021/ja905368d.

[102] C.N.R. Rao, S. Natarajan, R. Vaidhyanathan, Metal Carboxylates with Open Architectures, Angew. Chem. Int. Ed. 2004 (2004) 1466–1496.

[103] D. Maspoch, D. Ruiz-Molina, K. Wurst, N. Domingo, M. Cavallini, F. Biscarini, et al.,

A nanoporous molecular magnet with reversible solvent-induced mechanical and magnetic properties., Nat. Mater. 2 (2003) 190–195. doi:10.1038/nmat834.

[104] N. Roques, D. Maspoch, I. Imaz, A. Datcu, J.-P. Sutter, C. Rovira, et al., A three-dimensional lanthanide-organic radical open-framework., Chem. Commun. (Camb). (2008) 3160–3162. doi:10.1039/b802196a.

[105] N. Roques, D. Maspoch, F. Luis, A. Camón, K. Wurst, A. Datcu, et al., A hexacarboxylic open-shell building block: synthesis, structure and magnetism of a three-dimensional metal–radical framework, J. Mater. Chem. 18 (2008) 98. doi:10.1039/b713705b.

[106] Z.-Z. Lu, R. Zhang, Y.-Z. Li, Z.-J. Guo, H.-G. Zheng, Solvatochromic Behavior of a Nanotubular Metal−Organic Framework for Sensing Small Molecules, J. Am. Chem. Soc. 133 (2011) 4172–4174.

[107] C.-Y. Sun, X.-L. Wang, C. Qin, J.-L. Jin, Z.-M. Su, P. Huang, et al., Solvatochromic Behavior of Chiral Mesoporous Metal–Organic Frameworks and Their Applications for Sensing Small Molecules and Separating Cationic Dyes, Chem. Eur. J. 19 (2013) 3639–3645.

[108] B. V. Harbuzaru, A. Corma, F. Rey, J.L. Jordá, D. Ananias, L.D. Carlos, et al., A miniaturized linear ph sensor based on a highly photoluminescent self-assembled Europium(III) metal-organic framework, Angew. Chemie - Int. Ed. 48 (2009) 6476–6479. doi:10.1002/anie.200902045.

[109] J. Rocha, L.D. Carlos, F.A.A. Paz, D. Ananias, Luminescent multifunctional lanthanides-based metal-organic frameworks., Chem. Soc. Rev. 40 (2011) 926–940. doi:10.1039/c0cs00130a.

[110] D. Zacher, O. Shekhah, C. Wöll, R.A. Fischer, Thin films of metal-organic frameworks., Chem. Soc. Rev. 38 (2009) 1418–1429. doi:10.1039/b805038b.

[111] S.-Z. Zhan, M. Li, S.W. Ng, D. Li, Luminescent Metal–Organic Frameworks (MOFs) as a Chemopalette: Tuning the Thermochromic Behavior of Dual-Emissive Phosphorescence by Adjusting the Supramolecular Microenvironments, Chem. Eur. J. 19 (2013) 10217–10225.

[112] P. Horcajada, T. Chalati, C. Serre, B. Gillet, C. Sebrie, T. Baati, et al., Porous metal-organic-framework nanoscale carriers as a potential platform for drug delivery and imaging., Nat. Mater. 9 (2010) 172–178. doi:10.1038/nmat2608.

[113] C. McCusker, L. B.; Baerlocher, Introduction to Zeolite Science and Practice, Stud. Surf. Sci. Catal. 168 (2007) 13–37.

[114] K. Nakamoto, Infrared and Raman Spectra of Inorganic and Coordination Compounds: Part B: Applications in Coordination, Organometallic, and Bioinorganic Chemistry, 2008. doi:10.1002/9780470405888.

[115] X-ray Photoelectron Spectroscopy, (n.d.). http://en.wikipedia.org/wiki/X-ray_photoelectron_spectroscopy.

[116] O.M. Yaghi, M. O'Keeffe, N.W. Ockwig, H.K. Chae, M. Eddaoudi, J. Kim, Reticular synthesis and the design of new materials., Nature. 423 (2003) 705–714. doi:10.1038/nature01650.

[117] S. Kitagawa, R. Kitaura, S. Noro, Functional porous coordination polymers, Angew Chem Int Ed Engl. 43 (2004) 2334–2375. doi:10.1002/anie.200300610.

[118] G. Férey, Hybrid porous solids: past, present, future., Chem. Soc. Rev. 37 (2008) 191–214. doi:10.1039/b618320b.

[119] D. Zhao, D. Yuan, H.-C. Zhou, The current status of hydrogen storage in metal-organic frameworks., Energy Environ. Sci. 1 (2008) 222–235. doi:10.1039/b808322n.

[120] J.L.C. Rowsell, O.M. Yaghi, Strategies for hydrogen storage in metal-organic frameworks, Angew. Chemie - Int. Ed. 44 (2005) 4670–4679. doi:10.1002/anie.200462786.

[121] C. Yang, X. Wang, M.A. Omary, Fluorous Metal−Organic Frameworks for High-Density Gas Adsorption, J. Am. Chem. Soc. Comm. 129 (2007) 15454–15455.

[122] M. Hartmann, S. Kunz, D. Himsl, O. Tangermann, S. Ernst, A. Wagener, Adsorptive separation of isobutene and isobutane on Cu3(BTC) 2, Langmuir. 24 (2008) 8634–8642. doi:10.1021/la8008656.

[123] R. Kitaura, K. Seki, G. Akiyama, S. Kitagawa, Porous coordination-polymer crystals with gated channels specific for supercritical gases, Angew. Chemie - Int. Ed. 42 (2003) 428–431. doi:10.1002/anie.200390130.

[124] Y.K. Hwang, D.Y. Hong, J.S. Chang, S.H. Jhung, Y.K. Seo, J. Kim, et al., Amine grafting on coordinatively unsaturated metal centers of MOFs: Consequences for

catalysis and metal encapsulation, Angew. Chemie - Int. Ed. 47 (2008) 4144–4148. doi:10.1002/anie.200705998.

[125] J. Seo, D. Whang, H. Lee, S. Jun, J. Oh, Y. Jeon, et al., A homochiral metal-organic porous material for enantioselective separation and catalysis, Nature. 404 (2000) 982–986. doi:10.1038/35010088.

[126] S. Hermes, F. Schröder, R. Chelmowski, C. Wöll, R.A. Fischer, Selective nucleation and growth of metal-organic open framework thin films on patterned COOH/CF3-terminated self-assembled monolayers on Au(111), J. Am. Chem. Soc. 127 (2005) 13744–13745. doi:10.1021/ja053523l.

[127] P. Horcajada, C. Serre, M. Vallet-Regí, M. Sebban, F. Taulelle, G. Férey, Metal-organic frameworks as efficient materials for drug delivery, Angew. Chemie - Int. Ed. 45 (2006) 5974–5978. doi:10.1002/anie.200601878.

[128] P. Horcajada, C. Serre, G. Maurin, N.A. Ramsahye, F. Balas, M. Vallet-Regí, et al., Flexible porous metal-organic frameworks for a controlled drug delivery, J. Am. Chem. Soc. 130 (2008) 6774–6780. doi:10.1021/ja710973k.

[129] B. Panella, M. Hirscher, H. Pütter, U. Müller, Hydrogen adsorption in metal-organic frameworks: Cu-MOFs and Zn-MOFs compared, Adv. Funct. Mater. 16 (2006) 520–524. doi:10.1002/adfm.200500561.

[130] J. Liu, J.T. Culp, S. Natesakhawat, B.C. Bockrath, B. Zande, S.G. Sankar, et al., Experimental and Theoretical Studies of Gas Adsorption in Cu3(BTC)2: An Effective Activation Procedure, J. Phys. Chem. C. 111 (2007) 9305–9313. doi:10.1021/jp071449i.

[131] K. Schlichte, T. Kratzke, S. Kaskel, Improved synthesis, thermal stability and catalytic properties of the metal-organic framework compound CU3(BTC)(2), Microporous Mesoporous Mater. 73 (2004) 81–88. doi:10.1016/j.micromeso.2003.12.027.

[132] P. Krawiec, M. Kramer, M. Sabo, R. Kunschke, H. Froede, S. Kaskel, Improved hydrogen storage in the metal-organic framework Cu3(BTC)2., Adv. Eng. Mater. 8 (2006) 293–296. doi:10.1002/adem.200500223.

[133] Q.M. Wang, D. Shen, M. Bulow, M.L. Lau, S. Deng, F.R. Fitch, et al., Metallo-organic molecular sieve for gas separation and purification., Microporous Mesoporous Mater. 55 (2002) 217–230. doi:10.1016/S1387-1811(02)00405-5.

[134] L. Alaerts, E. Séguin, H. Poelman, F. Thibault-Starzyk, P.A. Jacobs, D.E. De Vos,

Probing the lewis acidity and catalytic activity of the metal-organic framework [Cu3(btc)2] (BTC = Benzene-1,3,5-tricarboxylate), Chem. - A Eur. J. 12 (2006) 7353–7363. doi:10.1002/chem.200600220.

[135] A. Vishnyakov, P.I. Ravikovitch, A. V. Neimark, M. Bülow, Q.M. Wang, Nanopore structure and sorption properties of Cu-BTC metal-organic framework, Nano Lett. 3 (2003) 713–718. doi:10.1021/nl0341281.

[136] Z.-Q. Li, L.-G. Qiu, T. Xu, Y. Wu, W. Wang, Z.-Y. Wu, et al., Ultrasonic synthesis of the microporous metal–organic framework Cu3(BTC)2 at ambient temperature and pressure: an efficient and environmentally friendly method, Mater. Lett. 63 (2009) 78–80.

[137] Y.K. Seo, G. Hundal, I.T. Jang, Y.K. Hwang, C.H. Jun, J.S. Chang, Microwave synthesis of hybrid inorganic-organic materials including porous Cu3(BTC)2 from Cu(II)-trimesate mixture, Microporous Mesoporous Mater. 119 (2009) 331–337. doi:10.1016/j.micromeso.2008.10.035.

[138] J.Y. Choi, J. Kim, S.H. Jhung, H.K. Kim, J.-S. Chang, H.K. Chae, Microwave Synthesis of a Porous Metal-Organic Framework, Zinc Terephthalate MOF-5, Bull. Korean Chem. Soc. 27 (2006) 1523–1534.

[139] M.M. Maik Schlesinger, Steffen Schulze, Michael Hietschold, Evaluation of synthetic methods for microporous metal–organic frameworks exemplified by the competitive formation of [Cu2(btc)3(H2O)3] and [Cu2(btc)(OH)(H2O)], Microporous Mesoporous Mater. 132 (2010) 121–127.

[140] A. Pichon, A. Lazuen-Garay, S.L. James, Solvent-free synthesis of a microporous metal–organic framework, CrystEngComm. 8 (2006) 211. doi:10.1039/b513750k.

[141] G.A. Tompsett, W.C. Conner, K.S. Yngvesson, Microwave synthesis of nanoporous materials, Chemphyschem. 7 (2006) 296–319. doi:10.1002/cphc.200500449.

[142] K. Schlichte, T. Kratzke, S. Kaskel, Improved synthesis, thermal stability and catalytic properties of the metal-organic framework compound Cu3(BTC)2, Microporous Mesoporous Mater. 73 (2004) 81–88. doi:10.1016/j.micromeso.2003.12.027.

[143] E. Biemmi, S. Christian, N. Stock, T. Bein, High-throughput screening of synthesis parameters in the formation of the metal-organic frameworks MOF-5 and HKUST-1, Microporous Mesoporous Mater. 117 (2009) 111–117. doi:10.1016/j.micromeso.2008.06.040.

[144] Z.Q. Li, L.G. Qiu, T. Xu, Y. Wu, W. Wang, Z.Y. Wu, et al., Ultrasonic synthesis of the microporous metal-organic framework Cu3(BTC)2 at ambient temperature and pressure: An efficient and environmentally friendly method, Mater. Lett. 63 (2009) 78–80. doi:10.1016/j.matlet.2008.09.010.

[145] Z. Ni, R.I. Masel, Rapid Production of Metal−Organic Frameworks via Microwave-Assisted Solvothermal Synthesis, J. Am Chem. Soc. Comm. 128 (2006) 12394–12395.

[146] P. Amo-Ochoa, G. Givaja, P.J.S. Miguel, O. Castillo, F. Zamora, Microwave assisted hydrothermal synthesis of a novel CuI-sulfate-pyrazine MOF, Inorg. Chem. Commun. 10 (2007) 921–924. doi:10.1016/j.inoche.2007.04.024.

[147] H. Yang, S. Orefuwa, A. Goudy, Study of mechanochemical synthesis in the formation of the metal-organic framework Cu3(BTC)2 for hydrogen storage, Microporous Mesoporous Mater. 143 (2011) 37–45. doi:10.1016/j.micromeso.2011.02.003.

[148] X.J. Z.-Q. Li, L.-G. Qiu, T. Xu, Y. Wu, W. Wang, Z.-Y. Wu, Ultrasonic synthesis of the microporous metal–organic framework Cu3(BTC)2 at ambient temperature and pressure: an efficient and environmentally friendly method, Mater. Lett. 63 (2009) 78–80.

[149] R. Senthil Kumar, S. Senthil Kumar, M. Anbu Kulandainathan, Efficient electrosynthesis of highly active Cu3(BTC)2-MOF and its catalytic application to chemical reduction, Microporous Mesoporous Mater. 168 (2013) 57–64. doi:10.1016/j.micromeso.2012.09.028.

[150] Sonochemistry in “Organic chemistry portal,” (n.d.).

[151] G. Férey, G. Ferey, Hybrid porous solids: past, present, future., Chem. Soc. Rev. 37 (2008) 191–214. doi:10.1039/b618320b.

[152] L.J. Murray, M. Dinca, J.R. Long, Hydrogen storage in metal-organic frameworks, Chem. Soc. Rev. 38 (2009) 1294–1314. doi:10.1039/b802256a.

[153] F. Nouar, J.F. Eubank, T. Bousquet, L. Wojtas, M.J. Zaworotko, M. Eddaoudi, Supermolecular building blocks (SBBs) for the design and synthesis of highly porous metal-organic frameworks, J. Am. Chem. Soc. 130 (2008) 1833–1835. doi:10.1021/ja710123s.

[154] R.E. Morris, P.S. Wheatley, Gas storage in nanoporous materials., Angew. Chem. Int. Ed. Engl. 47 (2008) 4966–4981. doi:10.1002/anie.200703934.

[155] J.R. Li, R.J. Kuppler, H.C. Zhou, Selective gas adsorption and separation in metal-organic frameworks, Chem. Soc. Rev. 38 (2009) 1477–1504. doi:Doi 10.1039/B802426j.

[156] J. Lee, O.K. Farha, J. Roberts, K. a Scheidt, S.T. Nguyen, J.T. Hupp, Metal-organic framework materials as catalysts., Chem. Soc. Rev. 38 (2009) 1450–1459. doi:10.1039/b807080f.

[157] J. An, S.J. Geib, N.L. Rosi, Cation-triggered drug release from a porous zinc-adeninate metal-organic framework, J. Am. Chem. Soc. 131 (2009) 8376–8377. doi:10.1021/ja902972w.

[158] M. Allendorf, R. Houk, R. Bhakta, I.B. Nielsen, P. Doty, Scintillating Metal Organic Frameworks: A New Class of Radiation Detection Materials, MRS Proc. 1164 (2009). doi:10.1557/PROC-1164-L07-01.

[159] T. Uemura, N. Yanai, S. Kitagawa, Polymerization reactions in porous coordination polymers., Chem. Soc. Rev. 38 (2009) 1228–1236. doi:10.1039/b802583p.

[160] K.M.L. Taylor-Pashow, J. Della Rocca, Z. Xie, S. Tran, W. Lin, Postsynthetic modifications of iron-carboxylate nanoscale metal-organic frameworks for imaging and drug delivery, J. Am. Chem. Soc. 131 (2009) 14261–14263. doi:10.1021/ja906198y.

[161] N.A. Khan, J.W. Jun, J.H. Jeong, S.H. Jhung, Remarkable adsorptive performance of a metal-organic framework, vanadium-benzenedicarboxylate (MIL-47), for benzothiophene., Chem. Commun. (Camb). 47 (2011) 1306–1308. doi:10.1039/c0cc04759g.

[162] E. Haque, J.E. Lee, I.T. Jang, Y.K. Hwang, J.S. Chang, J. Jegal, et al., Adsorptive removal of methyl orange from aqueous solution with metal-organic frameworks, porous chromium-benzenedicarboxylates, J. Hazard. Mater. 181 (2010) 535–542. doi:10.1016/j.jhazmat.2010.05.047.

[163] P.T.W. S.M. Humphrey, Multiple areas of magnetic bistability in the topological ferrimagnet [Co3(NC5H3(CO2)2-2,5)2((3-OH)2(OH2)2], J. Am. Chem. Soc. 126 (2004) 13236–13237.

[164] H.R. Moon, J.H. Kim, M.P. Suh, Redox-active porous metal-organic framework producing silver nanoparticles from AgI ions at room temperature, Angew. Chemie - Int. Ed. 44 (2005) 1261–1265. doi:10.1002/anie.200461408.

[165] R.A.F. S. Hermes, F. Schroder, R. Chelmowski, C. Woll, Selective nucleation and growth of metal–organic open framework thin films on patterned COOH/CF3-terminated self-assembled monolayers on Au (1 1 1), J. Am. Chem. Soc. 127 (2005) 13744–13745.

[166] E. Haque, N. Khan, H.J. Park, S.H. Jhung, Synthesis of a metal-organic framework material, iron terephthalate, by ultrasound, microwave, and conventional electric heating: A kinetic study, Chem. - A Eur. J. 16 (2010) 1046–1052. doi:10.1002/chem.200902382.

[167] N.A. Khan, M.M. Haque, S.H. Jhung, Accelerated syntheses of porous isostructural lanthanide- benzenetricarboxylates (Ln-BTC) under ultrasound at room temperature, Eur. J. Inorg. Chem. (2010) 4975–4981. doi:10.1002/ejic.201000541.

[168] X.J. L.-G. Qiu, Z.-Q. Li, Y. Wu, T. Xu, Facile synthesis of nanocrystals of a microporous metal–organic framework by an ultrasonic method and selective sensing of organoamines, Chem. Commun. 364 (2008) 2–3644.

[169] X.J. Z.-Q. Li, L.-G. Qiu, W. Wang, T. Xu, Y. Wu, Fabrication of nanosheets of a fluorescent metal–organic framework [Zn(BDC)(H2O)]n (BDC = 1,4-benzenedicarboxylate): Ultrasonic synthesis and sensing of ethylamine Inorg. Chem. Commun., Inorg. Chem. Commun. 11 (2008) 1375–1377.

[170] W.-J. Son, J. Kim, J. Kim, W.-S. Ahn, Sonochemical synthesis of MOF-5., Chem. Commun. (Camb). (2008) 6336–6338. doi:10.1039/b814740j.

[171] H.L. and T.L.G. O. M. Yaghi, Construction of Porous Solids from Hydrogen-Bonded Metal Complexes of 1, 3, 5-Benzenetricarboxylic Acid, J. Am. Chem. Soc. 118 (1996) 9096–9101.

[172] B. Arstad, H. Fjellvåg, K.O. Kongshaug, O. Swang, R. Blom, Amine functionalised metal organic frameworks (MOFs) as adsorbents for carbon dioxide, Adsorption. 14 (2008) 755–762. doi:10.1007/s10450-008-9137-6.

[173] A. Tahmasian, A. Morsali, Ultrasonic synthesis of a 3D Ni(II) Metal-organic framework at ambient temperature and pressure: New precursor for synthesis of nickel(II) oxide nano-particles, Inorganica Chim. Acta. 387 (2012) 327–331. doi:10.1016/j.ica.2012.02.017.

[174] E. Haque, S.H. Jhung, Synthesis of isostructural metal-organic frameworks, CPO-27s,

with ultrasound, microwave, and conventional heating: Effect of synthesis methods and metal ions, Chem. Eng. J. 173 (2011) 866–872. doi:10.1016/j.cej.2011.08.037.

[175] T.Y. W. Zhou, H. Wu, Enhanced H2 adsorption in isostructural metal–organic frameworks with open metal sites: strong dependence of the binding strength on metal ions J. Am. Chem. Soc., 130 (2008), pp. 15268–15269, J. Am. Chem. Soc. 130 (2008) 15268–15269.

[176] B. Chen, X. Zhao, A. Putkham, K. Hong, E.B. Lobkovsky, E.J. Hurtado, et al., Surface interactions and quantum kinetic molecular sieving for H 2 and D2 adsorption on a mixed metal-organic framework material, J. Am. Chem. Soc. 130 (2008) 6411–6423. doi:10.1021/ja710144k.

[177] P.D.C. Dietzel, P.A. Georgiev, J. Eckert, R. Blom, T. Strässle, T. Unruh, Interaction of hydrogen with accessible metal sites in the metal-organic frameworks M(2)(dhtp) (CPO-27-M; M = Ni, Co, Mg)., Chem. Commun. (Camb). 46 (2010) 4962–4964. doi:10.1039/c0cc00091d.

[178] P.D.C. Dietzel, V. Besikiotis, R. Blom, Application of metal–organic frameworks with coordinatively unsaturated metal sites in storage and separation of methane and carbon dioxide, J. Mater. Chem. 19 (2009) 7362. doi:10.1039/b911242a.

[179] S.R. Caskey, A.G. Wong-Foy, A.J. Matzger, Dramatic tuning of carbon dioxide uptake via metal substitution in a coordination polymer with cylindrical pores, J. Am. Chem. Soc. 130 (2008) 10870–10871. doi:10.1021/ja8036096.

[180] T.K. Maji, R. Matsuda, S. Kitagawa, A flexible interpenetrating coordination framework with a bimodal porous functionality., Nat. Mater. 6 (2007) 142–148. doi:10.1038/nmat1827.

[181] L.J. Murray, M. Dinca, J.R. Long, Hydrogen storage in metal-organic frameworks, Chem. Soc. Rev. 38 (2009) 1294–1314. doi:10.1039/B802256A.

[182] P. Wang, T.A. Okamura, H.P. Zhou, W.Y. Sun, Y.P. Tian, Metal complex with terpyrindine derivative ligand as highly selective colorimetric sensor for iron(III), Chinese Chem. Lett. 24 (2013) 20–22. doi:10.1016/j.cclet.2012.12.010.

[183] et al. S.S. Chen, M. Chen, S. Takamizawa, Porous cobalt(II)-imidazolate supramolecular isomeric frameworks with selective gas sorption property, Chem. Commun. 47 (2011) 4902–4904.

[184] S.M. Seyedi, R. Sandaroos, G.H. Zohuri, Novel cobalt(II) complexes of amino acids-Schiff bases catalyzed aerobic oxidation of various alcohols to ketones and aldehyde, Chinese Chem. Lett. 21 (2010) 1303–1306. doi:10.1016/j.cclet.2010.06.009.

[185] Y. Zhao, X. Zhou, T. Okamura, M. Chen, Y. Lu, W.-Y. Sun, et al., Silver supramolecule catalyzed multicomponent reactions under mild conditions, Dalt. Trans. 41 (2012) 5889. doi:10.1039/c2dt30134b.

[186] H. Furukawa, N. Ko, Y.B. Go, N. Aratani, S.B. Choi, E. Choi, et al., Ultrahigh porosity in metal-organic frameworks., Science. 329 (2010) 424–428. doi:10.1126/science.1192160.

[187] D. Yuan, D. Zhao, D. Sun, H.C. Zhou, An isoreticular series of metal-organic frameworks with dendritic hexacarboxylate ligands and exceptionally high gas-uptake capacity, Angew. Chemie - Int. Ed. 49 (2010) 5357–5361. doi:10.1002/anie.201001009.

[188] O.K. Farha, I. Eryazici, N.C. Jeong, B.G. Hauser, C.E. Wilmer, A.A. Sarjeant, et al., Metal-organic framework materials with ultrahigh surface areas: Is the sky the limit?, J. Am. Chem. Soc. 134 (2012) 15016–15021. doi:10.1021/ja3055639.

[189] M.C. So, S. Jin, H.J. Son, G.P. Wiederrecht, O.K. Farha, J.T. Hupp, Layer-by-layer fabrication of oriented porous thin films based on porphyrin-containing metal-organic frameworks, J. Am. Chem. Soc. 135 (2013) 15698–15701. doi:10.1021/ja4078705.

[190] H.J. Son, S. Jin, S. Patwardhan, S.J. Wezenberg, N.C. Jeong, M. So, et al., Light-harvesting and ultrafast energy migration in porphyrin-based metal-organic frameworks, J. Am. Chem. Soc. 135 (2013) 862–869. doi:10.1021/ja310596a.

[191] S.Y. Jin, H.J. Son, O.K. Farha, G.P. Wiederrecht, J.T. Hupp, Energy Transfer from Quantum Dots to Metal-Organic Frameworks for Enhanced Light Harvesting, J. Am. Chem. Soc. 135 (2013) 955–958. doi:Doi 10.1021/Ja3097114.

[192] C.A. Kent, B.P. Mehl, L. Ma, J.M. Papanikolas, T.J. Meyer, W. Lin, Energy transfer dynamics in metal-organic frameworks, J. Am. Chem. Soc. 132 (2010) 12767–12769. doi:10.1021/ja102804s.

[193] C.A. Kent, D. Liu, L. Ma, J.M. Papanikolas, T.J. Meyer, W. Lin, Light harvesting in microscale metal-organic frameworks by energy migration and interfacial electron transfer quenching, J. Am. Chem. Soc. 133 (2011) 12940–12943. doi:10.1021/ja204214t.

[194] L.E. Kreno, K. Leong, O.K. Farha, M. Allendorf, D. Van Richard P., J.T. Hupp, Metal-Organic Framework Materials as Chemical Sensors., Chem. Rev. (Washington, DC, United States). 112 (2012) 1105–1125. doi:10.1021/cr200324t.

[195] C.-Y. Sun, X.-L. Wang, X. Zhang, C. Qin, P. Li, Z.-M. Su, et al., Efficient and tunable white-light emission of metal-organic frameworks by iridium-complex encapsulation., Nat. Commun. 4 (2013) 2717. doi:10.1038/ncomms3717.

[196] Y. Cui, Y. Yue, G. Qian, B. Chen, Luminescent functional metal-organic frameworks, Chem. Rev. 112 (2012) 1126–1162. doi:10.1021/cr200101d.

[197] M.L. Aubrey, R. Ameloot, B.M. Wiers, J.R. Long, Metal–organic frameworks as solid magnesium electrolytes, Energy Environ. Sci. 7 (2014) 667. doi:10.1039/c3ee43143f.

[198] A. Shigematsu, T. Yamada, H. Kitagawa, Wide control of proton conductivity in porous coordination polymers., J. Am. Chem. Soc. 133 (2011) 2034–6. doi:10.1021/ja109810w.

[199] S. Horike, D. Umeyama, S. Kitagawa, Ion conductivity and transport by porous coordination polymers and metal-organic frameworks, Acc. Chem. Res. 46 (2013) 2376–2384. doi:10.1021/ar300291s.

[200] W. Lin, S. Wu, Rational Design of Non-Centrosymmetric Metal-Organic Frameworks for Second-Order Nonlinear Optics, in: Met. Fram., 2010: pp. 193–213. doi:10.1002/9780470606858.ch6.

[201] Q.L. H. Pang, F. Gao, Q. Chen, R. Liu, Dendrite-like Co3O4 nanostructure and its applications in sensors, supercapacitors and catalysis, Dalt. Trans. 41 (2012) 5862–5868.

[202] et al. D. Wang, W. Ni, H. Pang, , Preparation of mesoporous NiO with a bimodal pore size distribution and application in electrochemical capacitors, Electrochim. Acta. 55 (2010) 6830–6835.

[203] H.-Y. Shi, B. Deng, S.-L. Zhong, L. Wang, A.-W. Xu, Synthesis of zinc oxide nanoparticles with strong, tunable and stable visible light emission by solid-state transformation of Zn(ii)–organic coordination polymers, J. Mater. Chem. 21 (2011) 12309. doi:10.1039/c1jm10809c.

[204] W.Y.S. L.N. Jin, Q. Liu, Shape-controlled synthesis of Co3O4 nanostructures derived from coordination polymer precursors and their application to the thermal decomposition of ammonium perchlorate., CrystEngComm. 14 (2012) 7721–7726.

[205] M.O. W. Cho, S. Park, Coordination polymer nanorods of Fe-MIL-88B and their utilization for selective preparation of hematite and magnetite nanorods., Chem. Commun. 47 (2011) 4138–4140.

[206] S. Jung, W. Cho, H.J. Lee, M. Oh, Self-template-directed formation of coordination-polymer hexagonal tubes and rings, and their calcination to ZnO rings, Angew. Chemie - Int. Ed. 48 (2009) 1459–1462. doi:10.1002/anie.200804816.

[207] A.M. M.Y. Masoomi, Applications of metal–organic coordination polymers as precursors for preparation of nano-materials, Coord.chem, Chem. Rev. 256 (2012) 2921–2943.

[208] K. Gedrich, I. Senkovska, N. Klein, U. Stoeck, A. Henschel, M.R. Lohe, et al., A highly porous metal-organic framework with open nickel sites, Angew. Chemie - Int. Ed. 49 (2010) 8489–8492. doi:10.1002/anie.201001735.

[209] P. Maniam, N. Stock, Investigation of porous ni-based metal-organic frameworks containing paddle-wheel type inorganic building units via high-throughput methods, Inorg. Chem. 50 (2011) 5085–5097. doi:10.1021/ic200381f.

[210] H. Kumagai, Y. Oka, M. Akita-Tanaka, K. Inoue, Hydrothermal synthesis and characterization of a two-dimensional nickel(II) complex containing benzenehexacarboxylic acid (mellitic acid), Inorganica Chim. Acta. 332 (2002) 176–180. doi:10.1016/S0020-1693(01)00786-1.

[211] D.J. Tranchemontagne, J.L. Mendoza-Cortés, M. O'Keeffe, O.M. Yaghi, Secondary building units, nets and bonding in the chemistry of metal-organic frameworks., Chem. Soc. Rev. 38 (2009) 1257–1283. doi:10.1039/b817735j.

[212] A.U. Czaja, N. Trukhan, U. Müller, Industrial applications of metal-organic frameworks., Chem. Soc. Rev. 38 (2009) 1284–1293. doi:10.1039/b804680h.

[213] J.W. Yoon, Y.K. Seo, Y.K. Hwang, J.S. Chang, H. Leclerc, S. Wuttke, et al., Controlled reducibility of a metal-organic framework with coordinatively unsaturated sites for preferential gas sorption, Angew. Chemie - Int. Ed. 49 (2010) 5949–5952. doi:10.1002/anie.201001230.

[214] P. Horcajada, S. Surblé, C. Serre, D.-Y. Hong, Y.-K. Seo, J.-S. Chang, et al., Synthesis and catalytic properties of MIL-100(Fe), an iron(III) carboxylate with large pores., Chem. Commun. (Camb). (2007) 2820–2822. doi:10.1039/b704325b.

[215] B.D. Cullity, Elements of X-Ray Diffraction, Am. J. Phys. 25 (1957) 394. doi:10.1119/1.1934486.

[216] Y.K. Seo, J.W. Yoon, J.S. Lee, U.H. Lee, Y.K. Hwang, C.H. Jun, et al., Large scale fluorine-free synthesis of hierarchically porous iron(III) trimesate MIL-100(Fe) with a zeolite MTN topology, Microporous Mesoporous Mater. 157 (2012) 137–145. doi:10.1016/j.micromeso.2012.02.027.

[217] P. O.M., Thermodynamics in Physical Chemistry (in Russian), (1991).

[218] K.S.W. Sing, Reporting physisorption data for gas/solid systems with special reference to the determination of surface area and porosity (Recommendations 1984), Pure Appl. Chem. 57 (1985) 603–619.

[219] Karnaukhov A.P, Adsorption: Texture of Dispersed and Porous Materials (in Russian), 1999.

[220] P. Horcajada, S. Surblé, C. Serre, D.-Y. Hong, Y.-K. Seo, J.-S. Chang, et al., Synthesis and catalytic properties of MIL-100(Fe), an iron(III) carboxylate with large pores., Chem. Commun. (Camb). (2007) 2820–2822. doi:10.1039/b704325b.

[221] F. Zhang, J. Shi, Y. Jin, Y. Fu, Y.J. Zhong, W. Zhu, Facile synthesis of MIL-100(Fe) under HF-free conditions and itsapplication in the acetalization of aldehydes with diols., Chem. Eng. J. 259 (2015) 183–190.

[222] I. Ahmed, J. Jeon, N.A. Khan, S.H. Jhung, Synthesis of a metal-organic framework, iron-benezenetricarboxylate, from dry gels in the absence of acid and salt, Cryst. Growth Des. 12 (2012) 5878–5881. doi:10.1021/cg3014317.

[223] A.U. Czaja, N. Trukhan, U. Muller, Industrial applications of metal-organic frameworks, Chem. Soc. Rev. 38 (2009) 1284–1293. doi:10.1039/b804680h.

[224] O.M. Yaghi, H. Li, T.L. Groy, Construction of Porous Solids from Hydrogen-Bonded Metal complexes of 1,3,5-tricarboxylic acid.pdf, J. Am. Chem. Soc. 118 (1996) 9096–9101. doi:S0002-7863(96)00746-9.

[225] C.R. Wade, M. Dincă, Investigation of the synthesis, activation, and isosteric heats of CO2 adsorption of the isostructural series of metal–organic frameworks M3(BTC)2 (M = Cr, Fe, Ni, Cu, Mo, Ru), Dalt. Trans. 41 (2012) 7931. doi:10.1039/c2dt30372h.

[226] J. Jänchen, D. Ackermann, H. Stach, W. Brösicke, Studies of the water adsorption on Zeolites and modified mesoporous materials for seasonal storage of solar heat, Sol. Energy. 76 (2004) 339–344. doi:10.1016/j.solener.2003.07.036.

[227] F.P.S.S.K.. H.S.J.J.H.M.H. Henninger, Novel adsorbents for solar cooling applications, in: Proc. Int. Conf. Sol. Air- Cond., Otti Technology Kolleg, Stafflestein, 2005: pp. 39–44.

[228] S.K. Henninger, H. a. Habib, C. Janiak, MOFs as adsorbents for low temperature heating and cooling applications, J. Am. Chem. Soc. 131 (2009) 2776–2777. doi:10.1021/ja808444z.

[229] W.-Y.S. Li-Na Jin, Qing Liu, Room temperature solution-phase synthesis of flower-like nanostructures of [Ni3(BTC)2·12H2O] and their conversion to porous NiO, Chinese Chem. Lett. 24 (2013) 663–667.

[230] K.S.W. SING, D.H. EVERETT, R.A.W. HAUL, L. MOSCOU, R.A. PIEROTTI, ROUQUEROL, et al., REPORTING PHYSISORPTION DATA FOR GAS/SOLID SYSTEMS with Special Reference to the Determination of Surface Area and Porosity, Pure App!. Chem. 57 (1985) 603–619.

[231] A.P. Karnaukhov, Adsorption: Texture of Disperse and Porous Materials., Sci. Novosib. Russ. (1999).

[232] J.-P. TAN Hai-Yan, LIU Cheng, WANG Zhao-Hui, WU, Simple Preparation, Structure and Conductivity of Nickel( ) Ⅱ Benzenetricarboxylate Ni3(BTC)2·12H2O, Chinese J. Struct. Chem. 33 (2014) 401–406.

Publications

1. Farrukh Israr, Duk Kyung Kim, Yeongmin Kim, Seung Jin Oh, Kim Choon Ng, Wongee Chun, **Synthesis of porous Cu-BTC with ultrasonic treatment: Effects of ultrasonic power and solvent condition**, *Ultrasonics Sonochemistry*, 29 (2016) 186-193.
2. Farrukh Israr, Duk Kyung Kim, Yeongmin Kim, Seung Jin Oh, Kim Choon Ng, Wongee Chun, **Hydrothermal Synthesis of Fe based MOFs with Energy Economy Approach**, *J. Energy Engineering*, 24 (2015) 55-58.
3. Farrukh Israr, Duk Kyung Kim, Yeongmin Kim, Seung Jin Oh, Kim Choon Ng, Wongee Chun, **Cost Effective and low energy consuming hydrothermal synthesis of Ni based MOF**, *J. Energy Engineering*, 24 (2015) 51-54.
4. Jun-Ho Hyun, Farrukh Israr, Yoon-Joon Lee, Wongee Chun, **A Performance Study on Silica Gel Adsorption Desalination System Utilizing Low Temperature Heat Source**, *J. Korean Solar Energy Society*. 33 (2013) 39-46.
5. Kuan Chen, Seung Jin Oh, Farrukh Israr, Sanket Kolhe, Sang Woong Shin, Wongee Chun, **Optimization of Operational and Constitutional Geometric Parameters for Acoustic energy Output**, *J. Energy & Climate Change*. 8 (2013) 74-93.